



# ZnO nanostructure synthesis for the photocatalytic degradation of azo dye methyl orange from aqueous solutions utilizing activated carbon

Ahmed Jaber Ibrahim <sup>a,\*</sup>

<sup>a</sup>Scientific Research Center, Al-Ayen University, ThiQar 64011, Iraq

## ARTICLE INFO:

Received 3 Sep 2022

Revised form 29 Oct 2022

Accepted 18 Nov 2022

Available online 29 Dec 2022

## Keywords:

Degradation,  
Zinc oxide,  
Nanostructure,  
Methyl orange,  
Photocatalytic

## ABSTRACT

In this study, zinc acetate (as a precursor) and activated carbon carboxylic acid derivative were used to create the nanostructure of zinc oxide (ZnO) as a matrix. The carboxylic acid derivative was produced by modifying the oxidized activated carbon with nitric acid (AC-COOH). The modified activated carbon's surface was then impregnated with zinc to load it. By using BET, XRD, and SEM to characterize the ZnO nanostructure, it was discovered that it was composed of nanoparticles with a surface area capacity of 17.78 m<sup>2</sup> g<sup>-1</sup> and a size range of 21–31 nm. The photocatalytic hydrolysis of the dye methyl orange in an aqueous medium served as a test case for the catalyst's performance. The primary variables were considered, including pH, catalyst dose, stirring effect, and starting dye concentration. Measurements of activity below UV light revealed satisfactory outcomes for photocatalytic hydrolysis of the methyl orange (MO). In addition, the efficiency of the methyl orange (MO) photolysis catalyst prepared with unmodified activated carbon was also evaluated. The outcomes proved that zinc oxide (ZnO), made using a derivative carboxylic acid of activated carbon molecules by a matrix, had more good photocatalytic action than zinc oxide (ZnO) made by the real activated carbon matrix.

## 1. Introduction

Reactive dye-containing effluents from various sectors frequently generate environmental issues [1]. The ecosystem of the receiving surface waterways is severely harmed by this pollution [2]. Many researchers' efforts have focused on removing pollutants and toxins from wastewater from different sectors [3]. A variety of chemical and physical procedures, such as membranes [4], adsorption methods [5], and photolysis, have been employed to remove dyes [6] presently. Several researchers

have recently used photolysis as one of the advanced oxidation processes (AOPs) to get rid of dyes from wastewater [7]. Without altering the substrate, the photocatalytic reaction is catalyzed by light and can proceed more quickly [8]. Under the right circumstances, semiconductors function as catalysts due to the down breaking energy between the capacitance and conduction bands [9]. The process of photocatalysis requires two levels of different, equal energy. The movement of the electrons caused by the absorption of this energy leads to a hole (h<sup>+</sup>) and a pair of electrons(e<sup>-</sup>). Both the oxidation of the electron donor species and the reduction of the electron acceptor species might include electrons [10]. To degrade pollutants, many materials are

\*Corresponding Author: [Ahmed Jaber Ibrahim](mailto:Ahmed Jaber Ibrahim)

Email: [ahmed.jibrahim@alayen.edu.iq](mailto:ahmed.jibrahim@alayen.edu.iq)

<https://doi.org/10.24200/amecj.v5.i04.200>

utilized as photocatalysts, including  $\text{TiO}_2$ ,  $\text{ZnO}$ ,  $\text{ZrO}_2$ ,  $\text{CdS}$ ,  $\text{MoS}_2$ , and  $\text{WO}_3$  [11].  $\text{TiO}_2$  is one of these materials frequently used as a photocatalyst and has seen the most application to date.  $\text{TiO}_2$  has benefits like environmental safety, non-toxicities, chemical constancy, and the capacity for restoration and reuse. However,  $\text{TiO}_2$  has drawbacks, including a high price tag and a UV absorption band. The importance of  $\text{ZnO}$  as a suitable  $\text{TiO}_2$  alternative in photocatalysis has lately increased [12]. One richest structures, zinc oxide, has a variety of advantages. As a result,  $\text{ZnO}$  has several uses in various scientific projects [13].  $\text{ZnO}$  has been produced using a variety of techniques, including the soft chemical method [14], the sol-gel method [15], the vapor-phase growth [16], the vapor-liquid-solid process [17], electrophoretic deposition [18], thermal evaporation [19], homogeneous precipitation [20], chemical vapor deposition [21], chemical bath deposition [22], etc. In the aforementioned investigations,  $\text{ZnO}$  nanoparticles were only occasionally generated through the activated carbon layer and by an auxiliary matrix approach, as recommended by Park et al. [23]. In this study, the photocatalytic activity of the generated  $\text{ZnO}$  was used to break down the azo dye methyl orange. Additionally,  $\text{ZnO}$  was produced using modified activated carbon (containing carboxyl functional groups).

## 2. Materials and Methods

### 2.1. Reagents

All chemical substances were obtained with a high degree of purity, including caustic soda ( $\text{NaOH}$ , CAS Number: 1310-73-2, Sigma), hydrochloric acid ( $\text{HCl}$ , CAS Number: 7647-01-0, Sigma, Germany), activated carbon (AC, CAS Number: 7440-44-0, Sigma), zinc acetate dihydrate ( $\text{Zn}(\text{CH}_3\text{CO}_2)_2 \cdot 2\text{H}_2\text{O}$ , CAS Number: 5970-45-6, Sigma), nitric acid ( $\text{HNO}_3$ , CAS Number: 7697-37-2, Sigma, Germany), and azo dye methyl orange ( $\text{C}_{14}\text{H}_{14}\text{N}_3\text{O}_3\text{SNa}$ , CAS Number: 547-58-0, Sigma). Methyl orange was dissolved in 100 mL of deionized water (DI), 0.010 g at a time, to create a stock solution ( $100 \text{ g mL}^{-1}$ ). All working solutions were made at the necessary concentration using distilled water to dilute the stock solution.

### 2.2. Equipment

An ultraviolet-visible spectrophotometer (model 2600) to record Rayleigh UV-Vis spectra. A Metrohm pH meter (model 744) to adjust the working solution's pH to the desired values. Field emission-scanning electron microscope (FE-SEM) (model SU5000) to know the characterization of the sample's surface and shape morphology. X-ray diffraction instrument (XRD) (model B8 ADVANCE) to record patterns via BRUKER. The transformer coupled plasma (TCP) (model VISTA-PRO) to measure the presence of zinc in the samples. Spectrophotometer (IR-470 Shimadzu) to record the Infrared (IR) spectrum of samples. At the analytical chemistry laboratory of the college of education (Ibn Al-Haitham) at the University of Baghdad, experiments in the photocatalytic bleaching and degradation of dye MO were carried out at a photoreactor framework prepared there for it.

### 2.3. Synthesizing Zinc Oxide nanoparticles by modified activated carbon particles

#### 2.3.1. Activated carbon surface modification

According to Chang et al. [24], adding carboxyl functional groups to the surface of activated carbon caused the carbon particles to become activated. To eliminate metal ions and other impurities, a hydrochloric solution (10% v/v) solution was first used to clean the activated carbon powder for 24 hours. Following that, 300 ml of a 32.5 % (v/v)  $\text{HNO}_3$  solution was stirred with 10 g of pure activated carbon added, and the mixture was heated at  $60 \text{ }^\circ\text{C}$  for five hours. The heterogeneous mixture had filtered and neutralized with DI water (deionized water) by wash and then dried below decreased pressure for eight hours at  $80 \text{ }^\circ\text{C}$ . the carboxylic derivative of activated carbon makes up the final product (AC-COOH).

#### 2.3.2. Synthesizing nanoparticles of zinc oxide

As a precursor for manufacturing  $\text{ZnO}$  nanoparticles, 100 mL of zinc acetate solution was mixed with 2 g of carboxylate-activated carbon (AC-COOH) in different concentrations for 12 hours. The solution was filtered, dried for 18 hours at  $80 \text{ }^\circ\text{C}$ , and then

calcined for 4 hours at 500 °C in an electric oven. Different concentrations of zinc acetate dihydrate were explored to create zinc nanoparticles by examining the impact of the concentration of zinc acetate precursor on the description of zinc oxide (particle size, percentage values, photocatalytic capabilities, etc.). To do this, ZnO nanoparticles were created using solutions containing concentrations of 0.09, 0.02, and 0.01 M (Molarity) zinc acetate dihydrate, respectively. XRD spectra of three samples were taken to verify the production of ZnO nanoparticle forms. The XRD bandwidth pattern and Scherrer's Equation 1 [25, 26] were used to measure the crystal size of three samples.

$$D = K (\lambda / \beta \cos \theta) \quad (\text{Eq.1})$$

Where D represents the size of crystalline particle in units of a nanometer (nm), The coefficient is K (that equals 0.89),  $\lambda$  represents the wavelength of the X-ray radiation in a unit of a nanometer (nm),  $\beta$  means FWHM (full width at half maximum) is an experimental value in radians (rad) and diffraction angle expressed in degrees had represented  $\theta$ .

### 2.3.3. Synthesis of Zinc Oxide nanoparticles utilizing unmodified activated carbon

2.0 g of activated carbon had put in 200 mL of hydrochloric solution (10% v/v) to eliminate impurities for twenty-four hours to study the surface modification phase of activated carbon particles in the formation of Zinc Oxide (ZnO). After that, the product was added to a concentration of 0.09 M zinc acetate dihydrate solution for 12 hours, and the resulting combination was then filtered. The finished product was dried at 80 °C for 18 hours before being calcined in an electric oven for 4 hours at 500 °C. To determine the sample's crystal size using Scherrer's equation, XRD spectra were taken on a sample made with unmodified activated carbon.

### 2.4. Procedure of methyl orange decomposition in photocatalytic experiments

Initially, a 250 mL beaker was filled with 100 mL of methyl orange (MO) solution with a concentration

of 10 mg L<sup>-1</sup> and a pH of 6. The solution was then supplemented with 20 mg of Zinc Oxide (ZnO) photocatalyst. Methyl orange was adsorbed onto Zinc Oxide (ZnO) nanoparticles after being combined with the solution utilizing a magnetic stirring device in a dark environment for half hour (30 min). Afterward confirming the balance of adsorption, 0.2 mL of the solution was placed into a test tube and then centrifuged for five minutes at 3000 rpm to collect the photocatalyst deposition particles. A spectrophotometer captured the solution's adsorption spectra in the 200–600 nm range. After the absorption spectrum was recorded, the combination was put into a photoreactor, and a UV light was turned on. Twenty minutes after exposure to UV light, ten samples were collected at intervals of one, and their absorption spectra were recorded. The control solution's adsorption spectrum was recorded similarly without including a photocatalyst.

### 2.5. Procedure of batch adsorption

To find the best circumstances for bleaching and degrading MO (methyl orange) in the existence of Zinc Oxide (ZnO) photocatalysts, batch experiments were carried out. It was thoroughly explored how relevant factors including methyl orange (MO) concentration, pH, solution stirring, photocatalyst dose, and solution oxygen affected the outcomes. One variable at a time optimization was utilized to improve factors that affected the reaction. With this procedure, studies were carried out in a batch setting with 100 mL of dye solution (10 mg L<sup>-1</sup>) placed into a beaker (250 ml). The magnetic stirrer was used to mix the suspensions for 30 minutes in the dark before centrifuging them for 5 minutes at 3000 rpm. A UV-Vis spectrophotometer was used to evaluate the clear supernatant. Equation (2) was used to determine the rate of bleaching and dye degradation [27].

$$R = (C_0 - C_t \div C_0) \times 100 \quad (\text{Eq. 2})$$

Where R (percentage) represents the dye removal effectiveness,  $C_0$  represents the dye's starting concentration (mg L<sup>-1</sup>), and  $C_t$  represents the dye's concentration at time t following adsorption (mg L<sup>-1</sup>).

### 3. Results and Discussion

#### 3.1. Study of Nanoparticles' characteristics

##### 3.1.1. X-Ray Diffraction (XRD) examination

The XRD spectra of three produced zinc oxide (ZnO) samples are shown in Figure 1 to illustrate that the nanoparticles formed appropriately. Figures 1 show that the sample's hexagonal zinc

oxide crystallization has been verified. Table 1 compares the XRD pattern characteristics for three produced samples and the reference sample [22]. It can be seen from the XRD spectrum in Figure 1 and the data in Table 1 that as zinc acetate dihydrate concentration increased, ZnO peak density too increased, and spectral noise intensity

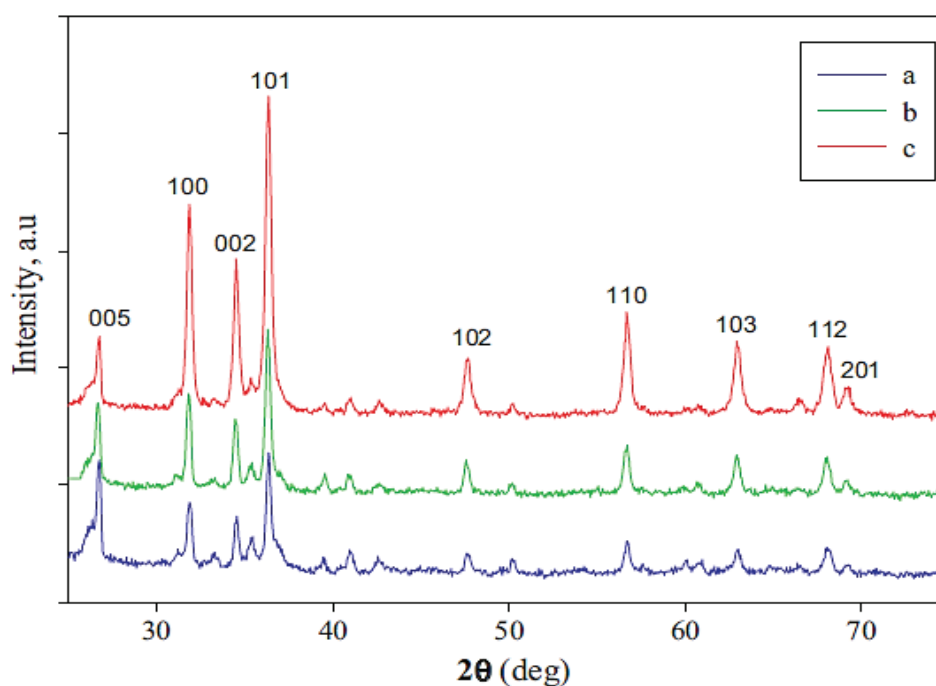


**Fig. 1.** XRD spectra of synthetic ZnO nanoparticles at various concentrations of zinc acetate dihydrate (a:0.01 M; b: 0.02 M; c: 0.09 M)

**Table 1.** Compares the standard sample with the XRD samples (a), (b), and (c), as well as a sample made with unmodified carbon

Standard sample		Samples						the sample produced utilizing unmodified carbon		
		A		b		C				
<u>hkl</u>	d (Å)	I/I <sup>0</sup>	d (Å)	I/I <sup>0</sup>						
100	2.82	58	2.81	68	2.82	67	2.81	69	2.75	32
002	2.61	45	2.60	86	2.60	55	2.60	53	2.52	91
101	2.48	100	2.47	100	2.48	100	2.48	100	2.32	100
110	1.63	33	1.63	42	1.63	40	1.63	37	1.51	33

d angstrom distance(Å) between plates, I peak intensity, I<sup>0</sup> maximum intensity to planes 100 and 002, 101 and 110

decreased. This data may result from increased ZnO nanostructure production with rising zinc acetate concentration. This data may be the result of increased ZnO nanostructure production with rising zinc acetate concentration. According to Liu et al. [20], the intensity of peak 005 in XRD spectra is associated with carbon impurities that became less intense as zinc acetate dihydrate concentration

was raised. Figure 2 displays the XRD spectrum of the carbon-free synthetic sample. The production of hexagonal ZnO has been confirmed based on Table 1 and the differentiation of the XRD data of the produced samples (unmodified activated carbon and the standard sample). Three samples that were created using both modified and unmodified carbon are shown in Table 2 by their crystal sizes.

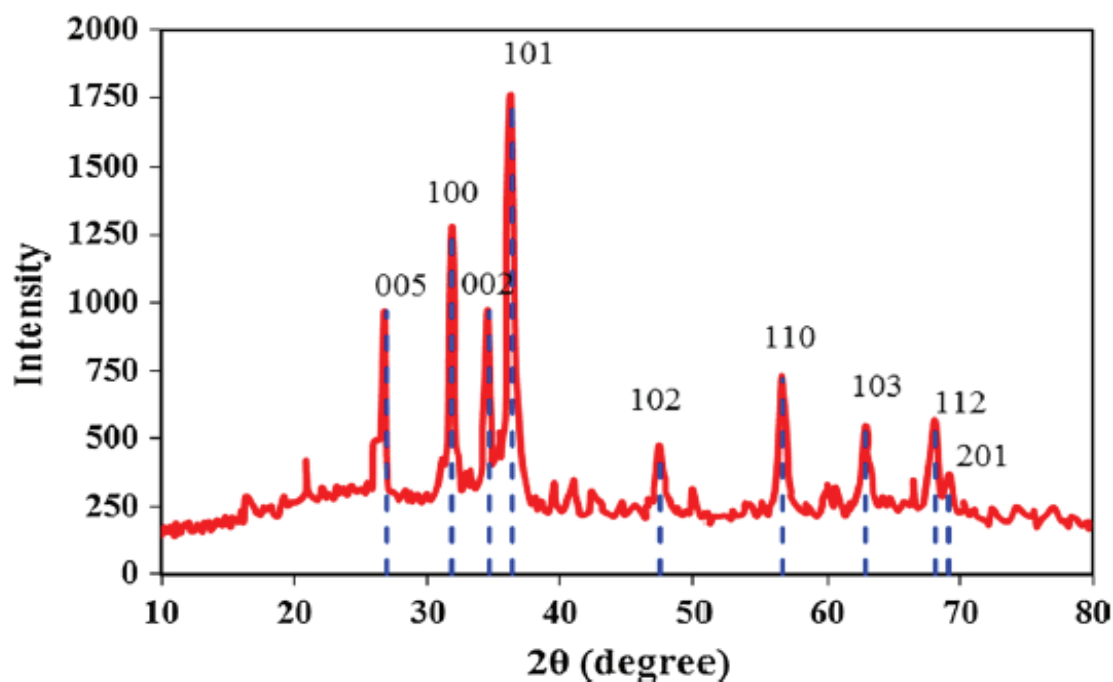


Fig. 2. XRD spectra sample using unmodified carbon and 0.09 M of zinc acetate dihydrate.

Table 2. Scherrer's equation-derived estimated particle size

Planes	Sample size (nm)			the sample produced utilizing unmodified carbon
	A	b	C	
101	26	25	22	24.50
100	27	28	24	36.66
002	33	27	25	25.34

### 3.1.2. Study analysis using TCP, BET, and SEM

The ZnO percent (%) in samples was calculated using TCP analysis. ZnO content was 9.94, 10.74, and 31.81 % in samples a, b, and c, respectively, according to TCP analysis. These findings suggest that raising the zinc acetate concentration leads to an increase in the samples' ZnO content. ZnO percent was 19.8% for unmodified carbon in the TCP measurement, demonstrating that ZnO % is decreased in the absence of surface modification of activated carbon. The specific surface area of produced ZnO nanoparticles was measured using BET analysis (only for sample c). The specific surface area of this material is higher than the specific surface area of traditional ZnO particles ( $4.49 \text{ m}^2 \text{ g}^{-1}$ ), according to the results of the BET study, which also revealed a total pore volume of  $0.1 \text{ cm}^3 \text{ g}^{-1}$  and average pore width of 51.6 nm [28]. The inclusion of activated carbon in the produced ZnO accounts for this elevated amount. ZnO, activated carbon, and AC-ZnO surface morphology and textural characterization are significant criteria that could improve the efficiency of the photocatalytic activity [29]. SEM images of samples a, b, and c as shown in Figure 3, were taken to evaluate the morphology feature of produced ZnO nanoparticles. It is evident that when the concentration of zinc acetate rises, ZnO particles fill the pores of the activated carbon, achieving uniform coverage on a large portion of the activated carbons. Even though

the large holes in the activated carbon were filled with ZnO particles, which prevent the porosity of the carbon surface, sample C nevertheless displays a porous nature with a sizable amount of surface area and pore volume [30].

### 3.2. Study Ultraviolet-Visible (UV-Vis) spectroscopic examination

Two adsorption bands at wavelengths of 464 and 272 nm can be seen in the methyl orange adsorption spectra. While the breakdown of the azo link, which results in bleaching, causes the absorption band at 464 nm to drop, the methyl orange absorption band decreases at 272 nm due to the phenyl rings degrading and completing mineralization. As seen in Figure 4, decolorization rates are very low, and there is no total degradation or mineralization when ZnO photocatalyst is not present. In contrast to what is depicted in Figure 5, complete bleaching and degradation take place when ZnO nanoparticles are present as a catalyst. For additional research, Figure 6 shows the absorption trend over time at wavelengths of 464 nm and 272 nm under three different circumstances: Ultraviolet radiation, dark medium, and ultraviolet radiation with the catalyst present.

The following figure demonstrates that dye methyl orange completely bleaches and degrades in the presence of a ZnO catalyst within 200 minutes; still, these processes were nonexistent in the absence of

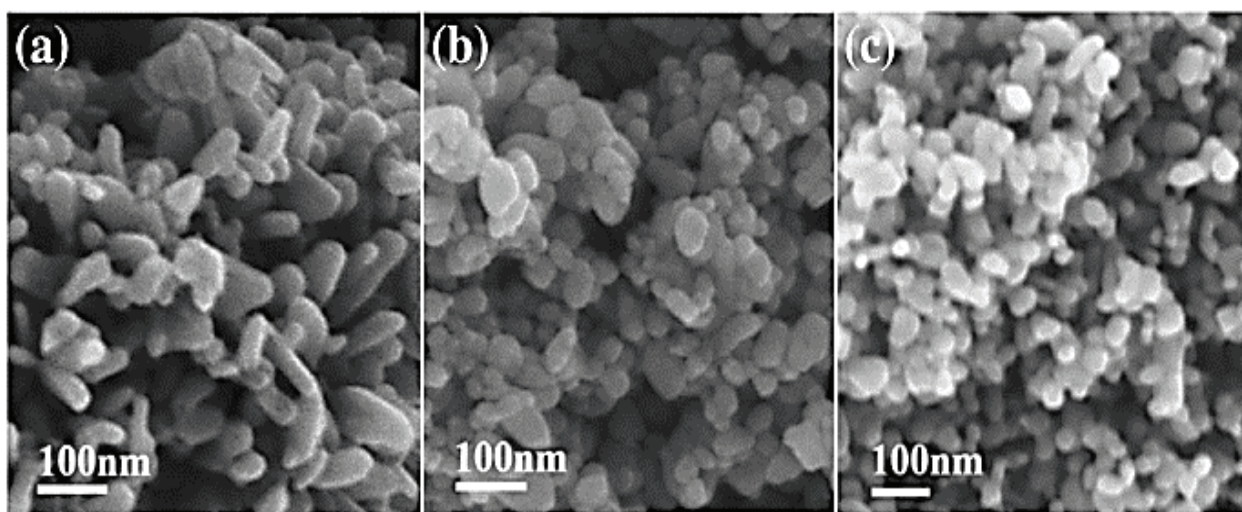
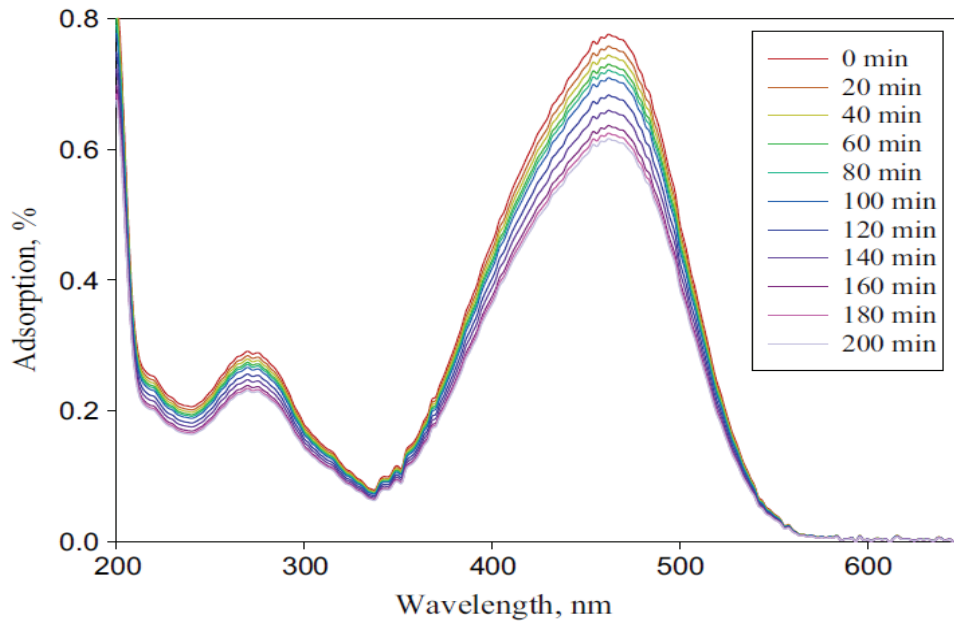


Fig. 3. SEM characterization for three samples (a, b, and c)

a photocatalyst. After swirling the dye and catalyst combination in the dark for 20 minutes, data analysis revealed that no simple degradation occurred and that the adsorption of dye methyl orange onto the

surface catalyst was stable. As a result, dye and catalyst mixtures were swirled for 30 minutes in complete darkness in each experiment to guarantee that adsorption equilibrium was reached.



**Fig. 4.** Shows the reaction system's adsorption spectrum without a ZnO photocatalyst, with  $10 \text{ mg L}^{-1}$  of methyl orange as the catalyst.

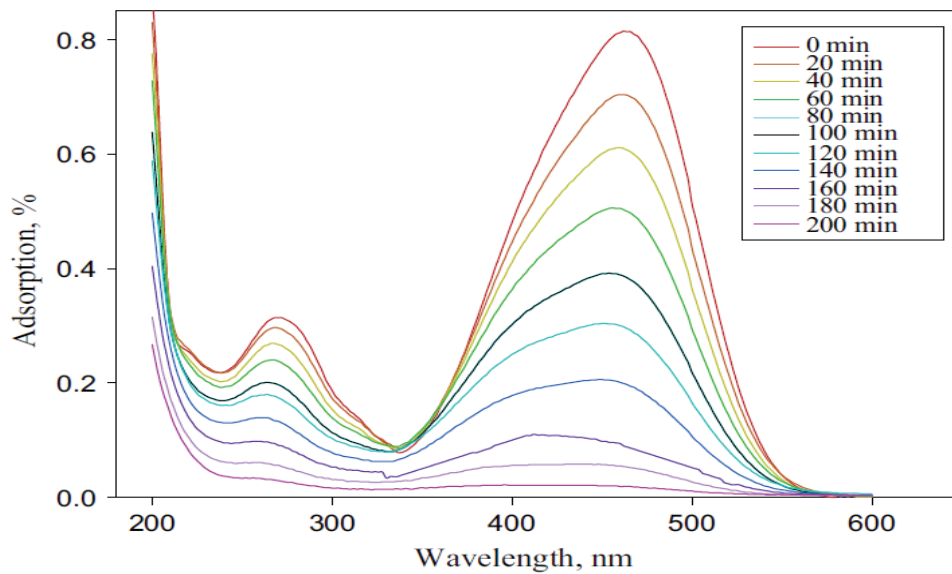


**Fig. 5.** Shows the reaction system's adsorption spectrum at pH 6,  $200 \text{ mg L}^{-1}$  of ZnO photocatalyst, and  $10 \text{ mg L}^{-1}$  of methyl orange.

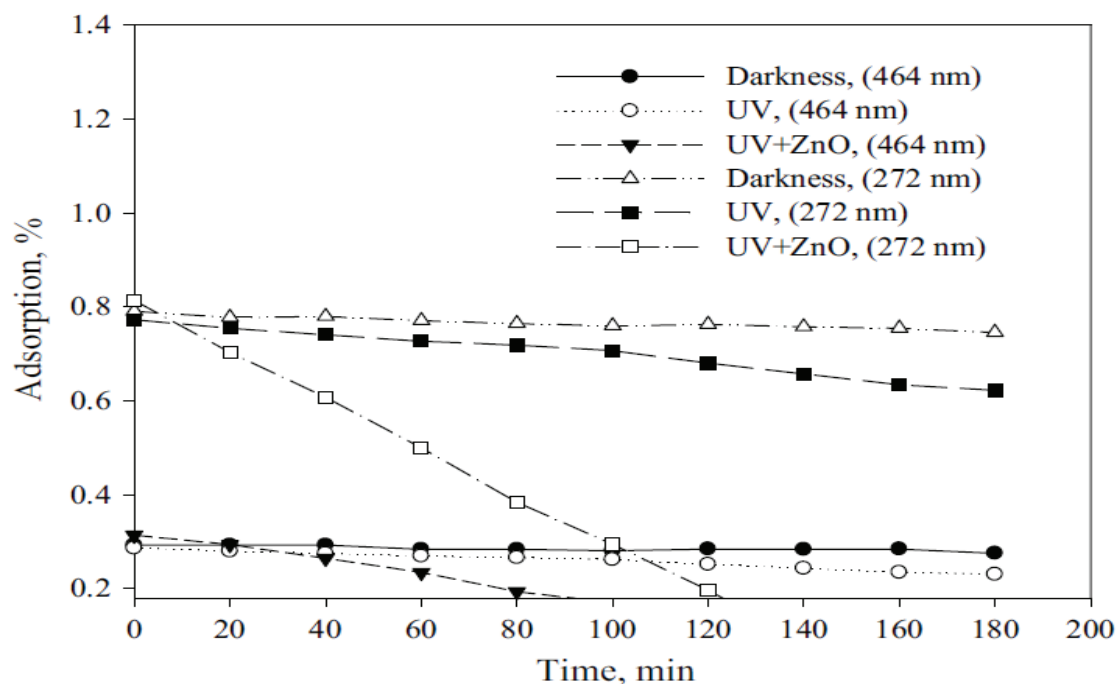


**Fig. 6.** The light absorption at wavelengths of 272 and 464 nm changes over time under the conditions at pH 6, 200 mg L<sup>-1</sup> of photocatalyst, and 10 mg L<sup>-1</sup> of methyl orange.

### 3.3. pH effect

The pH significantly affects the adsorption capacity of the adsorbent and removal efficiency by changing the adsorption chemistry of the adsorbent-adsorbate [31]. The appropriate contact time was used to dissolve 20 mg of photocatalyst into 100 mL of MO solution (10 mg L<sup>-1</sup>) for the pH-related experiments. To change the pH of the solution, 0.1 M HCl and 0.1 M NaOH solution were utilized. Figure 7 shows how the pH of the solution affects how quickly MO is bleached and degraded by AC-ZnO. It is clear that pH six results in the fastest bleaching and dye degradation of methyl orange (MO). Therefore, pH six was chosen for additional research. Changes in the electrostatic attraction between the dye MO and the ZnO surface can explain this removal process's pH-dependent behavior. In comparison to acidic circumstances (where the driving force is higher), the pollutant

adheres to the adsorbent particles more effectively under optimal electrostatic attraction [32]. ZnO's surface charge is positive at low pH 9 [33]. As a result, anions are more likely to bind to ZnO in an aqueous environment at a low pH of 9. However, the pKa for methyl orange has been reported to be 3.8 ± 0.02 [34]. As a result, at pH values higher than pKa, the concentration of methyl orange in its anionic form is greater than in its cationic form. The amount of methyl orange that could be adsorbed onto ZnO increased as the solution pH was raised to 6. The rate of bleaching and dye degradation was shown to decrease at increasing pH values above 6, because the hydroxyl radical's oxidation potential decreases with the rising pH of the solution [35]. Additionally, the anionic form of methyl orange competes with OH ions in the solution due to the greater OH content, which lowers the capacity of methyl orange to bind to ZnO [36].

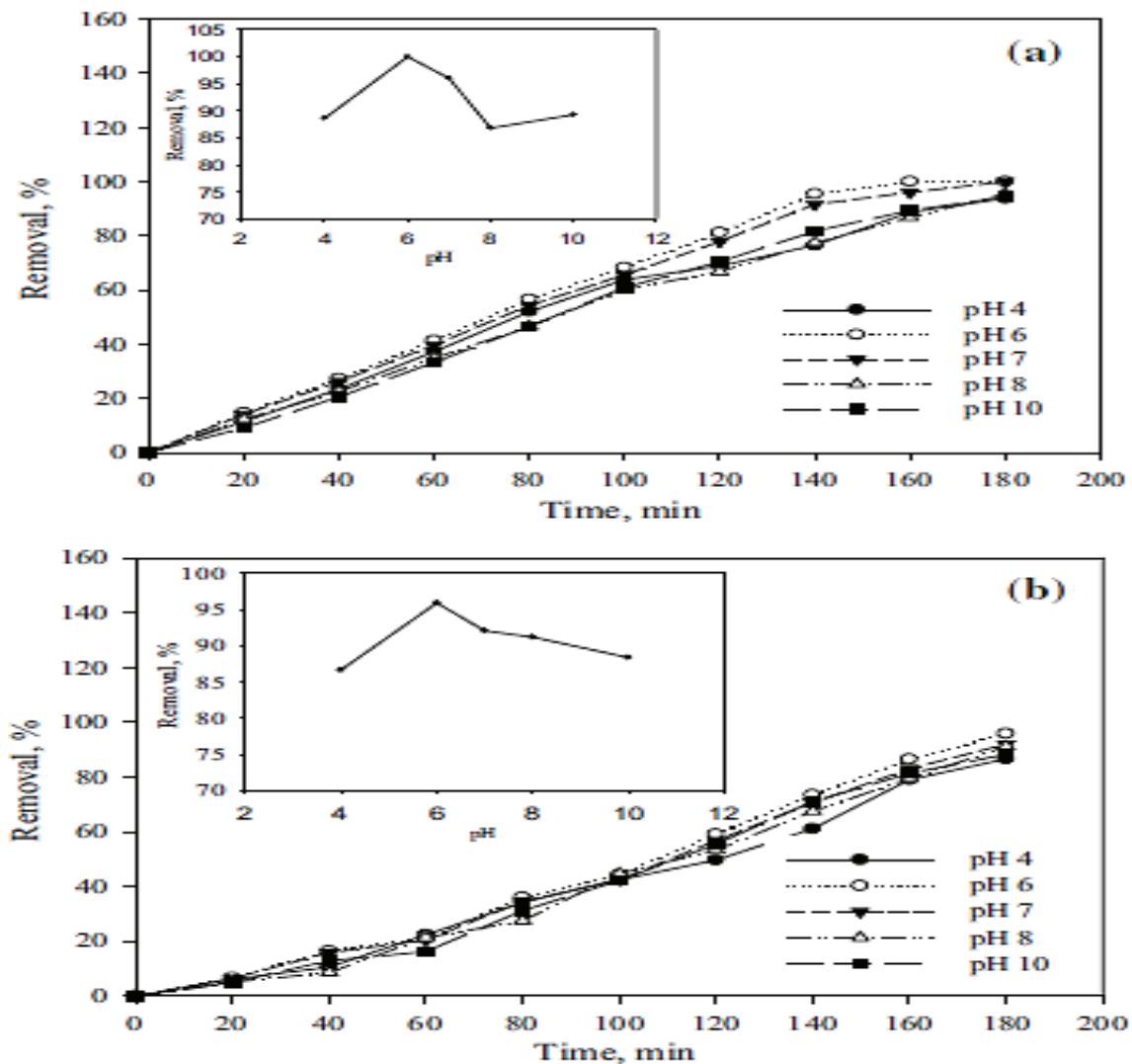
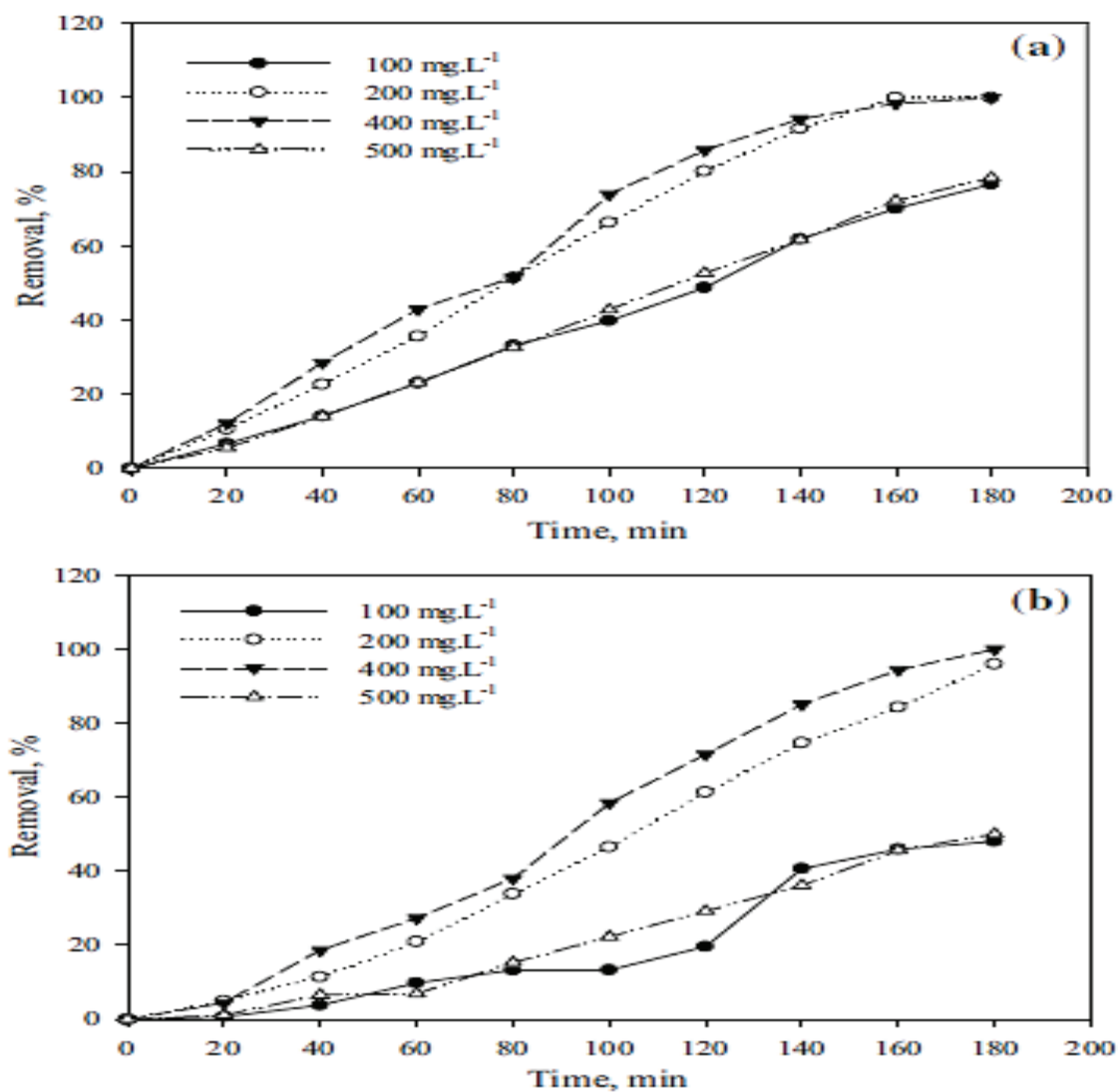


Fig. 7. The pH effects of methyl orange under the conditions of 200 mg L<sup>-1</sup> photocatalysts, and 10 mg L<sup>-1</sup> methyl orange on; (a) the rate of bleaching, (b) the rate of dye degradation

### 3.4. Photocatalyst dosage effects

To investigate the effects of photocatalyst dose on the bleaching and degradation of MO, a solution with a primary methyl orange concentration of 10 mg L<sup>-1</sup> and a reaction duration of 180 min was added to a range of photocatalyst doses from 100 to 500 mg L<sup>-1</sup>. Figure 8 depicts the findings of these analyses. The result demonstrated that bleaching and degradation increased when the catalyst concentration was raised to 200 mg L<sup>-1</sup>. When the catalyst concentration was increased to 400 mg L<sup>-1</sup>, bleaching and degradation did not change noticeably, but when the catalyst

concentration was increased to 500 mg L<sup>-1</sup>, bleaching and degradation decreased. As catalyst concentration grew, more surface active sites were available. As a result, there is an increase in the generation of hydroxyl radicals, which increases ZnO's photocatalytic activity. UV light cannot penetrate the catalyst's surface when the milky solution is in excess. As a result, these occurrences can reduce the generation of hydroxyl radicals, reducing the effectiveness of dye deterioration and solution pH discoloration [33,37]. For subsequent research, a dose of 200 mg L<sup>-1</sup> photocatalysts was used.



**Fig. 8.** Effect of catalyst amount of methyl orange under the conditions of pH 6, 180 minutes, and  $10 \text{ mg L}^{-1}$  of methyl orange on; (a) the rate of bleaching (b) the rate of dye degradation

### 3.5. MO concentration effects

Several methyl orange (MO) concentrations ( $5\text{--}20 \text{ mg L}^{-1}$ ) at a reaction duration of 180 min and a primary pH of 6 were studied to ascertain the impact of primary MO concentration on the method's effectiveness. Figure 9 displays the outcomes of these analyses. The findings showed that raising the initial dye concentration reduced bleaching and degradation. This might be brought on by a decline in the number of active surface

sites. As a result, the generation of hydroxyl radicals declines, which may result in decreased photocatalytic activity. Furthermore, as the dye concentration increases, the distance of a photon into a dye solution shortens. To conduct additional research, MO at a concentration of  $10 \text{ mg L}^{-1}$  was chosen because, at higher dye concentrations, the dye molecules may absorb more sunlight than the catalyst, which could reduce the catalyst's effectiveness [38, 39].

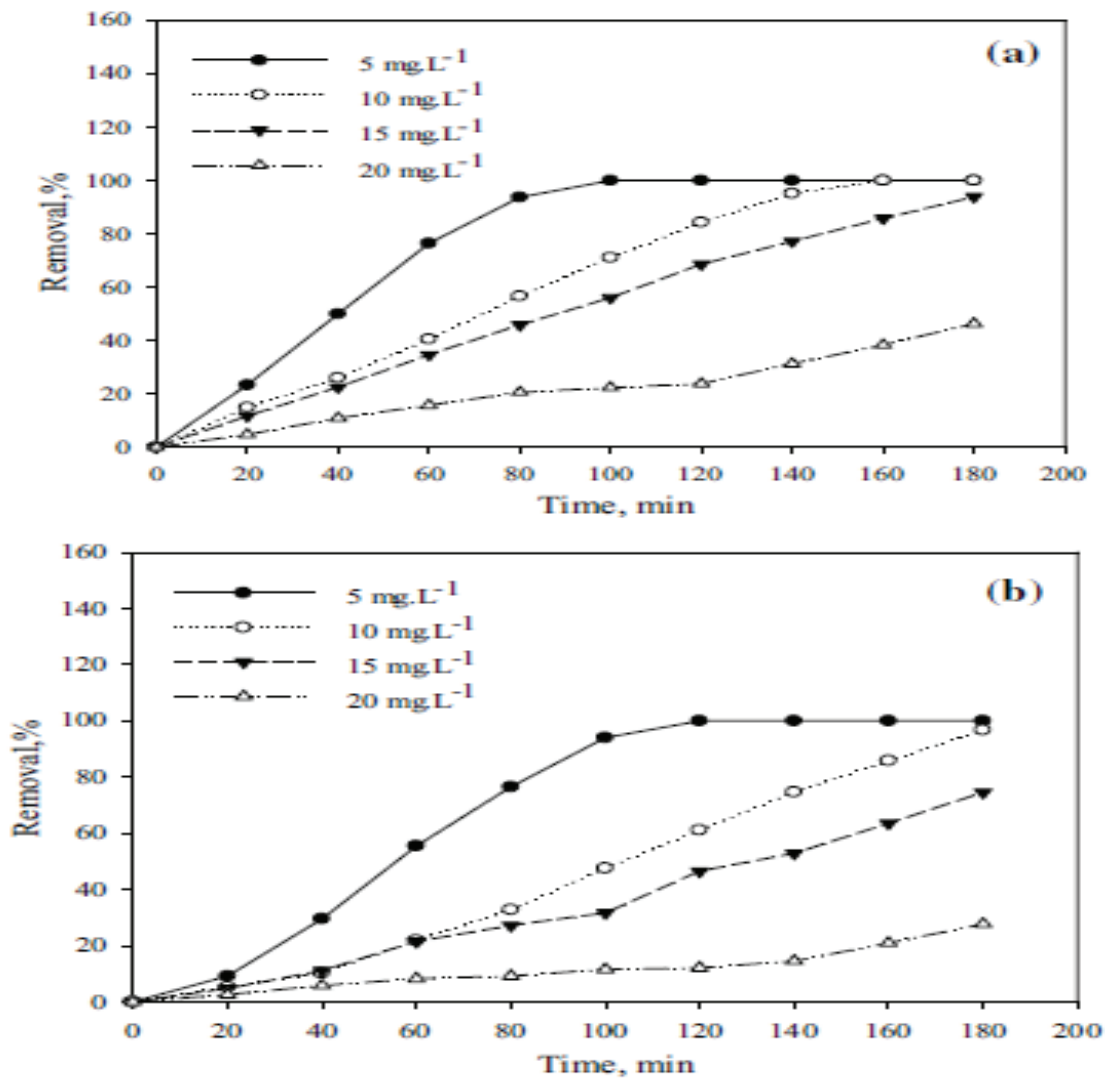


**Fig. 9.** Effect of primary concentration of MO under the conditions of pH 6, and 200 mg L<sup>-1</sup> photocatalysts on; (a) the rate of bleaching (b) the rate of dye degradation

### 3.6. Effects of stirring the mixture

To find out how stirring the solution affected the bleaching and degradation of MO, specific tests were conducted at reaction periods of 180 minutes, pH levels of 6, primary MO concentrations of 10 mg L<sup>-1</sup>, and catalyst doses of 200 mg L<sup>-1</sup>. Figure 10 percent (%) the findings of these analyses. The results show that swirling

the solution exacerbated the bleaching and deterioration. First, agitation causes turbulence in the solution, which promotes the solution's absorption of oxygen. In the synthesis of hydroxyl radicals, soluble oxygen is crucial. Second, stirring the solution shortens the time needed for equilibrium by accelerating MO transfer and surface diffusion [40].

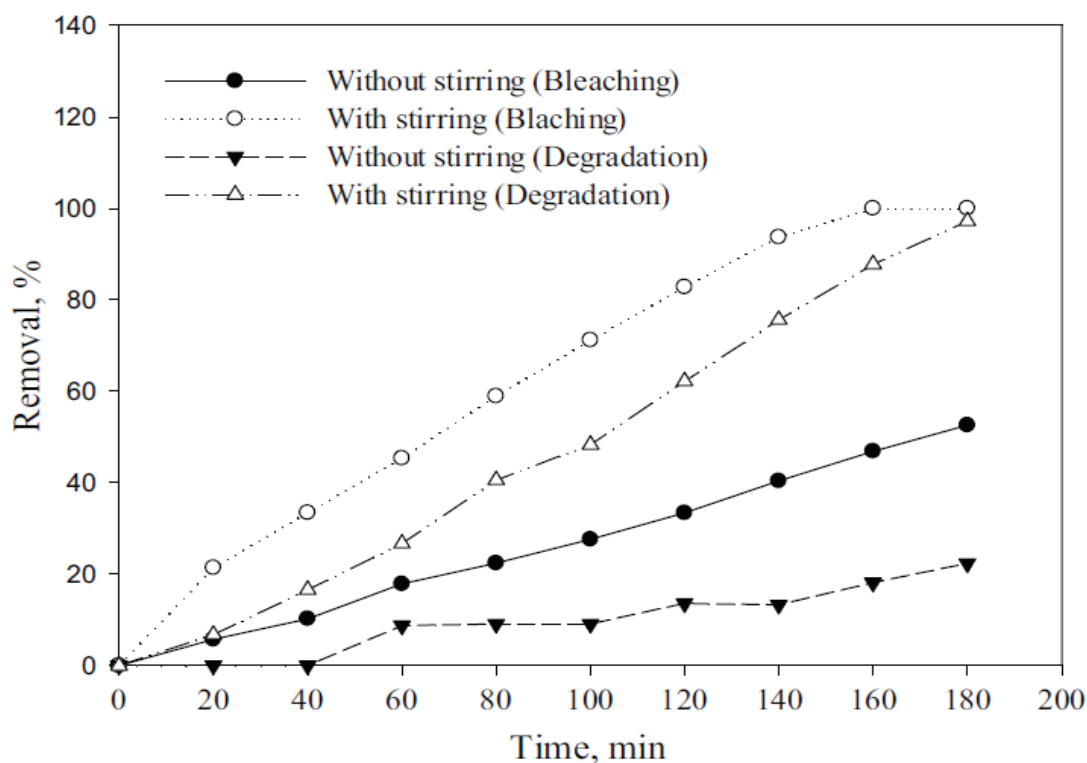


**Fig. 10.** Effect of solution stirring under the conditions of pH 6, 20 mg L<sup>-1</sup> photocatalysts, and 10 mg L<sup>-1</sup> methyl orange on the rate of bleaching and dye degradation

#### 4. Conclusion

In the current work, methyl orange from aqueous solutions was subjected to a dye degradation process employing ZnO as a photocatalyst. The results showed that the AC-ZnO system successfully destroyed the MO dye. When ZnO was present, the rate of deterioration was high, but when ZnO wasn't there, the degradation rate decreased. The best dye degradation conditions were found at a pH of 6.0 with 200 mg L<sup>-1</sup> of photocatalyst for 10 mg L<sup>-1</sup> of MO based on agitating the dye solution in an air environment. The outcomes also demonstrated that synthetic photocatalysts in the actual world had much high efficacy and that recovering and reusing photocatalysts hurt the degradation rate and bleaching. The current study offered a novel, cost-effective adsorbent with great promise for treating wastewater contaminated with dyes.

#### 5. Conflicts of interest

There are no conflicts to declare

#### 6. Acknowledgements

This research is supported by the Physical Chemistry Lab., Chemist Department, College of Education for pure science (ibn-al Haitham), University of Baghdad.

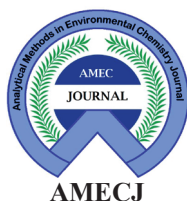
#### 7. References

- [1] C. Karthikeyan, P. Arunachalam, K. Ramachandran, A. M. Al-Mayouf, S. Karuppuchamy, Recent advances in semiconductor metal oxides with enhanced methods for solar photocatalytic applications, *J. Alloy Comp.*, 828 (2020) 154281. <https://doi.org/10.1016/j.jallcom.2020.154281>.

- [2] X. Nie, S. Wu, P. Lv, H. Ke, F. Huang, Q. Wei, Chameleon-inspired iridescent structural color textiles with reversible multiple stimulus-responsive functions, *Chem. Eng. J.*, 433 (2022) 134410. <https://doi.org/10.1016/j.cej.2021.134410>.
- [3] T. S. Naidu, C. M. Sheridan, L. D. van Dyk, Basic oxygen furnace slag: Review of current and potential uses, *Miner. Eng.*, 149 (2020) 106234. <https://doi.org/10.1016/j.mineng.2020.106234>.
- [4] F. M. Valadi, A. Ekramipooya, M. R. Gholami, Selective separation of Congo Red from a mixture of anionic and cationic dyes using magnetic-MOF: Experimental and DFT study, *J. Mol. Liq.*, 318(2020) 114051. <https://doi.org/10.1016/j.molliq.2020.114051>
- [5] K. Dahmani, D. E. Kherroub, A. Boucherdoud, B. Bestani, Removal of Ca (II) and Mg (II) hardness by ion exchange resins and soda ash for seawater pretreatment to reduce scale formation in evaporators multi-stage flash desalination, *Desalin. Water Treat.*, 221 (2021) 23-30. <https://doi.org/10.5004/dwt.2021.27020>.
- [6] X. Nie, S. Wu, P. Lv, H. Ke, F. Huang, Q. Wei, Chameleon-inspired iridescent structural color textiles with reversible multiple stimulus-responsive functions, *Chem. Eng. J.*, 433 (2022) 134410. <https://doi.org/10.1016/j.cej.2021.134410>.
- [7] N. Daneshvar, S. Aber, M. S. Dorraji, A. R. Khataee, M. H. Rasoulifard, Photocatalytic degradation of the insecticide diazinon in the presence of prepared nanocrystalline ZnO powders under irradiation of UV-C light, *Separ. Purif. Tech.*, 58 (2007) 91-98. <https://doi.org/10.1016/j.seppur.2007.07.016>.
- [8] D. F. Katowah, S. M. Saleh, S. A. Alqarni, R. Ali, G. I. Mohammed, M. A. Hussein, Network structure-based decorated CPA@CuO hybrid nanocomposite for methyl orange environmental remediation, *Sci. Rep.*, 11 (2021) 1-21. <https://doi.org/10.1038/s41598-021-84540-y>.
- [9] D. Vaya, P. K. Surolia, Semiconductor based photocatalytic degradation of pesticides: An overview, *Environ. Tech. Innovat.*, 20 (2020) 101128. <https://doi.org/10.1016/j.eti.2020.101128>.
- [10] A.R. Khataee, M.B. Kasiri, L. Alidokht, Application of response surface methodology in the optimization of photocatalytic removal of environmental pollutants using nanocatalysts, *Environ. Technol.*, 32(15) (2011) 1669-1684. <https://doi.org/10.1080/09593330.2011.597432>.
- [11] K. Jain, A. S. Patel, V. P. Pardhi, S. J. S. Flora, Nanotechnology in wastewater management: a new paradigm towards wastewater treatment, *Molecules*, 26 (2021) 1797. <https://doi.org/10.3390/molecules26061797>.
- [12] M. Amini, M. Kamkar, F. Rahmani, A. Ghaffarkhah, F. Ahmadijokani, M. Arjmand, Multilayer structures of a ZnO. 5NiO. 5Fe<sub>2</sub>O<sub>4</sub>-reduced graphene oxide/PVDF nanocomposite for tunable and highly efficient microwave absorbers, *ACS Appl. Elect. Mater.*, 3 (2021) 5514-5527. <https://doi.org/10.1021/acsaelm.1c00940>.
- [13] L. A. Goulart, G. O. Santos, K. I. Eguiluz, G. R. Salazar-Banda, M. R. Lanza, C. Saez, M. A. Rodrigo, Towards a higher photostability of ZnO photo-electrocatalysts in the degradation of organics by using MMO substrates, *Chemosphere*, 271 (2021) 129451. <https://doi.org/10.1016/j.chemosphere.2020.129451>.
- [14] S. Zhong, D. Xiong, B. Zhang, X. Yang, T. Yang, G. Tian, H. Zhang, W. Yang, W. Deng, Structurally unraveling the photocarrier behavior of Cu<sub>2</sub>O/ZnO heterojunction photodetectors, *ACS Photo.*, 9 (2022) 268-274. <https://doi.org/10.1021/acsp Photonics.1c01490>.
- [15] M. Zare, K. Namratha, S. Alghamdi, Y. H. E. Mohammad, A. Hezam, M. Zare, Q. A. Drmosh, K. Byrappa, B. N. Chandrashekar, S. Ramakrishna, X. Zhang, Novel green biomimetic approach for synthesis of ZnO-Ag

- nanocomposite; antimicrobial activity against food-borne pathogen, biocompatibility and solar photocatalysis, *Sci. Rep.*, 9 (2019)1-15. <https://doi.org/10.1038/s41598-019-44309-w>.
- [16] P. K. Aspoukeh, A. A. Barzinjy, S. M. Hamad, Synthesis, properties and uses of ZnO nanorods: a mini review, *Int. Nano Lett.*, (2021)1-16. <https://doi.org/10.1007/s40089-021-00349-7>.
- [17] M. A. Desai, A. N. Vyas, G. D. Saratale, S. D. Sartale, Zinc oxide superstructures: recent synthesis approaches and application for hydrogen production via photoelectrochemical water splitting, *Int. J. Hydrogen Energ.*, 44 (2019) 2091-2127. <https://doi.org/10.1016/j.ijhydene.2018.08.042>.
- [18] M. Qamar, S. A. Zaidi, M. Rafatullah, M. Qutob, S. J. Kim, Q. A. Drmosh, Role of post-hydrothermal treatment on the microstructures and photocatalytic activity of TiO<sub>2</sub>-based nanotubes, *Catalysts*, 12 (2022) 702. <https://doi.org/10.3390/catal12070702>.
- [19] S. Mishra, P. Supraja, P. R. Sankar, R. R. Kumar, K. Prakash, D. Haranath, Controlled synthesis of luminescent ZnS nanosheets with high piezoelectric performance for designing mechanical energy harvesting device, *Mater. Chem. Phys.*, 277 (2022) 125264. <https://doi.org/10.1016/j.matchemphys.2021.125264>.
- [20] A. Czyżowska, A. Barbasz, A review: zinc oxide nanoparticles—friends or enemies?, *Int. J. Environ. Health Res.*, 32 (2022) 885-901. <https://doi.org/10.1080/09603123.2020.1805415>.
- [21] M. S. Nasrollahzadeh, M. Hadavifar, S. S. Ghasemi, M. Arab Chamjangali, Synthesis of ZnO nanostructure using activated carbon for photocatalytic degradation of methyl orange from aqueous solutions, *Appl. Water Sci.*, 8 (2018) 1-12. <https://doi.org/10.1007/s13201-018-0750-6>.
- [22] B. Yulianto, L. Nulhakim, M. F. Ramadhani, M. Iqbal, A. Nuruddin, Improved performances of ethanol sensor fabricated on Al-doped ZnO nanosheet thin films, *IEEE Sens. J.*, 15 (2015) 4114-4120. <https://doi.org/10.1109/JSEN.2015.2410995>.
- [23] B. Ghanbarzadeh, S. A. Oleyaei, H. Almasi, Nanostructured materials utilized in biopolymer-based plastics for food packaging applications, *Crit. Rev. Food Sci. Nutr.*, 55 (2015) 1699-1723. <https://doi.org/10.1080/10408398.2012.731023>.
- [24] Z. Abid, A. Abbas, A. Mahmood, N. F. Rana, S. J. Khan, L. Duclaux, K. M. Deen, N. M. Ahmad, Water treatment using high performance antifouling ultrafiltration polyether sulfone membranes incorporated with activated carbon, *Polymers*, 14 (2022) 2264. <https://doi.org/10.3390/polym14112264>.
- [25] C. F. Holder, R. E. Schaak, Tutorial on powder X-ray diffraction for characterizing nanoscale materials, *ACS Nano*, 13 (2019) 7359-7365. <https://doi.org/10.1021/acsnano.9b05157>.
- [26] A. A. KHAMIS, A comparison of recent analytical methods for analysis of arsenic, *The Libyan Conference on Chemistry and Its Applications (LCCA)*, 1 (2021) 17-24. <http://repository.uob.edu.ly/handle/123456789/1617>.
- [27] F. Nekouei, H. Noorizadeh, S. Nekouei, M. Asif, I. Tyagi, S. Agarwal, V. K. Gupta, Removal of malachite green from aqueous solutions by cuprous iodide–cupric oxide nano-composite loaded on activated carbon as a new sorbent for solid phase extraction: isotherm, kinetics and thermodynamic studies, *J. Mol. Liq.*, 213 (2016) 360-368. <https://doi.org/10.1016/j.molliq.2015.07.058>.
- [28] T. Li, X. Ren, L. Bao, M. Wang, W. Bao, L. Chang, Effect of lignite as support precursor on deep desulfurization performance of semicoke supported zinc oxide sorbent in hot coal gas, *RSC Adv.*, 10 (2020) 12780-12787. <https://doi.org/10.1039/C9RA10884J>.
- [29] M. R. Al-Mamun, S. Kader, M. S. Islam, M. Z. H. Khan, Photocatalytic activity improvement and application of UV-TiO<sub>2</sub> photocatalysis

- in textile wastewater treatment: A review, *J. Environ. Chem. Eng.*, 7 (2019) 103248. <https://doi.org/10.1016/j.jece.2019.103248>.
- [30] P. Muthirulan, M. Meenakshisundaram, N. Kannan, Beneficial role of ZnO photocatalyst supported with porous activated carbon for the mineralization of alizarin cyanin green dye in aqueous solution, *J. Adv. Res.*, 4 (2013) 479-484. <https://doi.org/10.1016/j.jare.2012.08.005>.
- [31] F. Nekouei, H. Noorizadeh, S. Nekouei, M. Asif, I. Tyagi, S. Agarwal, V. K. Gupta, Removal of malachite green from aqueous solutions by cuprous iodide–cupric oxide nano-composite loaded on activated carbon as a new sorbent for solid phase extraction: isotherm, kinetics and thermodynamic studies, *J. Mol. Liq.*, 213 (2016) 360-368. <https://doi.org/10.1016/j.molliq.2015.07.058>.
- [32] Z. Noorimotlagh, R. Darvishi Cheshmeh Soltani, G. Shams Khorramabadi, H. Godini, M. Almasian, Performance of wastewater sludge modified with zinc oxide nanoparticles in the removal of methylene blue from aqueous solutions, *Des. Water Treat.*, 57 (2016) 1684-1692. <https://doi.org/10.1080/19443994.2014.977954>.
- [33] K. Bisaria, S. Sinha, R. Singh, H. M. Iqbal, Recent advances in structural modifications of photo-catalysts for organic pollutants degradation—a comprehensive review, *Chemosphere*, 284 (2021) 131263. <https://doi.org/10.1016/j.chemosphere.2021.131263>.
- [34] S. M. Saleh, ZnO nanospheres based simple hydrothermal route for photocatalytic degradation of azo dye, *Spectrochim. Acta Mol. Biomol. Spectros.*, 211 (2019) 141-147. <https://doi.org/10.1016/j.saa.2018.11.065>.
- [35] M. A. Hassaan, A. Pantaleo, L. Tedone, M. R. Elkatory, R. M. Ali, A. E. Nembr, G. D. Mastro, Enhancement of biogas production via green ZnO nanoparticles: Experimental results of selected herbaceous crops, *Chem. Eng. Comm.*, 208 (2021) 242-255. <https://doi.org/10.1080/00986445.2019.1705797>.
- [36] J. Saini, V. K. Garg, R. K. Gupta, N. Kataria, Removal of Orange G and Rhodamine B dyes from aqueous system using hydrothermally synthesized zinc oxide loaded activated carbon (ZnO-AC), *J. Environ. Chem. Eng.*, 5 (2017) 884-892. <https://doi.org/10.1016/j.jece.2017.01.012>.
- [37] V. I. Parvulescu, F. Epron, H. Garcia, P. Granger, Recent progress and prospects in catalytic water treatment, *Chem. Rev.*, 122 (2021) 2981-3121. <https://doi.org/10.1021/acs.chemrev.1c00527>.
- [38] S. G. Kumar, K. K. Rao, Zinc oxide based photocatalysis: tailoring surface-bulk structure and related interfacial charge carrier dynamics for better environmental applications, *RSC Adv.*, 5 (2015) 3306-3351. <https://doi.org/10.1039/C4RA13299H>.
- [39] N. Sobana, B. Krishnakumar, M. Swaminathan, Synergism and effect of operational parameters on solar photocatalytic degradation of an azo dye (Direct Yellow 4) using activated carbon-loaded zinc oxide, *Mater. Sci. Semicond. Process.*, 16 (2013) 1046-1051. <https://doi.org/10.1016/j.mssp.2013.01.002>.
- [40] M. Ghaedi, G. Negintaji, F. Marahel, Solid phase extraction and removal of brilliant green dye on zinc oxide nanoparticles loaded on activated carbon: new kinetic model and thermodynamic evaluation, *J. Ind. Eng. Chem.*, 20 (2014) 1444-1452. <https://doi.org/10.1016/j.jiec.2013.07.030>.



# Review Article: Development of biodegradable films using nanocellulose for food packaging application

Asha Valsalan<sup>a,\*</sup>, and Paramasivan Sivaranjana<sup>a</sup>

<sup>a</sup>Department of Chemistry, School of Advanced Sciences, Kalasalingam Academy of Research and Education Krishnankoil, Srivilliputhur, Tamil Nadu 626126

## ARTICLE INFO:

Received 16 Aug 2022

Revised form 20 Oct 2022

Accepted 11 Nov 2022

Available online 30 Dec 2022

## Keywords:

Nano cellulose,  
Biodegradable Films,  
Food Packaging,  
Extraction methods,  
Test methods,  
Tensile and physical characteristics

## ABSTRACT

Due to the development of nanotechnology and changing customer demands for food safety and hygiene, the food packaging industry is growing significantly. In today's worldwide market, active packaging offers a number of advantages over traditional wrapping because of its capacity to absorb or release substances to improve the shelf life of food. Traditional food packaging materials are difficult to recycle and are made from nonrenewable fossil fuels. The development of biodegradable films using Nano cellulose can be a good replacement for synthetic plastic packaging materials and can be a good solution for this problem. Other than that it has multiple advantages regarding tensile and physical properties, also as reducing health hazards. Tensile and physical characteristics are improved and water vapor permeability is decreased with the addition of cellulose nanoparticles to the biodegradable films/biodegradable composite films. The production of biodegradable materials employing Nano cellulose has been covered in this review study in four different ways, including extracts from agricultural waste, rice husk, various plant extracts, and biopolymer composite material in food packaging. The reason for using Nano cellulose-based biodegradable films in food packaging is also reviewed in this article. The key points for future research in overcoming the problems related to Nano cellulose and biodegradable films are also predicted in the paper.

## 1. Introduction

The rapid population expansion, high standards of living, and high rates of energy and goods consumption all contribute to significant levels of waste generation that, if not properly disposed or recycled, represent serious risks to the environment [1]. Plastic waste is a non-biodegradable component that can linger in the environment for hundreds of years. Both people and animals should avoid them because of how much land they consume.

Additionally, as plastics are petroleum-based materials, the ongoing engineering of plastics, which results in the depletion of petroleum, offers additional issues [2]. Over the past few decades, petroleum-based materials have been widely used in a variety of industries, especially for food wrapping because of their affordability, exciting technological features, as well as mechanical and physical capabilities. The bulk of plastics made from fossil fuels is bad for both public health and the environment [3]. In order to replace petroleum-based goods in food packaging applications, more renewable alternatives are being sought after. A large amount of the numerous tones of

\*Corresponding Author: [Asha Valsalan](mailto:Asha Valsalan)

Email: [id-bs.ashav@sbccemail.in](mailto:id-bs.ashav@sbccemail.in)

<https://doi.org/10.24200/amecj.v5.i04.207>

inedible plant debris produced each year gets landfilled. Reusing lignocellulose biomass wastes has received attention recently as a healthy and practical substitute for the usage of fossil fuels. Due to the enormous amount of agricultural waste produced annually, this reuse serves two purposes: Reducing landfill overflow and Reducing reliance on fossil fuels, with all the attendant environmental advantages [4]. They might also be referred to as bio-waste. Sludge from wastewater treatment plants, food manufacturing plant waste, and trade trash are all examples of biodegradable wastes [5]. Nowadays, biodegradable wastes are used in an effective manner for the manufacturing of various products, especially in the food packaging industries. The food packing sector is currently looking for lightweight, biodegradable packaging in an effort to utilize fewer resources, produce less waste, save transportation costs, maintain the freshness of food materials, and also to reduce health hazards [6]. Plastic food packaging materials are replaced by producing biodegradable films incorporated with Nano cellulose extracted from various types of biodegradable wastes like agri-waste, plant extracts, biodegradable polymers, etc. Biodegradable films are produced by adding some additives with them during the manufacturing process. Biodegradable films are an alternative to petroleum-based and plastic-based films.

## 2. Experimental

### 2.1. Nano Cellulose

Using various extraction methods, native cellulose is converted into the distinctive and natural molecule known as Nano cellulose. The amazing properties of Nano cellulose, such as its distinct surface chemistry, exceptional physiochemical toughness, and abundance of hydrophilic groups for alteration, are increasingly attracting attention. In addition to being environmentally friendly, it has significant biological qualities such as recyclability, bioactivity, and non-toxicity [7]. The term “Nano cellulose” refers to a class of cellulosic nanoparticles with at least one dimension up to 100 nm. Cellulose nanofibers (CNF), cellulose nanocrystals (CNC), and bacterial Nano cellulose (BNC) are the three varieties of “Nano cellulose” that may be identified by their diameters [8]. The picture of Nano cellulose is depicted in Figure 1.

### 2.2. Basic Extraction method of Nano cellulose

Many techniques have been developed to extract Nano cellulose from cellulose fiber. The diverse extraction methods led to a variety in the kinds and quality of the Nano cellulose that was produced. The three fundamental extraction techniques are acid degradation, enzymatic hydrolysis, and mechanical procedure. Acid hydrolysis is one of the main techniques for eliminating Nano cellulose



**Fig. 1.** The picture of Nano cellulose [8]

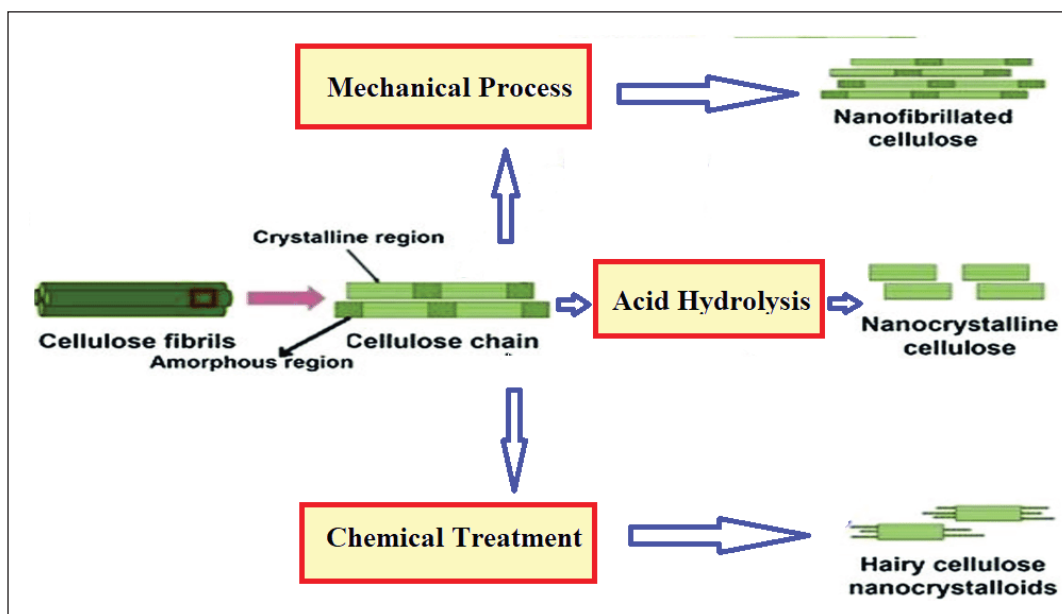


Fig. 2. The illustration of Nano cellulose extraction from lignocellulose biomass [9]

from cellulosic products. Because cellulose chains include equally arranged and unstructured regions, the organized regions survive acid degradation while the disorganized regions break down quickly. The acid most frequently used for acid hydrolysis is sulfuric acid. Enzymes are used in the biological process known as enzymatic hydrolysis to degrade or modify fibrous material. The biological treatment with enzymes may typically be carried out under modest conditions, although a lengthy procedure is needed. To solve this problem, enzymatic hydrolysis is always used in conjunction with other methods. A mechanical process isolates cellulose fibrils, resulting in Micro reinforcing materials cellulose, by using a powerful shear force to split the cellulose fibres along their longitudinal axis. The three mechanical processes that are most frequently used are ball milling, high-pressure homogeneity, and ultrasonication [9]. The separation of Micro cellulose from biomass including lignocellulose is depicted in Figure 2.

### 2.3. Types of Nano cellulose

Below is an explanation of the three different types of Nano cellulose: cellulose nanofibers (CNF), cellulose nanocrystals (CNC), and bacterial Nano cellulose (BNC).

#### 2.3.1. Cellulose Nanofibers (CNF)

Length, elastic, and intertwined nanoscale fibers known as “cellulose nanofibers” (CNF) can be recovered from lignocellulose-containing crops. Due to their superior hardness, rigidity, lightweight, environmental friendliness, and recyclability, CNFs are being researched for usage in a variety of applications, including electronics, packaging, and nanocomposites [10]. CNF have crystalline and amorphous regions, and they resemble ropes. When dried, CNF form a highly connected network as a result of strong intermolecular hydrogen bonding [11]. The SEM picture of CNF is displayed in the following Figure 3.

#### 2.3.2. Cellulose Nanocrystals (CNC)

The particles known as cellulose nanocrystals (CNC) are small, stiff, and rod-shaped. It is also known as Cellulose Nano whiskers. They are typically created through the process of strong acid hydrolysis, which separates the stiff crystalline sections from the amorphous phases of cellulose strands [11]. Researchers in both research and industrial applications have shown a great deal of interest in cellulose nanocrystals (CNCs) because of their intriguing structural features and distinctive physicochemical properties, like amazing structural

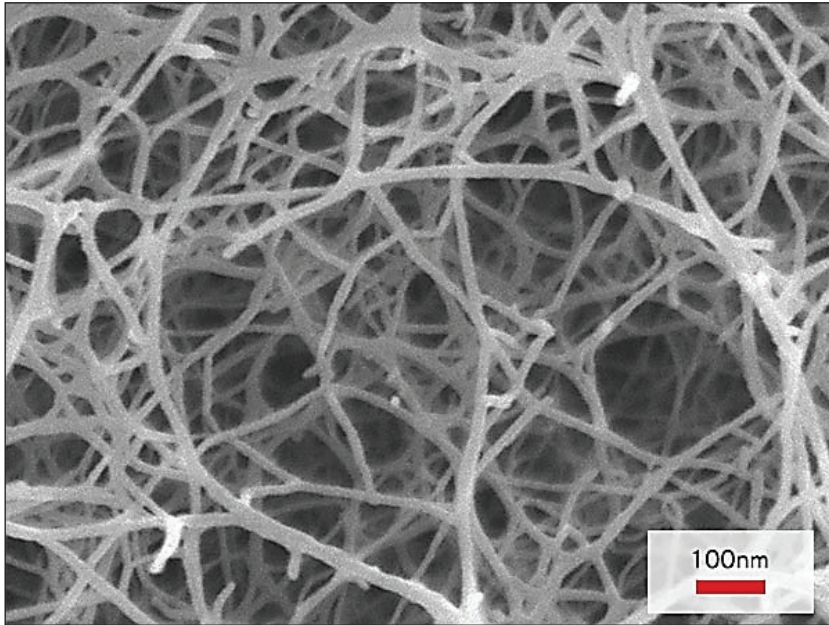


**Fig. 3.** SEM of Cellulose Nanofibers (CNF) [11]

rigidity, large surface region, numerous hydroxyl groups for chemical treatment, lightweight, and biodegradability. CNCs are a strong candidate for use in a variety of industries. In addition, cellulose nanocrystal extraction and surface modification continue to advance in response to producers' growing demand for cellulose nanocrystal-based goods [12]. Figure 4, presents the image of CNC.

### 2.3.3. Bacterial Nano cellulose (BNC)

Bacterial Nano cellulose (BNC), a naturally occurring biopolymer of enormous significance in many technical domains, has exceptional physicochemical and biological features. Specific species of bacteria generate bacterial Nano cellulose (BNC), a promising natural biopolymer, as an exopolysaccharide of D glucopyranose. BNC

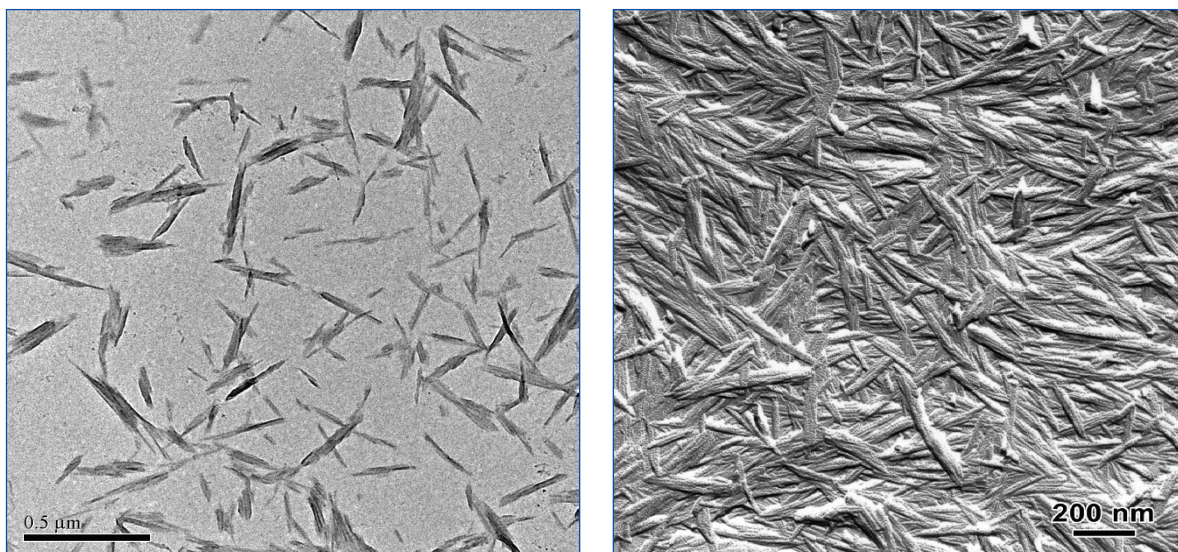


**Fig. 4.** Cellulose Nanocrystals (CNC) [12]

is 99 percent water but has excellent mechanical properties. Due to its ability to store water and its Nanostructured form, which is similar to the extracellular matrix protein collagen, BNC is particularly suitable for cellular immobilization and adhesion. Bacterial Nano cellulose is suited for a variety of uses since it has a number of unique characteristics and is a product that is generally regarded as safe (GRAS) [13]. The picture of BNC [14] is displayed in the Figure 5.

#### **2.4. Reason for using Nano cellulose based biodegradable films in food packaging**

The main objective of food packaging is to preserve the production of agricultural products through storage and delivery. As a result, it's critical to grow the shelf life of food goods by avoiding issues such as microbial deterioration and chemical pollutants, carbon dioxide, water vapor permeation, flammable substances, dampness, and light exposure as well as outside

physical influences. The materials used for packaging must ensure physical safety and establish suitable physicochemical conditions to ensure food quality [15]. Hence Nano cellulose incorporated biodegradable films thus produced plays a vital role as a food packaging material by overcoming all these defects due to their beneficial amount of physical, chemical, water solubility, and water absorption properties. These properties are discussed briefly in the upcoming sections. In this paper, a review based on development of biodegradable films using Nano cellulose from various extracts and useful analyzing in food packaging applications was presented. This review paper's structure is followed as: the experimental section evaluates the existing research on biodegradable films using Nano cellulose in four different directions, the results section gives the summary of this paper, another section comes out with the key points to be researched in the future and conclusion.

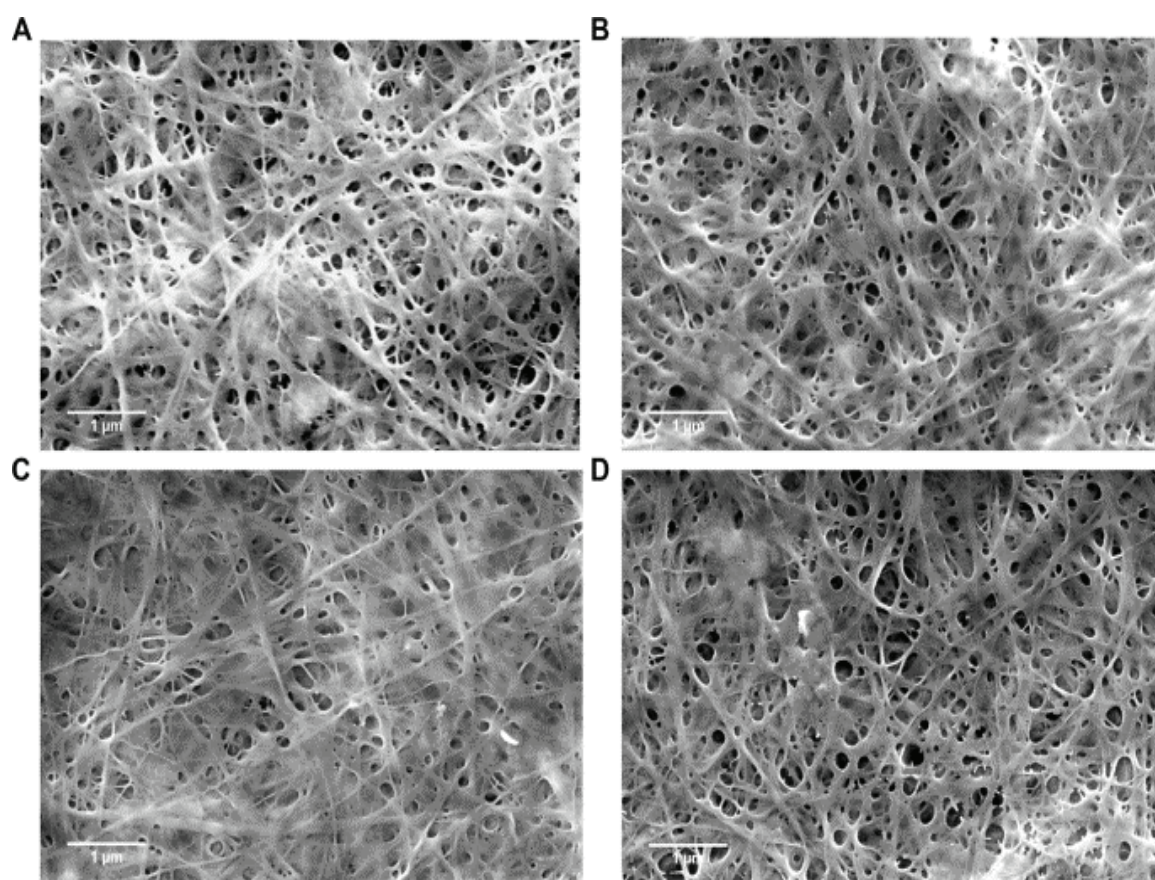


**Fig. 5.** Bacterial Nano cellulose (BNC: A-D) [14]

### 3. Results of literature review

This section reviews the development of biodegradable films using Nano cellulose from – agricultural waste, rice Husk, various plant extracts, and biopolymer composite material in food packaging. Agricultural Waste: Agro-wastes come from a variety of materials, including rice husks, wheat straw, palm oil fibers, pineapple, orange, and tomato pomace, grape pomace, lemon peels, and sugarcane bagasse [16]. Agro-industrial waste is a byproduct of agricultural-based businesses that is frequently rich in lignocellulose resources and bioactive compounds. The industries where these pollutants are frequently disposed of in uncontrolled procedures have weak regulations for their management. These actions have had a negative impact on the ecology and the economy as a whole. Due to this, extensive research has been done to extract useful materials from these wastes [17]. Rice husk is a lignocellulose biomass, that comes under non-woody biomass sources. Non-woody plants are ones that have frail stems and are susceptible to yearly regrowth to the ground. They go by the name herbaceous plants as well [18]. Some of the Plant extracts used for Nano cellulose production, that we have discussed in the upcoming section are as follows: sugarcane bagasse, olive tree pruning scraps, yam beam, sunflower oil cake (SOC), Natural essential oil from the clove bud, buffered with fermented black tea and cellulose nanocrystals fiber. Biopolymer composites are reinforced polymer materials in which the polymer functions as a matrix resin that reaches the bundles of reinforcement and forms bonds with it [19]. The upcoming sections deeply describe the related works of the above-mentioned directions.

#### 3.1. Biodegradable films using Nano cellulose from agricultural waste

Ilya et al examined the effects of different sugar palm nano fibrillated cellulose (SPNFCs) reinforced sugar palm starch (SPS) concentrations on the morphological, structural, and physical characteristics of the bio nanocomposite film [20]. Starch granules and filaments from sugarcane plants

are regarded as agricultural waste. A suspended sentence of sugar palm Nano fibrillated cellulose (SPNFCs) with a mean duration of many  $\mu\text{m}$  in diameter and diameters of 5.5 and 0.99 nm was made from sugar palm fibres using a high-pressure homogenization technique. SPNFCs were then used to strengthen the sugarcane bagasse carbohydrate sequence for the creation of bio nanocomposites using a remedy technique. The miscibility of SPS and SPNFCs was shown to be good using FESEM analysis of the casting solution. The FTIR analysis proved that intramolecular hydrogen bonds existed between the SPS and SPNFCs and that they were compatible. SPS/SPNFC bio nanocomposite films outperform control carbohydrate bio nanocomposite films in terms of physical and mechanical properties. The segmental molecular chains of the carbohydrate bio composite became less mobile and flexible as a result of the addition of Nano-reinforcements, which decreased the elongation at break. The ductility strength and modulus of the nanocomposite films were dramatically increased from 6.80 to 10.68 MPa and 59.07 to 121.26 MPa, respectively, by the increase in SPNFC reinforcement from 0 to 1.0 wt. percent. Adriana Nicoletta Frone et al used plum shells' agricultural residues to Nano cellulose as a biopolymer reinforcement [21]. Cellulose nanocrystals (CN) and cellulose nanofibers (CF) are the two types of Nano cellulose derived from plum seed shells. For the first time, CN and CF of cherry fruit skins were used as reinforcing agents in a polylactic acid/poly(3-hydroxybutyrate) (PLA/PHB) matrix using a solution-casting technique. A cost-effective and successful strategy to utilize agricultural waste as a source of production for elevated goods is to adopt this technique. Some of the CF type's limitations in terms of morphological characterization and thermal performance include that type CN cellulose nanocrystals are more similar in shape, have a smooth texture, and have a larger image size. The melting temperature of CN was somewhat less than that of CF due to the sulfate groups added to the cellulose's external side during the hydrolysis process, which led to the dewatering

of the cellulose fiber and a decrease in thermal properties. Thermal and XRD tests showed that adding CN improved the PLA/PHB bio-composite film's thermostability and crystalline nature.

According to report of Reshmy et al, jackfruit (*Artocarpus heterophyllus*) skin was used as the hydrolysis source for pure Nano cellulose [22]. Using liquid water evaporation, the thin films were created using BS as the filling, activator, and NC as the substrate. Solvent casting Nano cellulose and various plasticizers were used to make various thin films. FT-IR and XRD were used to describe thin films, and FESEM was used to explore surface changes. The advantages of this strategy are as follows: (i) To avoid chlorine bleaching solutions for natural fibers, the raw material was bleached with a 4 percent soapnut solution. (i) A unique filling named *Boswellia serrata* (BS) was used to enhance the properties of NC thin films for future applications. The breakage of bonds between NC and plasticizers caused commodities to decay during food storage due to the large price of WHC for NC alone and NC/Gly/BS. This resulted in less moisture absorption and swelling compared to other thin films.

Sheng Xu et al stated that *Artemisia selengensis* stalks were used as a source of hemicelluloses (ASH) and cellulose nanocrystals to create biodegradable films (ASCNC) [23]. Acid hydrolysis was used to separate the ASCNC from the ASC. SEM, TEM and FTIR methods are used for the test results, and OT and WVP are also checked. The composite membranes enhanced by ASCNC exhibited increased durability and performed much better as a water vapor shield when contrasted to the reference ASH/PVA film. Additionally, compared with the control screen, the ASCNC-enhanced ASH/PVA composite material decreased light transmission considerably. In the morphology of composite films, the ASH/PVA film's cross-section had many voids, and the structure was loose. With ASCNC loading reaching 9%, the composite film's tensile strength improved by 80.1 percent to 36.21 MPa, while the water vapor transfer rate fell by 15.45 percent when 12 percent ASCNC was added.

Banana pseudo-stems were proposed as a potential source of environmentally friendly Nano cellulose-based recyclable plastic as an agricultural waste by R. H. Fitri Faradilla et al [24]. This study looked closely at the impact of nanoclay (NC) and graphene oxide (GO) as nanofillers and glycerol as a lubricant on the mechanical, morphological, chemical, thermal, and impact resistance of banana pseudo-stem Nano cellulose films. TEM, SEM, FEI NOVA 230, AFM, Bruker, X-ray diffraction (XRD), analytical Xpert multipurpose X-ray diffraction, thermogravimetric analysis, and differential scanning calorimetry, ATR-FTIR, Bruker IFS 66/S, and Mocon-OX-TRAN are the testing methods used to find the results. Synergistic effects were seen when nanoparticles and glycerin were combined. Tensile modulus and flexibility were both risen, and the contact area of the motion pictures was considerably higher than that of films containing only nanoparticles. The thermoplastic had a massive effect on the barrier properties of the composites, while the glycerol concentration was positively correlated with the water vapour permeability. Oxygen permeability, however, was reduced when glycerol content increased. Also, the films' tensile strength was found to be improved by NC and GO, but not their elasticity. These results strongly imply that the characteristics of the banana pseudo-stem Nano cellulose film may be altered by modifying the nature and amount of additional chemicals.

It was suggested to separate bulgur bran into cellulose and hemicellulose-rich components, opening the way for exploiting this under-utilized agro-industrial biomass by Didem Sutay Kocabas et al [25]. Commercial cellulose nanocrystal (CNC) and cellulose nanofiber (CNF) were added to the hemicellulose substrate to remove bottlenecks. The characteristics of plain and Nano cellulose-reinforced films were compared using the thermogravimetric analysis (TGA), differential scanning calorimetry (DSC), and Fourier transform infrared spectroscopy (FTIR) techniques. A dense architecture was discovered by SEM analysis of films reinforced with CNC and CNF. The

hemicellulose channel's tensile properties were significantly improved by adding CNC and CNF as fills. After adding Nano cellulose, the films' water vapour permeability (WVP), light transmittance, overall mismatching, and biocompatible all fell. Additionally, the hemicellulose precipitate contains lignin (6.70 percent), starch, potassium acetate, and other impurities. The proposed full-quadratic model was shown to have excellent accuracy within the 95 percent confidence interval ( $R^2 = 0.9877$ ). According to the findings, films with 10% (w/w) CNC and 10% (w/w) CNF incorporation had a 21.3 percent lower FWS when compared to neat pictures.

Krishnavani Pavalaydon et al extracted Micro cellulose from cassava peel and coco fiber using chemical processes such as mercerization, bleaching, and acid hydrolysis [26]. Taguchi design is the technique used in the process of Fourier-Transform(FT). The test techniques employed in the procedure include DLS, transmission electron microscopy, and infrared spectroscopic. Bio-nanocomposite films were created using the solvent casting method using polyvinyl alcohol (PVA) as the matrix. Excellent sources of Micro cellulosic include sugarcane bagasse and coir, which can be used to create bio-composites having good strength properties. Nanocellulose, which is made from bagasse, first appeared as crooked and minute circular particles. The highest tensile strength (38.2 MPa) was achieved for CNCs derived from coir at a CNC/PVA loading of 0.5 wt%, which is a 96.9 percent improvement in strength properties over the unstrengthened PVA substrate.

According to Vu Nang An et al, the goal of the study is to separate high-crystallinity Cellulose Nano Crystals (CNCs) from Vietnamese agricultural residues (Nypa Fruticans trunk, coconut husk fiber, and rice husk) [27]. Using a three-step process that involved pre-treatment with formic/peroxyformic acids, processing with hydrogen peroxide/sodium hydroxide, and disintegration by hydrolysis, so, CNCs were extracted from the aforementioned natural origin. After every phase of behavior, the thermophysical characteristics of the obtained

resources were examined using XRD, TGA, TEM, and FT-IR studies. Nano cellulose fibres were found to have improved thermal stability through thermogravimetric analysis, making them suitable for the creation of bio nanocomposites for a variety of uses, including the production of functional paper, flexible assistance for the synthesis of metal/oxide metallic nanoparticles, and cell wall filters. The amorphous portions of the cellulose structure have been utterly destroyed by the corrosive ions, remaining the crystalline structure unharmed. Because of this, CNCs are both shorter and have a higher CrI than cellulose. The CNCs nanofibers have a high crystalline index (almost 80%), increased heat stability, and indicating an extensive variety of applications. Hui Li et al aimed to isolate cellulose nanocrystals (CNC) from pea hull and test their capacity to strengthen carboxymethyl cellulose (CMC) film [28]. To better utilize and get rid of cheap and plentiful farmed pea husk trash, the needle-like CNC was finally recovered from the trash by alkalization, washing, and sulfuric acid degradation. The solvent casting process produced CNC, which was then used as a reinforcing component in the creation of compound products which was depended on CMC. The tests included scanning electron microscopy, ATR-FTIR and X-ray diffraction analysis, hand-held digital microscopy, gravimetric technique, and DSC. The CMC/CNC nanocomposites saw improvements in their thermal properties, ultraviolet layer, mechanical properties, and water vapor barrier. The lower the endothermic peak, the larger the additional concentration of CNC. This was due to a lower hygroscopic affinity caused by the addition of additional sulfate groups to the CMC/CNC nanocomposite. In comparison to pure CMC film, the 5-weight percent CNC reinforced composite film had a 53.4 percent lower water vapour absorption and a 50.8 percent better durability.

According to research of Jayachandra S. Yaradoddi et al, the objective is to transform carboxymethyl cellulose (CMC), which is generated from agricultural residues, into a workable, biodegradable plastic that often includes a packaging material [29].

Mixtures were created using CMC (trash generated), gelatin, agar, and varied levels of glycerol; 1.5 percent (sample A), 2 percent (sample B), and 2.5 percent (sample C) were added. CMC was recovered from agricultural residues, primarily cane sugar waste. Thermogravimetric analysis (TGA), Fourier Transform Infrared (FTIR) spectroscopy, and Differential Scanning Calorimetry (DSC) were used to describe the physiochemical parameters of each created biodegradable plastic (samples A, B, and C). Sample C, which was made with gelatin, CMC, agar, and 2.0 percent glycerol, was discovered to be the best combination and ideal for possible future use in food applications because it had identified the strengths like the smallest water vapour

permeability and the greatest recyclability rate when compared to other samples. As commercially available CMS is currently too expensive, farm waste-derived carboxymethyl cellulose (CMC) is used largely to reduce the cost of film development. As a consequence, sample C's (gelatin+CMC+agar) film functioned better than samples A and B related to the addition of glycerol at a softener concentration of 2.0 percent.

Table 1 shows the overall review of the techniques such as Nano cellulose produced, the material, testing method, advantages, limitations, and performance parameters. Table 1 explained the direction - Biodegradable films using Nano cellulose from agricultural waste.

**Table 1.** Review on Biodegradable films using Nano cellulose from agricultural waste

Technique	Nano cellulose Produced	Material	Testing Method	Advantages	Limitation	PP	Ref.
HPhM & SCM	SPNFCs	AW-SPF	FESEM and FTIR	MP > CSBNF	Reduced the elongation at break Affecting mobility and ductility of the biopolymer's segmental	TS=6.8 - 10.7 MPa Modulus= 59.1 - 121.3 MPa	[20]
Solution-casting method	CF and CN	Agri waste-PSS	Thermal and XRD analyses	Cost-effective and well-organized	Compared to the CF type, type CN's morphology is much more regular, its surface is finer, and its aspect ratio is higher.	The thermal stability was improved by the calculation of CN and crystallinity of the PLA/PHB biocomposite film	[21]
Acid hydrolysis, BS filler and NC	Solvent casting Nano cellulose	(i) Agri waste - Jackfruit peel (ii) Bleaching Agent - Soapnut solution	FT-IR, XRD and FESEM	(i) Chlorine bleaching solutions (i) <i>Boswellia serrata</i> (BS) improve the characteristics of NC thin films	Because of the tall value of WHC for NC alone and NC/Gly/BS, commodities spoiled during food storage due to breakdown of bonds between NC and plasticizers	When compared to other thin films, this resulted in less moisture absorption and swelling	[22]
Acid hydrolysis	Hemicelluloses (ASH) and cellulose nanocrystals (ASCNC)	Agri waste - <i>Artemisia selengensis</i> straw	SEM, TEM and FTIR methods, OT and WVP is also checked.	water vapour shield effectiveness, and light transmission reduction.	ASH/PVA film's cross section had a lot of voids and the structure was loose	With ASCNC loading reaching 9%, the composite film's tensile strength improved 80.1 percent to 36.21 MPa	[23]
Modified Nano cellulose film	Banana pseudo-stem Nano cellulose films	Agri waste - banana pseudo-stem	TEM, SEM, FEI NOVA 230, AFM, Bruker, XRD, ATR-FTIR,	(i) Enhanced tensile power and flexibility, (ii) The great materials' contact angle (iii) The film resistance affected by the plasticiser.	(i) Oxygen permeability, reduced when glycerol content increased (ii) Film's tensile strength was found to be improved by NC and GO, but not their elasticity	By varying the type and concentration of added additives, the properties of the banana pseudo-stem Nano cellulose film might be modified.	[24]

Bulgur bran hemi-cellulose	Cellulose nanocrystal (CNC) and Cellulose nanofiber (CNF)	Agri waste - Bulgur bran	TGA, DSC, FTIR	(i) Revealed a compact structure (ii) Increased the tensile strength	(i) Water vapor permeability (WVP), light transmittance, overall colour difference, and biodegradability all are decreased (ii) Contains lignin (6.70%), starch, potassium acetate	(i) Have great accuracy ( $R^2 = 0.9877$ ) (ii) 10% (w/w) CNC- and 10% (w/w) CNF incorporated films had a 21.3 percent decrease in FWS	[25]
Bleaching, Acid hydrolysis and Solvent casting process	Bio-nanocomposite films with polyvinyl alcohol (PVA)	Agri waste - Sugarcane bagasse and coir	FTIR, SEM, DLS	(i) Good bases of Nano cellulose (ii) employed to create bio-composites with good strength properties.	Bagasse-derived Nano cellulose emerged as irregular and tiny circular particles	The ultimate compressive strength (38.2 MPa) for CNCs of coir,	[26]
(i) Pre-treatment with HCOOH (ii) treatment with H <sub>2</sub> O <sub>2</sub> /NaOH (iii) disintegration	Cellulose Nano Crystals (CNC)	Vietnamese agricultural waste (Nypa Fruticans trunk, coconut husk fiber, and rice husk)	XRD, TGA, TEM, and FT-IR analyses	(i) Nano cellulose fibers have improved thermal stability (ii) The cellulose material's unstructured regions have been attacked and destroyed by the acidity ions	CNCs have a greater CrI than cellulose and have a shorter length than cellulose	CNCs nanofibers have a high crystalline index (almost 80%) and increased heat stability	[27]
(i) Alkali treatment, Bleaching, For CNC (ii) Solution casting For CMC	Cellulose nanocrystals (CNC)	Agri waste - Pea hull waste	SEM, ATR-FTIR analysis, Gravimetric Method, DSC	CMC/CNC hybrid sheets' UV barrier, mechanical properties, and heat resistance were enhanced.	The presence of more sulphate groups in the CMC/CNC composite film resulted in a decreased hygroscopic affinity	(i) 50.8 percent improvement in tensile strength (ii) 53.4 percent decrease in water vapor permeability	[28]
Bleaching	Carboxymethyl cellulose (CMC)	Agri waste - Sugar cane bagasse	TGA, FTIR, DSC	Sample C: (i) best formulation (ii) food packaging (iii) lowest water vapor permeability	Expensive	The film generated from sample C outperformed the other samples A and B	[29]

**PP:** Performance Parameters

**TS:** Tensile strength

**HPHM & SCM:** High-pressure homogenization method and Solution-casting method

**SPNFCs:** Starch reinforced with sugar palm Nano fibrillated cellulose

**AW-SPF:** Agriculture waste- Sugar palm fibers

**MP:** Mechanical properties

**CSBNF:** Control starch bio nanocomposite films

**CF:** Cellulose nanofibers **CN:** Cellulose nanocrystals

**PSS:** Plum seed shells

### 3.2. Biodegradable films using Nano cellulose from rice Husk

Rice Husks were cleaned, chemically hydrolyzed, and ultrasonically processed at a low temperature by Pedro Nascimento et al to produce Nano cellulose [30]. An agricultural sector byproduct called rice husk can be utilized to make Nano cellulose. SEM, TEM, XRD, FTIR, TGA, and DSC are the tests undergone to find the characterization of Nano cellulose-reinforced starch-glycerol films. When added as reinforcement to the starch films, the Nano cellulose created webs of connected, tiny fibers (about 100 nm in diameter) that reduced opacity, increased mechanical characteristics, and were less permeable to water vapor. The inclusion of 2.5 percent (w/w) of the nanostructures to

starch-glycerol films increased the mechanical characteristics, water vapor permeability, and opacity of starch films (made by extrusion). After the alkaline pre-treatment, the fibre surface has been less tiny as well as its actual construction has been altered. This outcome showed that the exterior non-cellulosic layer, which is made up of hemicelluloses and lignin, had been partially removed. The produced Nano cellulose displayed lower lignin levels than 0.35 percent, greater thermal strength than the raw substantial, and higher crystallinity (up 70%). Sumira Rashid et al used rice grains with short, medium, and long husks to extract Nano cellulose [31]. During the steps of delignification and acid hydrolysis, the noncellulose amorphous and noncrystalline cellulose fractions

were successfully removed because of increased crystallinity and altered infrared diffraction. Nanocelluloses are more heat resistant than cellulose. The results are obtained using the tests methods: SEM, TEM, AFM, NT-MDT, SOLVER NANO, ZP, ATR-FTIR, XRD, TGA, DSC, and HA. Delignification in conjunction with bleaching led to gradual depigmentation and turned the material's hue to white. The size, crystallinity, strength, and thermal stability of long husks built at the nanoscale were better than those of medium and short husks. Cellulose nanomaterials are totally consistent with fortifying biopolymers, according to J. F. Delgado et al [32]. The effects of rice husk cellulose nanofibers (RHCNF) and bacterial nanocellulose (BNC) on water vapour transport and mechanical behavior were examined in yeast biomass films made from dispersions (processed by greater homogenized and subsequently thermal treatment) at pH 6 and 11. BNC was created using a culture of the NRRL B-42 strain of *Gluconacetobacter xylinus*. The tests used to analyze the results are NMR, XRD, AFM, SEM, and WVP. Nano fibers could be successfully added to yeast matrices and both increased tensile strengths, while BNC was more effective than RHCNF at improving the mechanical properties of yeast films. Despite having identical diameters and costing more to produce than RHCNF, only BNC improved Young's modulus, elastic modulus, modulus of rupture, and mechanical hardness of the yeast matrix simultaneously. Although they had little effect at pH 6, both supplements had a 5-weight percent reduction in water vapor permeability in films made at pH 11. The impact of Nano cellulose on the film properties of edible coatings was studied by Jeya Jeevahan Jayaraj et al [33]. To produce Nano cellulose from rice husk, a three-stage biochemical process involving alkaline solution, whitening, and acid hydrolysis was applied. Using native potato starch, glycerin, and varying amounts of Nano cellulose, the edible coatings (potato starch films) were produced using the solution casting method (0 percent, 5 percent, 10 percent & 15 percent). AStM E96, Digital colorimetric method, and AStM D882 are the test analysis methods conducted to determine

the WVTR, Film color, and Powered strength of the comestible films. It was discovered that the addition of Small amounts of cellulosic had created films with a lower Water Vapor Transmission Rate (WVTR), more mechanical strength, and greater transparency compared to the control films. Mechanical strength did not increase as the Nano cellulose content was raised above 10%. With the rise in Nano cellulose percentage from 5 % to 15 %, the WVTR of bio nanocomposite edible films reduced. Starch granules only have between 40 and 60 percent visibility compared to Nano cellulose's greater than 95 percent visibility. According to A. Ganesh Babu et al, bio-films were produced utilizing the solution casting process employing liquid polyvinyl alcohol (PVA) and variable amounts (5-25wt percent) of rice husk flour as reinforcing filler [34]. FTIR, XRD, TGA, DSC, Tensile test, Surface morphology investigations, WVP, and Antibacterial tests were used to examine the impact of RHP on the PVA matrix. Some of the advantages are (i) Bio-films could tolerate temperatures of up to 350 °C (ii) The stronger interaction of polymer chains is present with lower WVP levels (iii) Exhibit strong antibacterial activity (iv) Bio-films were clearly homogenous, free of fractures and phase separation (v) Enhance the biofilm's thermo-mechanical properties. The presence of hydrogen bonding makes films less flexible. Tensile modulus and tensile properties steadily rise as RHP is infused into the matrix, reaching their maximum values at a concentration of 25 percent RHP in PVA and 23.32 MPa and 684 MPa, respectively. Himanshu Gupta et al focused on using leftover lignocellulose biomass (such as sugarcane bagasse and rice hulls) to make carboxymethyl cellulose (CMC), which is then transformed into a biodegradable film [35]. The methods of Mercerization and Etherification are used to create CMC from SCB Cellulose and Rice Hulls. The characterization is done by the FTIR, XRD, MC, and TS test methods. The biopolymer film made from sugarcane bagasse CMC had the highest strength and elongation when compared to films manufactured from conventional CMC and CMC made from rice

**Table 2.** Review on biodegradable films using Nano cellulose from rice husk

Technique	Nano cellulose Produced	Material	Analysis	Advantages	Limitation	PP	Ref.
(i)NC - Bleaching, Acid hydrolysis, and Ultrasonic (ii)SGF -Extrusion	(i)NC from rice hulls (ii)SGF	Rice hull	SEM, TEM, XRD, FTIR, TGA, DSC	(i)Reduced opacity (ii)Increased mechanical characteristics (iii)Less permeable to water vapor	Less dense fibre layer with lessral shape and the exterior non-cellulosic layer removed	(i)Displayed lower lignin levels than 0.35% (ii)Higher thermal stability than the raw material (iii) Higher crystallinity (up 70%)	[30]
Delignification and Acid hydrolysis	Nano cellulose	Rice grains with short, medium, and long husks	SEM, TEM, AFM, NT-MDT, SOLVER NANO, ZP, ATR-FTIR, XRD, TGA, DSC, HA	(i)Noncellulosic and noncrystalline cellulose removed (ii)Increased crystallinity (iii)Nanocelluloses are more heat resistant than cellulose and husks	Delignification led to gradual depigmentation and turned the material's hue to white	The size, crystallinity, strength, and thermal stability of long husks were better than medium and short husks	[31]
(i)Yeast biomass films - Dispersions at pH 6 and 11 (ii)RHCNF and BNC	Rice husk cellulose nanofibers (RHCNF) and Bacterial Nano cellulose (BNC)	(i)For RHCNF (ii)For BNC (iii)For Yeast Biomass Films	NMR, XRD, AFM, SEM, WVP	(i) BNC was more successful than RHCNF in enhancing the mechanical properties of yeast films (ii)BNC and RHCNF, both boosted tensile strengths	(i)Only BNC enhanced the yeast matrix's Young's modulus, tensile strength, (ii) BNC is more expensive than producing RHCNF	Water vapor permeability was reduced by 5 weight percent in both reinforcements in films created at pH 11.	[32]
(i)Nano cellulose - Alkaline treatment, Bleaching, and Acid hydrolysis (ii)Potato starch films - Solution casting method	Nano cellulose	(i)For NC – Rice Husk (ii)For Potato Starch Film - glycerol with varied NC (0 - 15 % )	AStM E96, Digital colorimetry method, AStM D882	(i)Lower Water Vapour Transmission Rate (WVTR) (ii)Greater mechanical strength (iii)Greater transparency	Mechanical strength did not increase as the Nano cellulose content was raised above 10%	(i)Rise in Nano cellulose percentage from 5 % to 15 % - WVTR of bio nanocomposite edible films reduced. (ii)The transparency of Nano cellulose is greater than 95%	[33]
Solution casting method	Polyvinyl alcohol (PVA)	Rice Hull powder as filler	FTIR, XRD, TGA, DSC, Tensile test, Surface morphology studies, WVP and Antibacterial testing	(i)Tolerate up to 350 °C (ii)High interaction of polymer chains (iii)Exhibit strong antibacterial activity (iv)Bio-films were clearly homogenous, electrical and thermal qualities.	Lower flexibility of films is caused by the existence of hydrogen bonds	Tensile strength and tensile modulus - 23.32 MPa and 684 MPa, at a concentration of 25 percent RHP in PVA.	[34]
Mercurization and Etherification	CMC from SCB Cellulose and Rice Hulls	Rice husk and Sugarcane bagasse	FTIR, XRD, MC, TS	(i)Had the highest tensile strength and elongation (ii)Improved machine-driven possessions (TS and Elongation)	(i) negatively affect the strength of the material (ii) the DS and TS of the rice hull CMC were lower than those of the SCB	With an increase in DS of CMC and as the degree of CMC substitution grew the film's opacity, moisture content, and solubility also increases	[35]

NC: Nano cellulose

SGF: Starch glycerol films

hull. The bio-composite material formed from mixed carbohydrate manufactured CMC solution has exhibited superior mechanical properties in comparison to the film made from blended Starch-Commercial CMC solution (TS and Elongation). Because rice husk contains a lot of sodium chloride and sodium glycolate, (i) it has an adverse effect on the material's strength properties and (ii) it has lower DS and TS than the SCB. The degree of

CMC substitution and the DS of CMC both grow as do the film's transparency, water levels, and solubility. Table 2, describes an overall review of the techniques such as Nano cellulose produced, the material, testing method, advantages, limitations, and performance parameters which was explained under the biodegradable films using Nano cellulose from the rice husk..

### 3.3. Biodegradable films using Nano cellulose

### *from Various Plant Extracts*

Using a more effective, economical enzymatic hydrolysis pathway, R. Reshmy et al proposed a straightforward method for the extraction of Nano cellulose from sugarcane bagasse [36]. It was possible to extract NC fibres from sugarcane bagasse. NC was produced by alkaline treatment, bleaching, and acid hydrolysis. The solvent casting method was used to create thin films. FT-IR, XRD, FESEM, DLS, and AStM D 2216 methods were used to characterize the films. Non-edible sustainable material usefulness, cost efficiency, simple ease of processing, minimal energy usage, non-hazardousness, and simple degradation rate are advantages of this upgraded technology. These thin films might degrade well in situations with soil, salt, acid, and alkaline conditions. Glycerol, a plasticizer, is present in NC, which lessens its tendency to inflate. The acid resistance is increasing due to the use of glycerol as a plasticizer and the reduction in weight loss from 50% to about 40% is a result of the plasticizers included in NC. Nano cellulose was suggested to be added to polyvinyl alcohol by Mónica Sánchez-Gutiérrez et al in order to enhance the technical prowess of the composite coating used for food packaging (PVA) [37]. PVA films reinforced with (L)CNFs derived from olive tree trimming leftovers were manufactured using the solvent casting method. Micro cellulosic was created from pulp that had been both dyed and unbleached using a mechanical and TEMPO preparation. The test methods are as follows: Perkin Elmer UV-Vis Lambda 25 spectrophotometer, FTIR, TGA, SEM, XRD, and AStM E96/E96M-10. From six percent for the pure PVA film to 50 percent and 24 percent, respectively. For unbleached and bleached Nano cellulose, the UV barrier was increased in terms of optical properties. Associated with pure PVA film, the antioxidant capacity of mechanical Nano cellulose films made without bleaching significantly increased (5.3%). The mechanical Nano cellulose films with a 5% unbleached component demonstrated noticeably greater

tensile strength as compared to pure PVA film. The 5 percent Nano cellulose films were also improved in terms of their thermal properties and impermeability. They offered an oxygen shield akin to aluminum layers and plastic films while reducing water vapour leakage by 38–59%. Because they are more sensitive to environmental conditions like humidity and temperature. (L) CNF-reinforced films obtained by mechanical pretreatment (MU and MB) needed a lengthier stabilization period than (L)CNF-reinforced films obtained through TEMPO pretreatment (TU and TB). This behavior is displayed by other materials, such as EVOH, which are greatly affected by the surrounding humidity. According to Mochamad Asrofi et al, a Yam Bean (YB) starch substrate and Micro Cellulosic Water Hyacinth Fiber (WHF) reinforcing were employed to develop bio nanocomposites utilizing the casting process [38]. The secret to creating good bio nanocomposites was adding Micro viscose as a solution to the YB starch matrix, allowing it to gel, and then briefly sonicating it. The effect of Nano cellulose suspension loading on the YB starch matrix was examined using mechanical testing, Scanning Electron Microscopy (SEM), X-Ray Diffraction (XRD), Thermogravimetric Analysis (TGA), Fourier Transform Infrared (FTIR), and wettability. After the addition of Nano cellulose, tensile strength (TS) and tensile modulus (TM) greatly increased. With higher Micro lignocellulosic content, heat resistance and water resistance were also improved. Bio-nanocomposites have a rougher fracture surface than pure YB starch sheets. The greatest amounts of Nano cellulose (1 wt. percent) were used to achieve the maximum values for TS (5.8 MPa) and TM (403 MPa). With just a little more than 1 weight percent of extra Nano cellulose, the bio-nanocomposite's crystallinity index (CrI) increased by more than 200 percent. Zineb Kassab et al proposed that Sunflower oil cake (SOC) was found to be a bio-sourced resource for the manufacture of cellulose nanocrystals (CNC) after chemical processing and sulfuric acid

hydrolysis [39]. This study also looked into the newly created CNC's polymer nanoreinforcing capabilities. PVA-based nanocomposite films with CNC30 concentrations of 1, 3, 5, and 8 weight percent were produced using the solvent casting technique. The rheological properties of CNC solutions at different percentages were evaluated using systemic resistance stiffness studies and cyclic dynamic experiments. When the mechanical and transparency properties of CNC-filled PVA nanocomposite films were examined at various CNC contents (1, 3, 5, and 8 wt%), clear nanocomposite products with high hardness properties were produced. The resultant CNC displayed remarkable saturated solution stabilization and gel-like properties at very low CNC concentrations. Nanocomposite materials with significantly better tensile characteristics were produced by incorporating CNC into a PVA polymeric matrix. The addition of CNC causes slight changes in the FTIR spectra of PVA nanocomposites that are filled with CNC. It is possible to see a tiny variation in the OH stretching vibration's intensity. When 8-weight percent CNC was added to PVA-based nanocomposite films, the tensile strength and elastic modulus improved by 107 and 78%, respectively. Swarup Roy and Jong-Whan Rhim showed that an extremely stable nanoscale Pickering emulsion(PE) was made using natural clove bud essential oil stabilized with nanocellulose fibre [40]. The PE was used to produce gelatin and agar functional films. The gelatin/agar-based bidirectional compound film was made using the solution casting technique, and the cellulose nanofiber-based PE was made by preparing a cellulose nanofiber solution. ASTM D 882–88, TGA, FESEM, FTIR, and Chroma meter are tests taken to predict the characterization. The inclusion of PE only slightly changed the mechanical properties and vapor impermeability of the gelatin/agar-based film, with no discernible impact on temperature. Without affecting the film's transparency, the inclusion of PE also gave it exceptional UV-barrier qualities. Additionally,

the composite film had strong antioxidant properties. The power of the gelatin/agar film was significantly impacted by the addition of PEC. The film has high transmittance to UV and visible light, with corresponding T280 and T660 values of 26.9%, 88.0%, and 1.4 %. The neat gelatin/agar film's minimally changed WVP was  $0.59 \times 10^{-9} \text{ gm.m}^{-2}\text{Pa}^{-1}\text{s}^{-1}$ . The utilization of static intermittent fed-batch (SIFB) equipment and a cheap medium, such as fermentation black tea, according to Chhavi Sharma et al, this study proposes a technique with industrial significance for the creation of inexpensive and environmentally friendly bacterial Nano cellulose (BNC) films [41]. Chitosan, a natural polymer, successfully altered the BNC film (BNC-chitosan film). SCOBY, black tea, and tomatoes were the materials used. The films were characterized using FE-SEM (Field Emission Scanning Electron Microscopy), ATR-FTIR (Attenuated Total Reflectance and Fourier Transform Infrared Spectrometry), X-ray diffraction (XRD), and thermogravimetric analysis (TGA). Because of their high tensile properties, crystallinity, air resistance, and tomato shelf life evaluation, BNC-chitosan coatings have a considerable potential to be used for economical encapsulation, which is unquestionably wanted by the packaging sector. The surface morphology of BNC changed after chitosan treatment. BNC yield was higher in this modified bioprocess ( $29.2 \text{ g L}^{-1}$ ) than in the standard static approach ( $13.3 \text{ g L}^{-1}$ ) with a BNC yield of  $29.2 \text{ g L}^{-1}$ . Segal method calculations showed that the CrI of BNC formed via the SIFB technique was 79.2 percent(%), which is nearly identical to the CrI of BNC previously shaped under the traditional fixed technique (79.4 %). The upcoming Table 3, describes an overall review of the techniques such as, Nano cellulose produced, the material, testing method, advantages, limitations, and performance parameters which was explained under the biodegradable films using Nano cellulose from various plant extracts.

### **3.4. Biodegradable films using Nano cellulose**

**Table 3.** Review on biodegradable films using Nano cellulose from various plant extracts

Technique Used	Nano cellulose Produced	Material	Analysis	Advantages	Limitation	Performance Parameters	Ref.
(i)NC - Alkaline treatment, Bleaching, and Acid hydrolysis (ii)Thin films - Solvent casting method	NC Fibres	Sugarcane bagasse	FT-IR, XRD, FESEM, DLS, AStM D 2216	Non-edible renewable feedstock utility, cost-effectiveness, easy processibility, less energy consumption, non-hazardous and easy degradability	Glycerol, a plasticizer, is present in NC, which lessens its tendency to inflate	(i)Acid resistance is increasing (ii) The reduction in weight loss from 50% to about 40% is a result of the plasticizers included in NC	[36]
(i)Nano cellulose - Mechanical and TEMPO preparation (ii) PVA films with (L)CNF reinforcement - Solvent casting	PVA films reinforced with (L) CNFs	Olive tree pruning scraps	Perkin Elmer UV/VIS FTIR, TGA, SEM, XRD, AStM E96/E96M-10.	(i)UV barrier was raised (ii)Antioxidant capacity of mechanical Nano cellulose films is increased (iii)Had higher tensile strength (iv)Thermal stability (v) Reduced water vapor permeability by 38–59% (vi) oxygen barrier	(L)CNF-reinforced films required a longer stabilisation period than (L) CNF-reinforced films obtained by TEMPO pretreatment	(i)UV barrier increased – 50% & 24% (ii)Antioxidant capacity increased – 5.3% (iii)Reduced water vapor permeability - 38–59%	[37]
(i)NC- Gelation and a brief Sonication (ii)Bionanocomposite Film - Casting method	(i)Nano cellulose - (WHF) (ii)Film - Yam Bean (YB)	Yam Beam	TT, SEM, XRD, TGA, FTIR, MA	(i)Tensile strength (TS) and Tensile modulus (TM) greatly increased (ii)Thermal stability and moisture resistance were also raised	Bio-nanocomposites have a rougher fracture surface than pure YB starch sheet	(i)TS- 5.8 MPa and TM -403 MPa (ii)CrI-increased by more than 200 percent	[38]
(i)Nano cellulose - Chemical processing and Sulfuric acid hydrolysis (ii)Film - Solvent casting method	(i)Cellulose nanocrystals (CNC) (ii)PVA-based nanocomposite films	Sunflower oil cake (SOC)	observations of constant rheological properties and cyclic dynamic tests	(i)Has transparent nanocomposite materials with potent mechanical properties (ii)Exhibited exceptional aqueous colloidal stability and gel-like behavior (iii)Has better tensile characteristics	(i)Addition of CNC causes slight changes in the FTIR of PVA nanocomposites with CNC. (ii)A tiny variation in the OH stretching vibration's intensity	Elastic mechanical and physical properties improved by 107 and 78%, respectively.	[39]
(i)Nano cellulose (ii) Film - Solution casting method	(i)Nano cellulose - CNFPE (ii)Film - Gelatin/Agar-based BCF	CBN stabilized with Nano cellulose fiber	AStM D 882–88, TGA, FESEM, FTIR, Chroma meter	(i)Increased the mechanical strength and decreased the vapor barrier qualities of the gelatin/agar-based film (ii)Good UV-barrier qualities (iii)Had strong antioxidant properties	The strength of the gelatin/agar film was significantly impacted by the addition of PEC	(i)High transparency to UV and visible light - 26.9 1.3 %, 88.0 1.4 % T280 and T660 (ii)Gelatin/agar film's WVP - 0.59 10 9 g.m./ m2. Pa.s	[40]
Static intermittent fed-batch (SIFB) technology	(i)NC - (BNC) (ii)Film - BNC-chitosan film	SCOBY, black tea and tomatoes	FESEM, ATR-FTIR, XRD, TGA	(i)Good mechanical strength (ii)Crystalline nature (iii)Resistance to air (iv)Shelf life evaluation of tomatoes	The surface morphology of BNC changed after chitosan treatment	(i)BNC yield was higher - 29.2 gL-1 (ii)CrI of BNC formed via SIFB method - 79.2 %	[41]

**WHF:** Water Hyacinth Fiber

**CNFPE:** Cellulose nanofiber-based PE

**CBNO:** Clove bud natural essential oil

**BCF:** Binary composite film

**BNC:** Bacterial Nano cellulose

Gelatin and carbohydrate substrates were examined by S.M. Noorbakhsh-Soltani et al for the integration of Nano-cellulose [42]. Chitosan enhances the mechanical, anti-fungal, and waterproofing properties of materials. The response

surface approach is used in the design and analysis of experiments. Acid hydrolysis is used to create Nano cellulose, which is then wet-processed and added to base matrices. Films are produced by film casting techniques. The strength properties,

storage of food, clarity in visible and ultraviolet light, and water contact angle are also conducted on the Nano-composite films. On the ideal films, DSC/TGA, SEM, TEM, XRD, and air permeability tests are also carried out. The advantages are include, (i) High elasticity, strength properties, extension to break, clarity, and possibly foodstuff storage properties of both gelatin and starch bases can be improved (ii) Decrease in UV transmittance (iii) Gelatin films offer greater transparency, elastic modulus, and break length than starch films. According to the results of the stress-strain curves, which measure the mechanical strength of nanocomposite films, some of the samples exhibit thinning, others exhibit thickening, and some exhibit a straightforward linear response. According to the results, increasing the amount of Nano cellulose to 10% raises the mechanical properties at the break to  $8121 \text{ MN m}^{-2}$ , while decreasing the ductility. Furthermore, chitosan content can be increased from 5% to 30% to enhance food storage for up to 15 days. Using the wire extension method, Yasmim Montero et al suggested making PBAT active films that were packed with nanocellulose and infused with cinnamon essential oil [43]. The connections among NC-EO-PBAT were investigated, and the results demonstrated that the direct closeness between the EO and the PBAT matrix changed the conformations of the polymer molecules. FT-Raman, FTIR, TGA, and WVP are the tests undergone for the process. The modified CNF films displayed a controlled Fickian diffusion, a greater essential oil release, reduced water vapor permeability, and effective filler dispersion. The film at 3085  $\text{cm}^{-1}$  lost its form and intensity after 3 wt% CNF was inserted. Fruits loaded in films with 0.5 weight percent modified-CNF have little weight reduction, better quality maintenance, and no fungal attack after 15 storage periods. According to the report of Syafiq et al, liquid casting was used to generate biodegradable nanocomposite films using sugar palm starch (SPS), sugar palm nanocrystalline cellulose (SPNCC), and cinnamon essential oil (EO) [44]. By using an acid hydrolysis technique, sugar palm Nano crystalline celluloses

(SPNCC) was created. Solution-cast SPS/SPNCC nanocomposite coatings with added cinnamon essential oil were created. The SEM, ASTM D 644, ASTM 570, FTIR, disk diffusion method (DDM), and Agar disc method (ADM) are the test methods used to find out the results. Mechanical characteristics experiments on films containing cinnamon EO revealed improved tensile strength and tensile stiffness numbers from 4.8 to 5.3 MPa and 122.49 to 130.52 MPa, respectively. In addition, the density was lowered from 1.38 to  $1.31 \text{ g cm}^{-3}$  and the moisture content was reduced from 13.65 to 12.33 percent, respectively. The results unambiguously demonstrate that the introduction of cinnamon essential oil caused a decrease in the films' elongation at break, from 18.14 to 3.35 percent.

The effects of dextran-coated silver nanoparticle loading on the robotic, boundary, and antibacterial activities of skinny movies produced from cellulose nanofibrils by solvent evaporation technique were shown by Vesna Lazić et al [45]. They showed an environmentally friendly and food-preservative packing material. The film is created using hybrid materials based on CNF and Ag NPs covered with dextran. The test methods employed to ascertain the properties of the film include TEM, SEM, ASTM D3985, and a Shimadzu AGS-X electromechanical universal testing machine. The advantages of adding dextran are as follows: (i) Acts as dispersing media (ii) it is an additive that seals out moisture (iii) It has insufficient oxygen penetrability (iv) Keeps the food safe from bacterial growth. These films also exhibit better Young's moduli while maintaining their flexibility and tensile strength. Both artificial substrates like hydroxyapatite and magnetite, as well as Ag NPs attached to macroporous polymer substrates, demonstrate lesser antibacterial activity against *S. aureus* than *E. coli*. The 99.9% suppression of *Escherichia coli* after five repetitive cycles of 24 h exposed to 0.9 percent NaCl aqueous solution was demonstrated, supported by a sustained release of  $\text{Ag}^+$  ions (underneath the toxicants dangerous criterion). Lower oxygen transmitting percentages from 2.07 to  $1.40\text{-}0.78 \text{ cm}^3 \text{ m}^{-2} \text{ d}^{-1}$ , hydrophilicity

from 20.8<sup>o</sup> to 52.4<sup>o</sup> for MilliQ water, and from 35<sup>o</sup>-37<sup>o</sup> to 62<sup>o</sup>-74<sup>o</sup> for 3 % acetic acid and 0.9 % NaCl simulant solutions were obtained.

Nano-chitosan (NCH), Nano-cellulose (NCL), and cellulose derivatives were employed by Narges Jannatyha et al as biodegradable biopolymers [46]. Various amounts of nano chitosan or nanocellulose were added using casting procedures to the carboxyl methyl cellulose (CMC) film solution (0.1, 0.5, and 1 percent). XRD, DSC, and DC are the test methods conducted to predict the results. Some of the advantages are: (i) When the concentration of the nanocomposite rose, the WVP of the polymer and nanofiller decreased (ii) By increasing concentration, the TS and elongation at the break of a nanocomposite film were improved (iii) CMC/NCH provides more benefits than CMC/NCL biopolymer when used as a biocompatible film (iv) Particularly at concentrations of 1%, physical characteristics like water solubility(WS), moisture content(MC), and moisture absorption(MA) were lowered by both CMC/NCH and NCL and also causes the nanofiller in CMC film to aggregate. The antibacterial properties of CMC and CMC/NCL are absent. The physical and thermal properties in CMC/NCH were lower than CMC/NCL for the concentration  $p < 0.05$ . The melting points (T<sub>g</sub>) of CMC, CMC/NCL 1 %, and CMC/NCH 1 % films were, 206.31 °C, 221.97 °C, and 200.91 °C, respectively. Nanofiller utilized (1%) WS decreased to 18% and 33% for CMC/NCL and CMC/NCH films, respectively. Sapuan et al reported that the mechanical, barrier and thermal characteristics of nanocellulose-reinforced polymer composites were improved [47]. Enhancing the useful qualities of TPS, PLA, and PBS for food packaging through the addition of Nano cellulose is undoubtedly advantageous. Thermoplastic starch (TPS), polylactic acid (PLA), and polybutylene succinate (PBS) were selected as the alternatives because they are easily accessible, biodegradable, and have high food contact properties. FESEM and SEM are the tests conducted. Reinforcing Nano cellulose has many advantages such as, (i) Tensile strength and elastic

modulus are improved by PLA biocomposites (ii) Poor water barrier was improved by TPS/Nano cellulose (iii) The mechanical and oxygen barrier characteristics of PLA and PBS were enhanced. In comparison to pure PBSA, CNN decreased the tensile strength and elongation at break. Their usable characteristics did not necessarily increase with increased Nano cellulose loading. If the amount of Nano cellulose in the polymers was too high, agglomeration took place. The hydrophilic Nano cellulose and hydrophilic PLA are unsuitable and result in weak matrix interaction, hence only low Nano cellulose loadings between 0.5 and 2 weight percent are required for the optimum results. On the other hand, the addition of 2% PA increased the strength of PBS/CNN by about 120%. (95:5). Table 4 describes an overall review of the techniques such as, Nano cellulose produced, the material, testing method, advantages, limitations, and performance parameters which was explained under the direction - Biodegradable films using Nano cellulose from polymer composite material in the food packaging.

#### 4. Discussion

Petroleum-based products have already been employed in a variety of industries, but packaged foods have benefited most from their minimal price and strong mechanical and physical properties. But it is non-biodegradable and also produces numerous health hazards. Plastic or petroleum-based food containers need to be replaced in order to do so, various types of research have been going on for producing biodegradable films using Nano cellulose extracted from various biodegradable wastes such as agri-waste, various plant extracts, non-woody biomass, biopolymer composite materials, etc. Nano cellulose is produced by various extraction methods and the basic method is discussed in the paper. The three primary methods utilized to create Nano cellulose from diverse extracts are acid degradation, enzymatic hydrolysis, and electromechanical process. The common method used to make biodegradable composite films is a solvent-casting method. The types of Nano

**Table 4.** Review on biodegradable films using Nano cellulose from polymer composite material in Food Packaging Reduced

Technique	Nano cellulose Produced	Material	Analysis	Advantages	Limitation	Performance Parameters	Ref.
(i)Nano cellulose - Acid hydrolysis (ii)Film - film casting technique	Nano-composite films	Gelatin, Starch, Chitosan	air permeability, tensile strength, food preservation, transparency in visible and UV light	(i) High elasticity, elastic modulus, extension to break, clarity can be improved. (ii) Decrease in UV transmittance (iii)In comparison to starch films, gelatin films have better transparency	the stress-strain curves , thinning, thickening, linear line response	(i)Nano cellulose content to 10%, tensile strength at break - increase to 8121 MN/m <sup>2</sup> , lowers the elongation at break (ii)Increasing the chitosan content from 5% to 30% - improve food preservation for up to 15 days	[42]
Wire extension method	NC-EO-PBAT Films	PBAT, Cellulose nanofibers, Cinnamon oil	FT-Raman, FTIR, TGA, WVP	(i)Fickian diffusion, (ii)Greater essential oil release (iii)Reduced water vapor permeability (iv)Effective filler dispersion	After the addition of 3 wt. % CNF, the film at 3085 cm <sup>-1</sup> lost its form and intensity	The fruits sealed in films with 0.5 weight percent modified-CNF have very little losing weight, better fresh preservation, and no fungal attack after 15 storage periods.	[43]
(i)Nano cellulose - Acid hydrolysis process (ii)Film - Solution casting method	(i)Nano cellulose - (SPNCC) (ii)Film - SPS/SPNCC	Sugar palm starch (SPS)/ (SPNCC) and Cinnamon essential oil (EO)	SEM, ASTM D 644, ASTM 570, FTIR, DDM, ADM	(i) Enhanced tensile strength and tensile modulus values (ii)The moisture content and density were decreased	Addition of cinnamon EO reduced the films' elongation at break to drop from 18.14 - 3.35 % to 13.9 - 5.57 %	(i) Enhanced TS and TM - 4.8 to 5.3 MPa and 122.49 to 130.52 MPa (ii) MC and thickness decreased - 13.65 to 12.33 % and 1.38 to 1.31 g cm <sup>-3</sup>	[44]
Solvent casting method	Ag NPs with dextran coating and CNF-based composite sheets	Dextran, coated AgNPs and Cellulose nanofibrils	TEM, SEM, ASTM D3985, a Shimadzu AGS-X electro-mechanical machine	1. Dextran (i) Act as dispersing (ii)Moisture-resistant sealable additive (iii) Reduced oxygen permeability 2.Films also exhibit better Young's moduli while maintaining their flexibility and tensile strength.	Ag NPs as well as inorganic supports like hydroxyapatite and magnetite both exhibit lower antibacterial efficacy against S. aureus than E. coli	(i)Reduced OTR - from 2.07 to 1.40-0.78 cm <sup>3</sup> (ii)Hydrophilicity - from 20.8° to 52.4° for MilliQ water, from 35-37° to 62-74° for 3 % acetic acid, 0.9 % NaCl simulant solutions yielding a 99.9 % inhibition of E-Coli	[45]
Casting technique	CMC/NCH and CMC/NCL	Nano-chitosan (NCH), Nano-cellulose (NCL), Cellulose derivative and (CMC)	XRD, DSC, DC	(i)Concentration of the nanocomposite rose, the VWP decreased (ii) Enhanced TS and elongation at break (iii)CMC/NCH provides more benefits than CMC/NCL (iv)At 1%, physical characteristics lowered by both CMC/NCH and NCL	(i)The antibacterial of CMC and CMC/NCL are absent (ii)The physical and thermal properties in CMC/NCH were lower than CMC/NCL for the concentration p < 0.05.	(i)Tg of CMC, CMC/NCL 1 %, and CMC/NCH 1 % films - 206.31 °C, 221.97 °C, and 200.91 °C. (ii)Nanofiller utilized (1%) WS decreased - 18% and 33% for CMC/NCL and CMC/NCH films	[46]
Technique stated as in citation [47]	Nano cellulose reinforced polymer composites	TPS, PLA, and PBS	FESEM and SEM	(i) Tensile strength and elastic modulus are improved by PLA biocomposites (ii) Poor water barrier were improved by TPS/Nano cellulose	(i)In comparison to pure PBSA, CNN decreased the tensile strength and elongation at break	(i)For best outcomes - between 0.5 % and 2 weight % are necessary (ii)Addition of 2 % PA enhanced the tensile strength of PBS/CNN by around 120 % (95:5)	[47]

SPNCC: Sugar palm nanocrystalline celluloses

cellulose are CNF, CNC, and BNC. The XRD, SEM, TEM, DSC, FTIR, and FE-SEM are some of the test methods used to characterize biodegradable composite films. The tensile properties and physical characteristics of biodegradable films

and biodegradable composite films are enhanced overall by the use of nanocellulose. Water vapor permeability, Moisture content, etc., are reduced thus enabling the biodegradable films more suitable and efficient for food packaging.

## 5. Challenges and Future Research

There are more recent advancements have emerged in the development of biodegradable films using Nano cellulose from various biodegradable extracts but there are still some parameters to be enhanced. Some of the key points to be noted for future research are as follows: (i) Due to the large variety of bio-based substrates and essential oils offered, it is difficult to make general recommendations for the creation of proactive packaging products when using them. Greater attention should be paid to sensory evaluation, making additional, and the synergistic effects of numerous essential oils in order to enhance the active packaging on various food products [48] (ii) BNC offers intriguing uses in food packaging, but these uses aren't being fully investigated because to the material's high production costs and difficult commercialization in the packaging industry [49] (iii) Even with new approaches that have enabled controlled delivery of antibacterial agents in the appearance of NC feasible, utilizing bio-polymers as natural resources with appropriate membrane characteristics, strength properties, and satisfying the regulations for packaged foods is still a difficult problem to tackle [49]. (iv) More research is necessary to determine the effectiveness and durability of Nano cellulose-based packaging technologies during the real food warehouse and transportation process [50]. (v) Biopolymer-based nanocomposites begin to replace conventional synthetic plastic products in the near future only if:

- I. It would be energy and cost-effective to isolate cellulose and turn it into nanoparticles;
- II. Hydrophilic polymers and hydrophobic natural fibers (cellulose) would be able to coexist without conflict;
- III. It is advisable to lessen the variability of the extracted fiber's characteristics
- IV. It is advisable to produce compatibilizers, coupling agents, and adhesives from renewable sources;
- V. Nanocomposites' biodegradability and life cycle assessment should be thoroughly studied;
- VI. It is necessary to create new processing technologies [51].

## 6. Conclusion

In this review paper, we have analyzed Nano cellulose, its types, and the basic extraction methods. The reason for using Nano cellulose-based biodegradable films in food packaging is also discussed. Also, we have explored the recent research on the development of biodegradable films using Nano cellulose from agricultural waste, rice husk, various plant extracts, and biopolymer composite materials on food packaging. The techniques used, other Nano cellulose produced, various test methods adopted to define the characteristics of the films, advantages, limitations, and performance parameters are discussed briefly in the experimental section. The result section summarizes the paper, and other sections give the future research points that should be considered. From this review, we learned that developing biodegradable films using Nano cellulose has various valuable parameters in food packaging. A notable replacement for synthetic products has been highlighted for nanocomposites, particularly those that contain Nano cellulose as reinforcement.

## 7. Funding and Conflict of Interest

The authors declare that no funds, grants, or other support were received during the preparation of this manuscript. I hereby declare that the disclosed information is correct and that no other situation of real, potential or apparent conflict of interest is known to me.

## 8. Acknowledgment

We would like to thank Sree Buddha College of Engineering, Pattoor, Kerala, and Chemistry department of Kalasalingam Academy of Research and Education, Krishnakovil, India.

## 9. References

- [1] S. Nanda, F. Berruti, Municipal solid waste management and landfilling technologies: a review, *Environ. Chem. Lett.*, 19 (2021) 1433-1456. <https://doi.org/10.1007/s10311-020-01100-y>.

- [2] S.H. Gebre, M.G. Sendeku, M. Bahri, Recent trends in the pyrolysis of non-degradable waste plastics, *Chem. Open*, 10 (2021) 1202-1226. <https://doi.org/10.1002/open.202100184>.
- [3] C. Amara, A. El Mahdi, R. Medimagh, K. Khwaldia, Nanocellulose-based composites for packaging applications, *Curr. Opin. Green Sustain. Chem.*, 31 (2021) 100512. <https://doi.org/10.1016/j.cogsc.2021.100512>.
- [4] J.R. Pires, V.G.L.D. Souza, A.L. Fernando, Production of nanocellulose from lignocellulosic biomass wastes: prospects and limitations, In *International Conference on Innovation*, *J. Eng. Entrep.*, 505 (2018) 719-725. [https://doi.org/10.1007/978-3-319-91334-6\\_98](https://doi.org/10.1007/978-3-319-91334-6_98).
- [5] V. Katinas, M. Marčiukaitis, E. Perednis, E.F. Dzenajavičienė, Analysis of biodegradable waste use for energy generation in Lithuania, *Renew. Sustain. Energ. Rev.*, 101 (2019) 559-567. <https://doi.org/10.1016/j.rser.2018.11.022>.
- [6] L.K. Ncube, A.U. Ude, E.N. Ogunmuyiwa, R. Zulkifli, I.N. Beas, Environmental impact of food packaging materials: A review of contemporary development from conventional plastics to polylactic acid based materials, *Materials*, 13 (2020) 4994. <https://doi.org/10.3390/ma13214994>.
- [7] G.K. Gupta, P. Shukla, Lignocellulosic biomass for the synthesis of nanocellulose and its eco-friendly advanced applications, *Front. Chem.*, 8 (2020) 1203. <https://doi.org/10.3389/fchem.2020.601256>.
- [8] S. Mondal, Chapter 11, Nanocellulose reinforced polymer nanocomposites for sustainable packaging of foods, cosmetics, and pharmaceuticals, *Sustainable nanocellulose and nanohydrogels from natural sources*, Elsevier, *Micro Nano Technol.*, (2020) 237-253. <https://doi.org/10.1016/b978-0-12-816789-2.00011-0>.
- [9] P. Phanthong, P. Reubroycharoen, X. Hao, G. Xu, A. Abudula, G. Guan, Nanocellulose: extraction and application, *Carbon Resour. Convers.*, 1 (2018) 32-43. <https://doi.org/10.1016/j.crcon.2018.05.004>.
- [10] M. Hietala, K. Varrio, L. Berglund, J. Soini, K. Oksman, Potential of municipal solid waste paper as raw material for production of cellulose nanofibres, *Waste Manage.*, 80 (2018) 319-326. <https://doi.org/10.1016/j.wasman.2018.09.033>.
- [11] J. Pennells, I.D. Godwin, N. Amiralian, D.J. Martin, Trends in the production of cellulose nanofibers from non-wood sources, *Cellulose*, 27 (2020) 575-593. <https://doi.org/10.1007/s10570-019-02828-9>.
- [12] A.K. Rana, E. Frollini, V.K. Thakur, Cellulose nanocrystals: Pretreatments, preparation strategies, and surface functionalization, *Int. J. Biol. Macromol.*, 182 (2021) 1554-1581. <https://doi.org/10.1016/j.ijbiomac.2021.05.119>.
- [13] C. Sharma, N.K. Bhardwaj, Bacterial nanocellulose: Present status, biomedical applications and future perspectives, *Mater. Sci. Eng. C*, 104 (2019) 109963. <https://doi.org/10.1016/j.msec.2019.109963>.
- [14] D. Abol-Fotouh, M.A. Hassan, H. Shokry, A. Roig, M.S. Azab, A.E.H.B. Kashyout, Bacterial nanocellulose from agro-industrial wastes: Low-cost and enhanced production by *Komagataeibacter saccharivorans* MD1, *Sci. reports*, 10 (2020) 1-14. <https://doi.org/10.1038/s41598-020-60315-9>.
- [15] E. Souza, L. Gottschalk, O. Freitas-Silva, Overview of nanocellulose in food packaging, *Recent Pat. Food Nutr. Agric.*, 11 (2020) 154-167. <https://doi.org/10.2174/2212798410666190715153715>.
- [16] C. Maraveas, Production of sustainable and biodegradable polymers from agricultural waste, *Polymers*, 12 (2020) 1127. <https://doi.org/10.3390/polym12051127> [www.mdpi.com/journal/polymers](http://www.mdpi.com/journal/polymers).
- [17] A.N.S. Ahmad Khorairi, N.S. Sofian-Seng, R. Othaman, H. Abdul Rahman, N.S. Mohd

- Razali, S.J. Lim, W.A. Wan Mustapha, A review on agro-industrial waste as cellulose and nanocellulose source and their potentials in food applications, *Food Rev. Int.*, (2021) 1-26. <https://doi.org/10.1080/87559129.2021.1926478>.
- [18] S.J. Owonubi, S.C. Agwuncha, N.M. Malima, G.B. Shombe, E.M. Makhatha, N. Revaprasadu, Non-woody biomass as sources of nanocellulose particles: A review of extraction procedures, *Front. Energ. Res.*, 9 (2021) 608825. <https://doi.org/10.3389/fenrg.2021.608825>.
- [19] J.P. Greene, *Automotive plastics and composites: Materials and processing*, William Andrew, Elsevier, (2021) 191-222. <https://doi.org/10.1016/B978-0-12-818008-2.00007-6>.
- [20] R.A. Ilyas, S.M. Sapuan, R. Ibrahim, H. Abral, M.R. Ishak, E.S. Zainudin, R. Jumaidin, Effect of sugar palm nanofibrillated cellulose concentrations on morphological, mechanical and physical properties of biodegradable films based on agro-waste sugar palm (*Arenga pinnata* (Wurmb.) Merr) starch, *J. Mater. Res. Technol.*, 8 (2019) 4819-4830. <https://doi.org/10.1016/j.jmrt.2019.08.028>.
- [21] A.N. Frone, D.M. Panaitescu, I. Chiulan, A.R. Gabor, C.A. Nicolae, M. Oprea, A.C. Puitel, Thermal and mechanical behavior of biodegradable polyester films containing cellulose nanofibers, *J. Therm. Anal. Calorim.*, 138 (2019) 2387-2398. <https://doi.org/10.1007/s10973-019-08218-4>.
- [22] R. Reshmy, E. Philip, P.H. Vaisakh, S. Raj, S.A. Paul, A. Madhavan, A. Pandey, Development of an eco-friendly biodegradable plastic from jack fruit peel cellulose with different plasticizers and *Boswellia serrata* as filler, *Sci. Total Environ.*, 767 (2021) 144285. <https://doi.org/10.1016/j.scitotenv.2020.144285>.
- [23] S. Xu, M. Jiang, Q. Lu, S. Gao, J. Feng, X. Wang, P. Ouyang, Properties of polyvinyl alcohol films composited with hemicellulose and nanocellulose extracted from *artemisia selengensis* straw, *Front. Bioeng. Biotechnol.*, 8 (2020) 980. <https://doi.org/10.3389/fbioe.2020.00980>.
- [24] R.H. Faradilla, G. Lee, J. Roberts, P. Martens, M. Stenzel, J. Arcot, Effect of glycerol, nanoclay and graphene oxide on physicochemical properties of biodegradable nanocellulose plastic sourced from banana pseudo-stem, *Cellulose*, 25 (2018) 399-416. <https://doi.org/10.1007/s10570-017-1537-x>.
- [25] D.S. Kocabaş, M.E. Akçelik, E. Bahçegül, H.N. Özbek, Bulgur bran as a biopolymer source: Production and characterization of nanocellulose-reinforced hemicellulose-based biodegradable films with decreased water solubility, *Ind. Crop. Prod.*, 171 (2021) 113847. <https://doi.org/10.1016/j.indcrop.2021.113847>.
- [26] K. Pavalaydon, H. Ramasawmy, D. Surroop, Comparative evaluation of cellulose nanocrystals from bagasse and coir agro-wastes for reinforcing PVA-based composites, *Environ. Dev. Sustain.*, 24 (2022) 9963-9984. <https://doi.org/10.1007/s10668-021-01852-9>.
- [27] V. Nang An, C. Nhan, H. Thuc, T.D. Tap, T.T.T. Van, P. Van Viet, L. Van Hieu, Extraction of high crystalline nanocellulose from biorenewable sources of Vietnamese agricultural wastes, *J. Polym. Environ.*, 28 (2020) 1465-1474. <https://doi.org/10.1007/s10924-020-01695-x>.
- [28] H. Li, H. Shi, Y. He, X. Fei, L. Peng, Preparation and characterization of carboxymethyl cellulose-based composite films reinforced by cellulose nanocrystals derived from pea hull waste for food packaging applications, *Int. J. Biol. Macromol.*, 164 (2020) 4104-4112. <https://doi.org/10.1016/j.ijbiomac.2020.09.010>.
- [29] J.S. Yaradoddi, N.R. Banapurmath, S.V. Ganachari, M.E.M. Soudagar, N.M. Mubarak, S. Hallad, H. Fayaz, Biodegradable carboxymethyl cellulose based material for sustainable packaging application, *Sci.*

- reports, 10 (2020) 1-13. <https://doi.org/10.1038/s41598-020-78912-z>.
- [30] P. Nascimento, R. Marim, G. Carvalho, S. Mali, Nanocellulose produced from rice hulls and its effect on the properties of biodegradable starch films, *J. Mater. Res.*, 19 (2016) 167-174. <https://doi.org/10.1590/1980-5373-mr-2015-0423>.
- [31] S. Rashid, H. Dutta, Characterization of nanocellulose extracted from short, medium and long grain rice husks, *Ind. Crop. Prod.*, 154 (2020) 112627. <https://doi.org/10.1016/j.indcrop.2020.112627>
- [32] J.F. Delgado, O. de la Osa, A.G. Salvay, E. Cavallo, P. Cerrutti, M.L. Foresti, M.A. Peltzer, Reinforcement of yeast biomass films with bacterial cellulose and rice Husk cellulose nanofibres, *J. Polym. Environ.*, 29 (2021) 3242-3251. <https://doi.org/10.1007/s10924-021-02109-2>.
- [33] J.J. Jayaraj, K. Renugadevi, P. Prakash, M. Harish, R.D. Kumar, Effect of nanocellulose extracted from rice husk on the film properties of native starch based edible films, In AIP Conference Proceedings, 2311, AIP Publishing LLC, (2020) 080015. <https://doi.org/10.1063/5.0033961>.
- [34] A. Ganesh Babu, S.S. Saravanakumar, Mechanical and physicochemical properties of green bio-films from poly (Vinyl Alcohol)/ nano rice hull fillers, *Polym. Bull.*, 79 (2022) 5365-5387. <https://doi.org/10.1007/s00289-021-03757-z>.
- [35] H. Gupta, H. Kumar, M. Kumar, A.K. Gehlaut, A. Gaur, S. Sachan, J.W. Park, Synthesis of biodegradable films obtained from rice husk and sugarcane bagasse to be used as food packaging material, *Environ. Eng. Res.*, 25 (2020) 506-514. <https://doi.org/10.4491/eer.2019.191> eISSN 2005-968X.
- [36] R. Reshmy, E. Philip, S.A. Paul, A. Madhavan, R. Sindhu, P. Binod, A. Pandey, A green biorefinery platform for cost-effective nanocellulose production: investigation of hydrodynamic properties and biodegradability of thin films, *Biomass convers. Biorefin.*, 11 (2021) 861-870. <https://doi.org/10.1007/s13399-020-00961-1>.
- [37] M. Sánchez-Gutiérrez, I. Bascón-Villegas, E. Espinosa, E. Carrasco, F. Pérez-Rodríguez, A. Rodríguez, Cellulose nanofibers from olive tree pruning as food packaging additive of a biodegradable film, *Foods*, 10 (2021) 1584. <https://doi.org/10.3390/foods10071584>.
- [38] M. Asrofi, H. Abrial, A. Kasim, A. Pratoto, M. Mahardika, F. Hafizulhaq, Characterization of the sonicated yam bean starch bionanocomposites reinforced by nanocellulose water hyacinth fiber (WHF): the effect of various fiber loading, *J. Eng. Sci. Technol.*, 13 (2018) 2700-2715. <https://jestec.taylors.edu.my/>
- [39] Z. Kassab, M. El Achaby, Y. Tamraoui, H. Sehaqui, R. Bouhfid, Sunflower oil cake-derived cellulose nanocrystals: Extraction, physico-chemical characteristics and potential application, *Int. J. Biol. Macromol.*, 136 (2019) 241-252. <https://doi.org/10.1016/j.ijbiomac.2019.06.049>.
- [40] S. Roy, J.W. Rhim, Gelatin/agar-based functional film integrated with Pickering emulsion of clove essential oil stabilized with nanocellulose for active packaging applications, *Colloids and Surf. A: Physicochem. Eng. Asp.*, 627 (2021) 127220. <https://doi.org/10.1016/j.colsurfa.2021.127220>.
- [41] C. Sharma, N.K. Bhardwaj, P. Pathak, Static intermittent fed-batch production of bacterial nanocellulose from black tea and its modification using chitosan to develop antibacterial green packaging material, *J. Clean. Prod.*, 279 (2021) 123608. <https://doi.org/10.1016/j.jclepro.2020.123608>.
- [42] S.M. Noorbakhsh-Soltani, M.M. Zerfat, S. Sabbaghi, A comparative study of gelatin and starch-based nano-composite films modified by nano-cellulose and chitosan for food packaging applications, *Carbohydr.*

- Polym., 189 (2018) 48-55. <https://doi.org/10.1016/j.carbpol.2018.02.012>.
- [43] Y. Montero, A.G. Souza, E.R. Oliveira, D. dos Santos Rosa, Nanocellulose functionalized with cinnamon essential oil: A potential application in active biodegradable packaging for strawberry, *Sustain. Mater. Technol.*, 29 (2021) e00289. <https://doi.org/10.1016/j.susmat.2021.e00289>.
- [44] R. Syafiq, S.M. Sapuan, M.R.M. Zuhri, Antimicrobial activity, physical, mechanical and barrier properties of sugar palm based nanocellulose/starch biocomposite films incorporated with cinnamon essential oil, *J. Mater. Res. Technol.*, 11 (2021) 144-157. <https://doi.org/10.1016/j.jmrt.2020.12.091>.
- [45] V. Lazić, V. Vivod, Z. Peršin, M. Stoiljković, I.S. Ratnayake, P.S. Ahrenkiel, V. Kokol, Dextran-coated silver nanoparticles for improved barrier and controlled antimicrobial properties of nanocellulose films used in food packaging, *Food Packag. Shelf Life*, 26 (2020) 100575. <https://doi.org/10.1016/j.fpsl.2020.100575>.
- [46] N. Jannatyha, S. Shojaee-Aliabadi, M. Moslehishad, E. Moradi, Comparing mechanical, barrier and antimicrobial properties of nanocellulose/CMC and nanochitosan/CMC composite films, *Int. J. Biol. Macromol.*, 164 (2020) 2323-2328. <https://doi.org/10.1016/j.ijbiomac.2020.07.249>
- [47] A. Nazrin, S.M. Sapuan, M.Y.M. Zuhri, R.A. Ilyas, R.S.F.K.S. Syafiq, S.F.K. Sherwani, Nanocellulose reinforced thermoplastic starch (TPS), polylactic acid (PLA), and polybutylene succinate (PBS) for food packaging applications, *Front. Chem.*, 8 (2020) 213. <https://doi.org/10.3389/fchem.2020.00213>.
- [48] S. Casalini, M. Giacinti Baschetti, The use of essential oils in chitosan or cellulose-based materials for the production of active food packaging solutions: a review, *J. Sci. Food Agric.*, (2022)1-21. <https://doi.org/10.1002/jsfa.11918>.
- [49] S.S. Ahankari, A.R. Subhedar, S.S. Bhadauria, A. Dufresne, nanocellulose in food packaging: A review, *Carbohydr. Polym.*, 255 (2021) 117479. <https://doi.org/10.1016/j.carbpol.2020.117479>.
- [50] C.G. Perdani, S. Gunawan, A short review: Nanocellulose for smart biodegradable packaging in the food industry, In IOP Conference Series, IOP Publishing, *Earth Environ. Sci.*, 924 (2021) 012032. <https://doi.org/10.1088/1755-1315/924/1/012032>.
- [51] U. Qasim, A.I. Osman, A.A.H. Al-Muhtaseb, C. Farrell, M. Al-Abri, M. Ali, D.W. Rooney, Renewable cellulosic nanocomposites for food packaging to avoid fossil fuel plastic pollution: a review, *Environ. Chem. Lett.*, 19 (2021) 613-641. <https://doi.org/10.1007/s10311-020-01090-x>.



# Preparation of chitosan films plasticized by lauric and maleic acids

Sara Hikmet Mutasher <sup>a</sup> and Hadi Salman Al-Lami <sup>a,\*</sup>

<sup>a</sup> Department of Chemistry, College of Science, University of Basrah, Basrah, Iraq

## ARTICLE INFO:

Received 5 Aug 2022

Revised form 14 Oct 2022

Accepted 25 Nov 2022

Available online 29 Dec 2022

## Keywords:

Chitosan,  
Lauric acid,  
Maleic acid,  
Films plasticizers,  
Mechanical properties,  
Solubility

## ABSTRACT

The energy crisis and environmental concerns have increased interest in natural polymers, and the bio-sourced materials field is experiencing rapid growth. A useful alternative to conventional plastic packaging manufactured from fossil fuels is packaging constructed of biodegradable polymers. Consideration has been given to the instrumental methods for examining modifications to the chemical composition and characteristics of modified chitosan. The molecular weight and the kind of plasticizer present in these materials are the two primary variables influencing their usability and performance. This study set out to physically blend chitosan with two different acids, lauric and maleic, to enhance chitosan cast films' physical and mechanical properties. Different plasticizer ratios appeared to have little effect on the various properties of the chitosan cast films. Examining the obtained films by FTIR implies that chitosan's native structure was unchanged. The films prepared had more flexibility and better solubility than those made with un-plasticized chitosan. It was evident from an analysis of the mechanical properties of the films that both acid plasticizers enhanced the mechanical properties of the chitosan.

## 1. Introduction

The interest in natural polymers has grown as a result of the energy crisis and environmental concerns, and the field of bio-sourced materials is currently expanding quickly. In this situation, the industry must look for new sources of organic, environmentally friendly, and biodegradable polymers to replace those derived from petroleum. Polysaccharides in this area have enormous potential for use in active and intelligent packaging, smart textiles and biomedical devices, environmental remediation, and other applications. Chitosan is a special cationic polysaccharide with an excellent

affinity for various surfaces and outstanding cosmetic properties, even when left unaltered. It is a naturally occurring cationic copolymer [1]. This biopolymer, which is abundant in nature (the second one after cellulose), holds much promise for various uses. It is a highly renewable, biodegradable, environmentally friendly, and non-toxic polymer. Indeed, chitosan has been successfully used as a scaffold for biomedical applications, water engineering, treatment, the food industry, films, coatings, and construction fields. The functionalization of its chemical structure often enhances its characteristics until it obtains properties equivalent to synthetic products [1]. The development of chitosan-based materials has attracted much attention

\*Corresponding Author: [Hadi Salman Al-Lami](mailto:Hadi.Salman.Al-Lami@uobasrah.edu.iq)

Email: [hadi.abbas@uobasrah.edu.iq](mailto:hadi.abbas@uobasrah.edu.iq)

<https://doi.org/10.24200/amecj.v5.i04.209>

due to their great qualities, such as, nontoxicity, biodegradability, biocompatibility, antibacterial properties, and biofunctional characteristics, not only in the biomedical sector but also in the field of food contact materials. The new or improved properties of chitosan would be obtained through the chemical modification of its structure via the blending or attaching of various chemicals. Therefore, chitosan does not present problems of handling and disposal that may be encountered with some of its synthetic counterparts [2]. Chitosan is a promising material based on its chemical modifications as dye-removing agents and metal ion adsorbents. Recently, the progress on chemical modifications of chitosan has been quite rapid, and we are confident that a more extensive range of applications of chitosan derivatives could be expected shortly [3, 4]. In the plastics sector, plasticizers have long been a popular element [5]. Examples of its numerous applications include packaging, consumer goods, medicines, structures, and construction [6]. However, the industry is moving away from phthalate-based plasticizers and toward bio-based plasticizers due to environmental and health concerns [7]. Low cost per volume, low volatility, diffusivity, low specific gravity, good miscibility, and strong intermolecular interactions between the plasticizer and the polymer resin are all desired properties of plasticizers. A well-plasticized product should be flexible at low temperatures, have a low elastic modulus, a low glass transition temperature, and have good tensile elongation but low tensile strength [8]. Physical blending is a practical and important method for altering chitosan to serve various applications. Chitosan-based films' structural and physical characteristics have been extensively researched for use in biomedical and other applications [9,10]. When polymer chains separate from one another, plasticizers fill the intermolecular spaces between them. This reduces chain retraction and increases free volume, enabling polymer chains to move more freely [11]. The chitosan and plasticizer hydrogen bonding interaction [12,13] regulates

the mechanical and physical characteristics of the films. The physically blended plasticization of extracted chitosan with lauric acid and maleic was carried out in this work. It also focuses on the possible changes in molecular structure and mechanical and water solubility properties to see if they can produce appropriate chitosan films for packaging, which is a potential application for chitosan.

## **2. Experimental**

### **2.1. Reagents and Materials**

Chitosan was obtained by the deacetylation process of chitin extracted from local shrimp shell waste as described in the literature [14,15]. It had a viscosity average molecular weight of  $2.702 \times 10^5$  g per mole as determined by the viscosity technique and a deacetylation degree of 80%. The acetic acid ( $\text{CH}_3\text{CO}_2\text{H}$ ; pure  $\geq 99\%$ ; CAS No.: 64-19-7), Lauric acid ( $\text{CH}_3(\text{CH}_2)_{10}\text{COOH}$ . CAS No.: 143-07-7) and maleic acid ( $\text{HO}_2\text{CCH}=\text{CHCO}_2\text{H}$ , MDL Number: MFCD00063177; PubChem ID: 24896549, CAS No.: 99110-16-7) used as plasticizers and acetic acid as a solvent were purchased from Sigma-Aldrich Company and utilized without further treatment. The tris-maleate buffer and sodium maleate buffer make of maleic acid and can be used for the pretreatment of poplar tracheid cell walls for the spectroscopic analysis of lignin.

### **2.2. Instruments**

An FTIR-8101M Shimadzu spectrometer in the  $4000\text{--}400\text{ cm}^{-1}$  range was used to investigate the chemical structures of the unplasticized and chemically plasticized chitosan films. The mechanical properties (tensile strength, Young's modulus, and %elongation at break) of the unplasticized chitosan and their plasticizer blend films were measured in the tensile mode (speed  $5\text{ mm min}^{-1}$ ) with a BTI-FR2.5TN.D14 (ZwickRoell, Germany) mechanical testing machine. The standard test method (ASTM D882-10) for tensile properties of thin plastic sheeting and films was used to determine the mechanical properties of the plasticized and unplasticized chitosan films in the

form of stripes of 20 x 2 mm. This test method covers the determination of tensile properties of plastics in the form of thin sheeting and films (less than 1.0 mm (0.04 in.) in thickness).

### 2.3. Preparation of the chitosan films

The unplasticized chitosan film was prepared by the solvent evaporation method by dissolving 1.0 g of chitosan in 100 ml of 2% (v/v) acetic acid solution under stirring at ambient temperature for 24 h. Then, it was poured into a leveled Petri dish of 50 mm in diameter. The film was removed from the dish, dried for 12 hours at 45°C, and then stored before determining its structural, physical, and mechanical properties [16]. In the same procedure, plasticized chitosan films with different ratios of various acid plasticizers were prepared, as shown in Table 1.

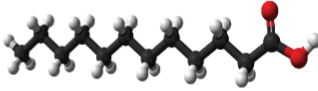
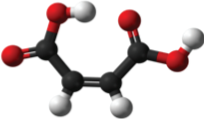
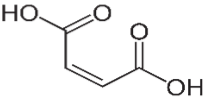
### 2.4. Film solubility

The amount of dry matter in the film that dissolves in water is used to calculate the solubility of the film. The solubility of the films was evaluated using previously described techniques with some changes [17]. In a nutshell, the films were divided into 2 cm × 2 cm squares and entirely dried before being stored. The films were weighed repeatedly until a stable weight that matched the fully dried films was attained; this weight was then used as the initial dry weight. The films were stirred at 25 °C for 24 hours while submerged in a glass beaker in 50 ml of deionized water. After being taken out of the beakers, the films were dried at 105 °C until they attained a constant weight. This quantity served as the final dry weight. The solubility percentage was calculated using equation 1 [18].

$$\text{Water Solubility (\%)} = \frac{\text{Initial Dry Weight} - \text{Final Dry Weight}}{\text{Initial Dry Weight}} \times 100$$

(Eq: 1)

Table 1. Plasticizers used and their ratio to Chitosan

Plasticizer	Chemical Structure	Chitosan: Plasticizer ratio
<u>Lauric acid</u>	 <chem>CH3(CH2)9CH2COOH</chem>	1:1, 1:2, 1:3, 2:1
<u>Maleic acid</u>	 	1:1, 1:2, 2:1

### 3. Results and Discussion

#### 3.1. Cast film formation and appearance

The films were easy to peel from the cast Petri dish and simple to handle and treat further. The cast films were transparent, uniform, thin, flexible, and manageable.

#### 3.2. FTIR characterization of unplasticized Chitosan films

Figure 1(black) displays the spectrum of the unplasticized chitosan film produced by casting a 2% acetic acid solution after it was removed from the Petri plate and before storage. The distinctive features of the chitosan spectrum in this study are analogous to those in other investigations [19,20]. Pure Cs exhibit characteristic polymer base-state peaks, including those at  $1037\text{ cm}^{-1}$  from the vibration of C-O groups,  $1562\text{ cm}^{-1}$  from NH bending, and  $1654\text{ cm}^{-1}$  from C=O stretching (amide I) O=C-NHR. The stretching vibration of free hydroxyl and the asymmetrical and symmetrical stretching of the N-H bonds in the amino groups

are correlated with the peaks between  $3610$  and  $3000\text{ cm}^{-1}$  that are present in all of the films under examination [21]. The bands at  $2912$  and  $2843\text{ cm}^{-1}$  indicate the vibrations of the aliphatic C-H [22].

#### 3.3. FTIR investigation of Cs-lauric acid blended films

Figures 1 illustrate the usual lauric acid peak, which occurs between  $2928$  and  $2844\text{ cm}^{-1}$  [23]. The amide II band for the C-O stretch of the acetyl group is represented by the band at  $1654\text{ cm}^{-1}$ , while the band represents the N-H stretch by the band at  $1597\text{ cm}^{-1}$ . The linked C-O stretch of the glucosamine residue is represented by the skeletal vibration at  $1072\text{ cm}^{-1}$ , and the asymmetric C-H bending of the  $\text{CH}_2$  group is indicated by the band at  $1377\text{ cm}^{-1}$  [24]. The bands at  $2916\text{ cm}^{-1}$  and  $2850\text{ cm}^{-1}$ , respectively, reflect the stretching vibrations of  $\text{CH}_2$  and  $\text{CH}_3$ , whereas the band at  $1753\text{ cm}^{-1}$  represents the stretching vibrations of C=O [25,26]. The band between  $1750$  and  $1700\text{ cm}^{-1}$  represents the carbonyl C=O stretching.

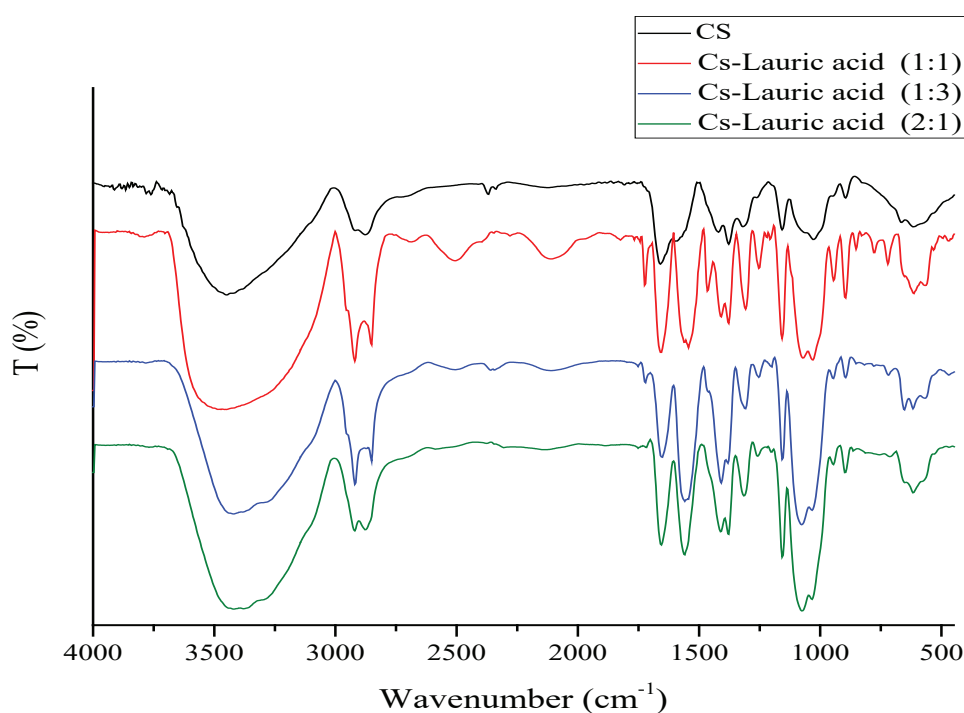


Fig. 1. FTIR spectra of Cs-lauric acid films

### 3.4. FTIR examination of Cs-maleic acid blended films

The FTIR spectra of the physical blend of chitosan with maleic acid films are shown in Figure 2. The spectra exhibited a peak in the 3500-2500  $\text{cm}^{-1}$ , which widened due to the OH groups of both diacids combining chitosan with each diacid individually. This suggests that integrating the two materials raised the proportion of hydroxyl groups rather than changing the type of functional groups in the backbone complex [27,28]. The outcome demonstrated that maleic acid successfully interacted with chitosan's amine group. Additionally, the diacid C=O band at 1701  $\text{cm}^{-1}$  [29] is present. Similar to this, the contributions of both diacid C-O bonds led to a wider chitosan C-O absorption at 1180  $\text{cm}^{-1}$ . Creating an amide link between maleic acid and the chitosan amine group is responsible for the remaining spectrum alterations.

At 1708  $\text{cm}^{-1}$ , the carbonyl C=O stretching

absorption became visible. The literature claims that pure diacid has two C=O peaks around 1700  $\text{cm}^{-1}$  and 1750  $\text{cm}^{-1}$ , respectively, and stands for free and hydrogen-bonded carboxylic acid groups [30]. The peak at 1750  $\text{cm}^{-1}$  vanished after the chitosan reaction, and there were no additional peaks in the 1735  $\text{cm}^{-1}$  region, indicating that esterification did not occur. According to a literature review on maleic acid amides, the cyclic amide analog emerged around 1770  $\text{cm}^{-1}$ , but the acyclic amide displayed classic C=O absorption near 1620  $\text{cm}^{-1}$  [31]. The cyclic structure cannot exist since there are no peaks in the 1770  $\text{cm}^{-1}$  area of the chitosantric acid spectra. Examining peaks in the 563–675  $\text{cm}^{-1}$  range proves that chitosan's native structure was unchanged. According to Mima et al. [32], these peaks are sharpest for 99 percent deacetylated chitosan and gradually fade away as acetylation increases (amide production), and this is the case here because the extracted chitosan used had about 81% degree of deacetylation.

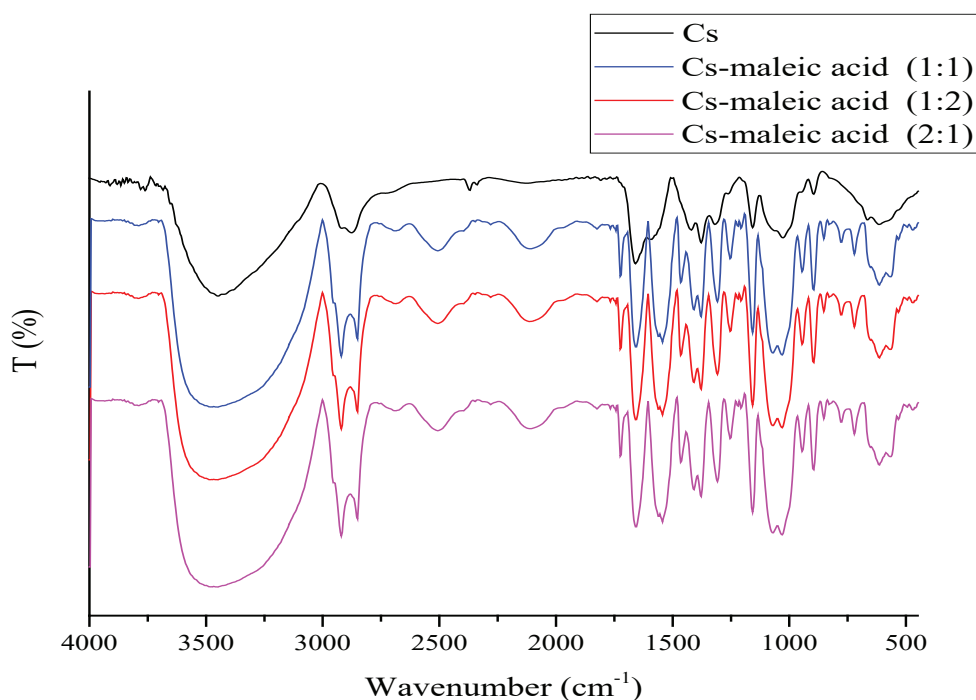


Fig. 2. FTIR spectra of Cs-maleic acid films.

### 3.5. Tensile properties of Chitosan films

Especially for single-use packaging when the material is stretched during use owing to continuous wear and tear, flexibility is an important property of plastics. The mechanical properties of synthetic bioplastics must be precisely studied to define their range of uses. Polymer films' strength and elasticity can be determined through mechanical testing. The amount to which the film subjected to the applied pull force reacts is defined by tensile strength measurements. A plasticizer is a substance that, when added to polymer materials, increases their elasticity. This plasticizer is necessary to get around the stiffness of films made with chitosan. The inter-polymer bond between chitosan polymer chains and plasticizers may become brittle and break. The plasticized and unplasticized chitosan films were tested in dry states according to ASTM D882-2010 "Standard Test Methods for tensile properties of thin plastic sheeting and films,"

### 3.6. Tensile properties of plasticized Cs: lauric acid films

The effect of the addition of lauric acid plasticizer resulted in a decrease of the tensile strength, Young modulus, and % elongation at break with an increasing amount of lauric acid, which was shown in Figures 3, 4, and 5. This leads to the indication that a level of interfacial adhesion may be lacking between chitosan and lauric acid. Adorna et al [33] obtained the same line of results. This happened because too many lauric acid plasticizer molecules were in a separate phase outside the phase of the plasticized blend. This suggests that there may not be enough interfacial adhesion between chitosan and lauric acid. The intermolecular force between the chains is reduced because of the conditions. It is concluded that the decrease in the measured mechanical properties of chitosan plasticized with increasing lauric acid plasticizer amount is in good accord with other reported results [34,35]. Their results were explained due to the plasticizer's effect on the promotion of intermolecular forces, thus lowering the high intramolecular forces inside the plasticized polymer mix chains.

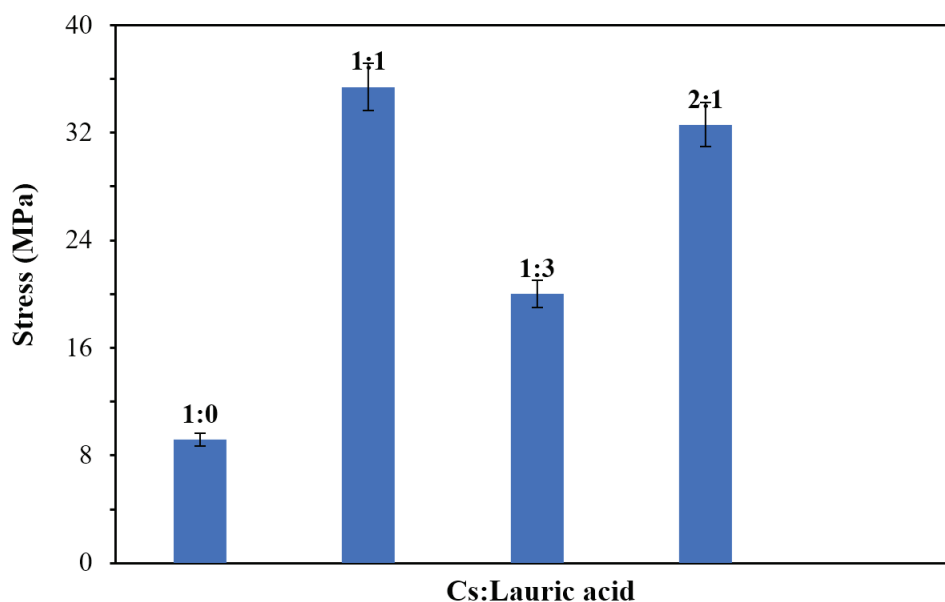
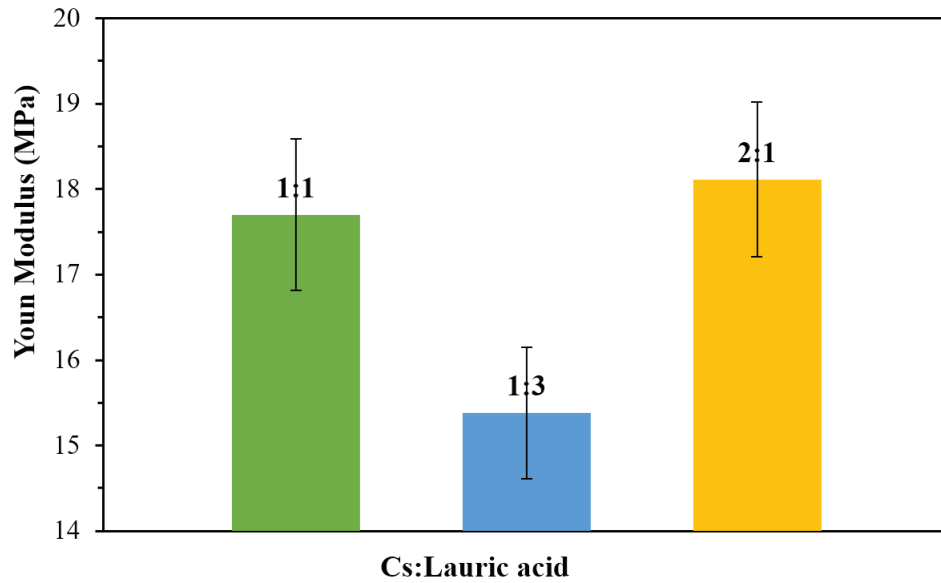
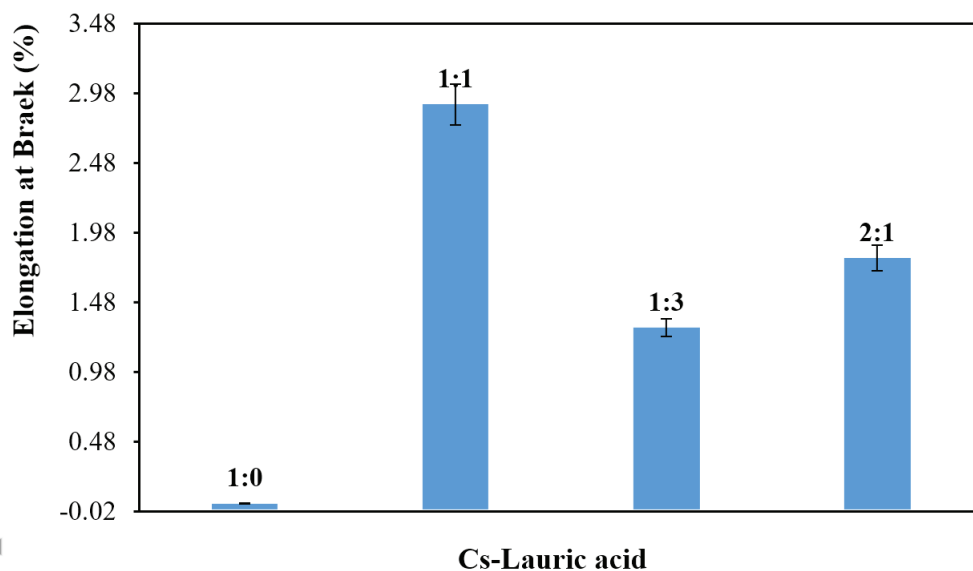


Fig. 3. The effect of Cs: Lauric acid ratios on the tensile strength of plasticized chitosan.



**Fig. 4.** The effect of Cs: Lauric acid ratios on the Young modulus of plasticized chitosan.



**Fig. 5.** The effect of Cs: Lauric acid ratios on the % elongation at break of plasticized chitosan.

### 3.7. Tensile properties of plasticized Cs: maleic acid films

Figures 6, 7, and 8 showed the effect of different ratios of chitosan: maleic acid plasticizer on the mechanical properties of the chitosan-based blended films, i.e., tensile strength, Young modulus, and %elengotion at the break, respectively. It can be observed that Cs: maleic acid films with a ratio of 2:1 showed higher stress at maximum load and Young's modulus

than those by (1:2) cross-linked by maleic acid, accompanied by an increase in the %elongation at break as well. This is because there is an excess of cross-linking bridges, resulting in lower chain stiffness and higher extendibility.

This result was also in agreement with Reddy and Yang [36] and Thessrimuang and Prachayawarakorn [37]. They reported using an acid plasticizer caused by excess cross-linking, which led to an increase in tensile strength, and this was the case here.

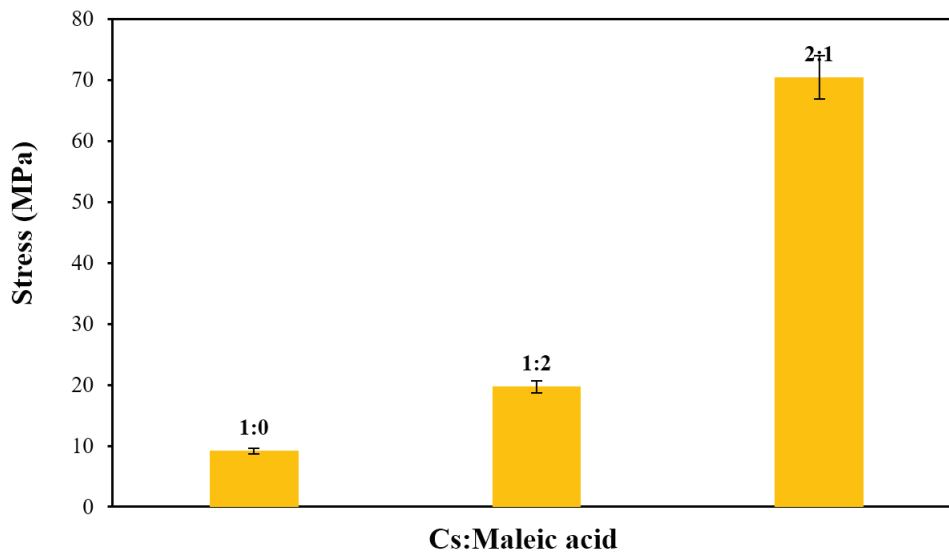


**Fig. 6.** The effect of Cs: Maleic acid ratios on the tensile strength of plasticized chitosan.

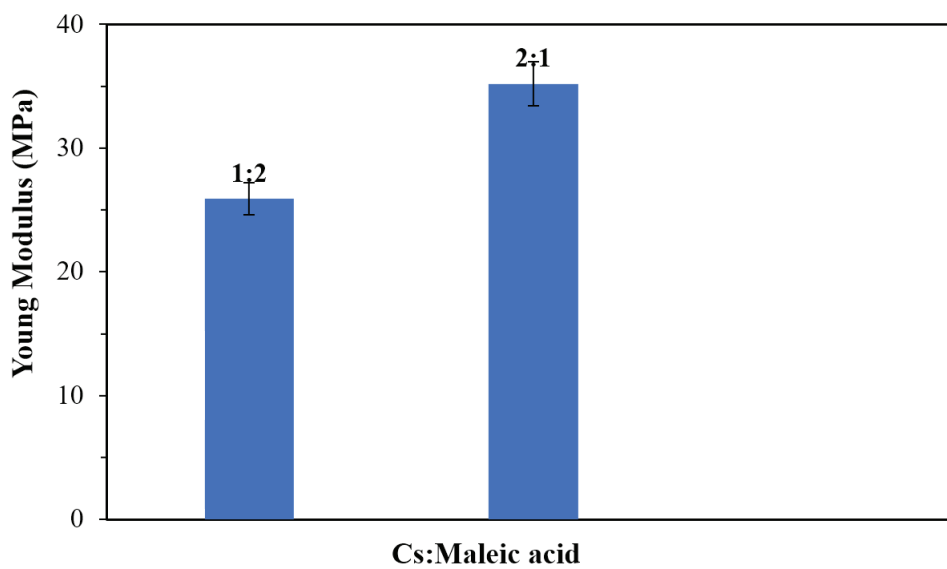


**Fig. 7.** The effect of Cs: Maleic acid ratios on the Young modulus of plasticized chitosan.

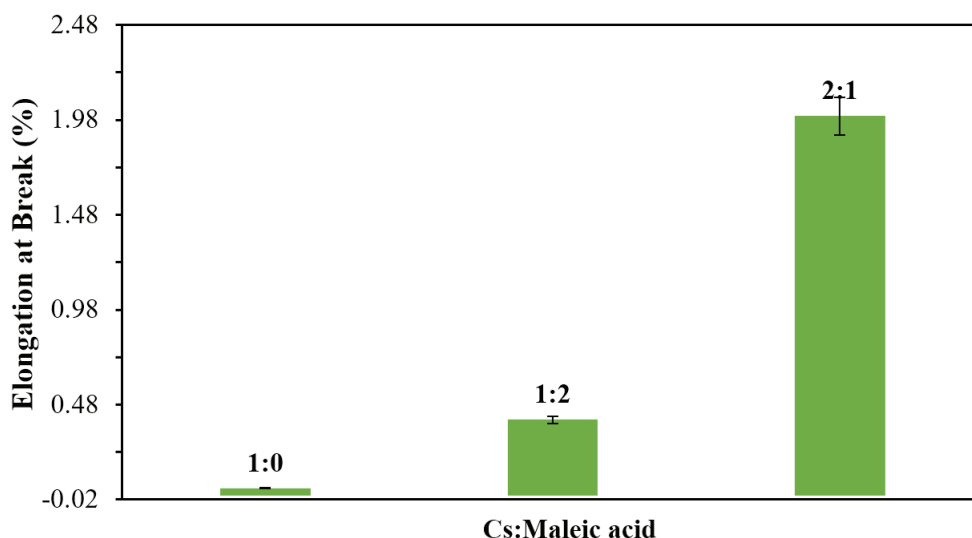


**Fig. 8.** The effect of Cs: Maleic acid ratios on the % elongation at break of plasticized chitosan.

### 3.8. Solubility of plasticized and un-plasticized Chitosan films

As measured by the film water solubility of chitosan films with various chitosan: plasticizers ratios (w/w), the impact of various plasticizers on the water barrier qualities of the materials was studied. The solubility of films in water was measured in triplicate. According to the type of plasticizer and its relative ratio, the films' water solubility increased, as shown in Table 2. This might be explained by the plasticizers' higher hydrophilicity than chitosan. By adjusting the kind and proportion of each plasticizer used in the production of those films, the solubility of chitosan/plasticizer films and blends may be controlled, opening up a wide range of industrial

applications. While it may be necessary for certain materials to be insoluble in specific applications to ensure the dependability and durability of the implemented product, film solubility may occasionally be desired before consumption. It will therefore rely on how each plasticizer is used when preparing the sample [38,39].

It may be worth mentioning here that the chitosan films always turned rubbery when submerged in water, but they never retained their structural integrity because the soluble plasticized portion of the film interfered with the structure. However, the type and concentration of the plasticizer can be adjusted to modify the solubility of the film, making it necessary for more potential applications.

**Table 2.** Solubility of some plasticized chitosan

Cs-Plasticizer	Ratio	SW 1 (%)	SW 2 (%)	SW 3 (%)	SW 4 (%)
Cs	0:0	2.1	2.8	3.3	3.9
Cs-Lauric acid	1:3	10.25	12.8	16.2	26.5
Cs-Maleic acid	2:1	2:1	48.7	53	55

The soluble plasticized part of the chitosan films interferes with the structure, which may be worth highlighting here. Despite usually turning rubbery when submerged in water, they never maintained their structural integrity. However, the kind and amount of the plasticizer can be altered to change how soluble the film is, necessitating it for more applications.

#### 4. Conclusions

The purpose of this research was to examine how the types of mono and di-acid plasticizers affected the molecular structure, solubility, and mechanical characteristics of chitosan cast films. To improve some of the physical and mechanical qualities of the resulting plasticized cast plasticized chitosan films, the characteristics of the original chitosan film were evaluated in conjunction with those of the other films. The instrumental techniques used to study changes in the chemical structure and properties of modified chitosan have been considered. Every plasticizer tested showed enhanced mechanical performance, and regardless of the kind or quantity utilized, they all demonstrated the typical plasticizer action of increasing elongation and decreasing film stiffness. Data demonstrating the possibility of using modified chitosan in food packaging as sustainably as possible have been presented.

#### 5. Acknowledgement

The authors wish to thank the Department of Chemistry, College of Science, University of Basrah for supporting this work.

#### 6. References

- [1] E.S. Al-Allaq, H.S. Al-Lami, A.H. Al-Mowali, Synthesis and adsorption study of some chitosan acidic derivatives as dispersants for ceramic alumina powders, *Egypt. J. Chem.*, 63 (2020) 2717-2736. <https://doi.org/10.21608/ejchem.2019.15492.1940>
- [2] A.A. Mizhir, A.A. Abdulwahid, H.S. Al-Lami, Adsorption of carcinogenic dye Congo red onto prepared graphene oxide-based composites, *Desalin. Water Treat.*, 202 (2020) 381–395. <https://doi.org/10.5004/dwt.2020.26141>
- [3] J. Ji, L. Wang, H. Yu, Y. Chen, Y. Zhao, H. Zhang, W.A. Amer, Y. Sun, L. Huang, M. Saleem, Chemical modifications of chitosan and its applications, *Polym-Plast. Technol.*, 53, (2014) 1494-1505. <http://dx.doi.org/10.1080/03602559.2014.909486>
- [4] S.H. Mutasher, H.S. Al-Lami, Chemically plasticized chitosan films by grafting succinic acid: Surface roughness and mechanical properties, *Int. J. Membr. Sci.*, 9 (2022) 33-39. <https://doi.org/10.15379/2410-1869.2022.09.02.01>
- [5] E. Czogała, R. Pankalla, Recent attempts in the design of efficient PVC plasticizers with reduced migration, *Materials*, 14 (2021) 844-872. <https://doi.org/10.3390/ma14040844>
- [6] O. Yesid, Polymer and polymeric composites in encyclopedia of polymer composites, Springer Berlin Heidelberg, 2014. <https://doi.org/10.1007/978-3-642-37179-0>
- [7] S.S. Muobom, A.M. Umar, Y. Soongseok, A.P. Brolin, A review on plasticizers and eco-friendly bioplasticizers: Biomass sources and market, *Int. J. Eng. Res.*, 9 (2020) 1138-1144. <https://doi.org/10.17577/IJERTV9IS050788>
- [8] K. Ledniowska, H. Nosal-Kovalenko, W. Janik, A. Krasuska, D. Stańczyk, E. Sabura, M. Bartoszewicz, A. Rybak, Effective, environmentally friendly PVC plasticizers based on succinic acid, *Polymers*, 14(2022) 1295-12305. <https://doi.org/10.3390/polym14071295>
- [9] R.K. Wanchoo, A. Thakur, A. Sweta, Viscometric and rheological behavior of chitosan hydrophilic polymer blends, *Chem. Bioch. Eng.*, 22 (2008)15-24. <https://hrcak.srce.hr/21394>
- [10] J. W. Rhim, H.M. Park, C.S. Ha, Bio-nanocomposites for food packaging applications, *Prog. Polym. Sci.*, 38 (2013)1629-1652. <https://doi.org/10.1016/j.progpolymsci.2013.05.008>
- [11] H. Lim, S.W. Hoag, Plasticizer effects on

- physical-mechanical properties of solvent cast soluplus films, *AAPS Pharm. Sci. Tech.*, 14 (2013) 903-910. <https://doi.org/10.1208/s12249-013-9971-z>
- [12] A. Silva-Weiss, V. Bifani, M. Ihl, P.J.A. Sobral, M.C. Gómez-Guillén, Structural properties of films and rheology of film-forming solutions based on chitosan and chitosan-starch blend enriched with Murata leaf extract, *Food Hydrocolloid*, 31 (2013) 458-466, <https://doi.org/j.foodhyd.2012.11.028>
- [13] J.M.F. Pavoni, C.L. Lucchese, I.C. Tessaro, Impact of acid type for chitosan dissolution on the characteristics and biodegradability of cornstarch/chitosan-based film, *Int. J. Biol. Macromol.*, 138 (2019) 693-703. <https://doi.org/10.1016/j.ijbiomac.2019.07.089>
- [14] M.S. Hossain, A. Iqbal, Production and characterization of chitosan from shrimp waste, *J. Bangladesh Agril. Univ.*, 12(2014) 153-160. <http://dx.doi.org/10.3329/jbau.v12i1.21405>
- [15] H.S. Al-Lami, A.A. Saleh, M.A. Jalal, S.H. Mutasher, The effect of synthesized chitosan grafted poly (N-L-lactide) on human genetic material, *InnovaCiencia*, 6 (2018) 1-10. <http://dx.doi.org/10.15649/2346075X.462>
- [16] A. Yadav, A. Kujur, A. Kumar, P.P. Singh, V. Gupta, B. Prakash, Encapsulation of bunium persicum essential oil using chitosan nanopolymer: Preparation, characterization, antifungal assessment, and thermal stability, *Int. J. Biol. Macromol.*, 142 (2020) 172-180. <https://doi.org/10.1016/j.ijbiomac.2019.09.089>
- [17] J. Hafsa, A. Smach, M. Khedher, M.R. Ben, B. Charfeddine, K. Limem, H. Majdoub, S. Rouatbi, Physical, antioxidant and antimicrobial properties of chitosan films containing Eucalyptus globulus essential oil, *LWT-Food Sci. Technol.*, 68 (2016) 356-364. <https://doi.org/10.1016/j.lwt.2015.12.050>
- [18] R. Priyadarshia, Sauraja, B. Kumara, Y.S. Negia, Chitosan films incorporated with citric acid and glycerol as an active packaging material for extension of green chilli shelf life, *Carbohydr. Polym.*, 195 (2018) 329-338. <https://doi.org/10.1016/j.carbpol.2018.04.089>
- [19] I.A. Farion, V.F. Burdukovskii, B.Ch. Kholkhoev, P.S. Timashev, R.K. Chailakhyan, Functionalization of chitosan with carboxylic acids and derivatives of them: Synthesis issues and prospects of practical use: A review, *Express Polym. Lett.*, 12 (2018) 1081-1111. <https://doi.org/10.3144/expresspolymlett.2018.95>
- [20] M.H. Zaboony, A.A. Saleh, H.S. Al-Lami, Synthesis, characterization and cytotoxicity investigation of chitosan-amino acid derivatives nanoparticles in human breast cancer cell lines, *J. Mex. Chem. Soc.*, 65 (2021) 178-188. <http://dx.doi.org/10.29356/jmcs.v65i2.1265>
- [21] J.F. Rubilar, R.M.S. Cruz, H.D. Silva, A.A. Vicente, I. Khmelinskii, M.C. Vieira, Physico-mechanical properties of chitosan films with carvacrol and grape seed extract, *J. Food Eng.*, 115 (2013) 466-474. <http://dx.doi.org/10.1016/j.jfoodeng.2012.07.009>
- [22] A.C.S. de Oliveira, T.A. Santos, J.C. Ugucioni, R.A. da Rocha, S.V. Borges, Effect of glycerol on electrical conducting of chitosan/ polyaniline blends, *J. Appl. Polym. Sci.*, 138 (2021) 14-18. <https://doi.org/10.1002/app.51249>
- [23] V.K. Mourya, N.N. Inamdar, Chitosan-modifications and applications: Opportunities galore, *React. Funct. Polym.*, 68 (2008) 1013-1051. <https://doi.org/10.1016/j.reactfunctpolym.2008.03.002>
- [24] S. K. Kim, N. Rajapakse, Enzymatic production and biological activities of chitosan oligosaccharides (COS): A review, *Carbohydr. Polym.*, 62(2005)357-368. <https://doi.org/10.1016/j.carbpol.2005.08.012>
- [25] Z. Cui, E. S. Beach, P.T. Anastas, Modification of chitosan films with environmentally benign reagents for increased water resistance, *Green Chem. Lett. Rev.*, 4 (2011) 35-40. <https://doi.org/10.1080/17518253.2010.500621>

- [26] C. Brasselet, G. Pierre, P. Dubessay, M. Dols-Lafargue, J. Coulon, J. Maupeu, A. Vallet-Courbin, H. de Baynast, T. Doco, P. Michaud, C. Delattre, Modification of chitosan for the generation of functional derivatives, *Appl. Sci.*, 9 (2019) 1321-1343. <https://doi.org/10.3390/app9071321>
- [27] H. A. Al-Mosawi, H. S. Al-Lami, N. A. Awad, Synthesis and characterization of some recycled polystyrene and chitosan-based copolymers for water hardness removal, *Bas. J. Sci.*, 39 (2021) 496-514. <https://doi.org/10.29072/basjs.2021311>
- [28] R.A. Lusiana, D. Siswanta, M. Mudasir, Preparation of citric acid crosslinked chitosan/poly(vinyl alcohol) blend membranes for creatinine transport, *Indo. J. Chem.*, 16(2016) 144-150. <https://doi.org/10.22146/ijc.21157>
- [29] K.M. Doll, R. L. Shogren, J.L. Willett, G.J. Swift, Solvent-free polymerization of citric acid and hexamethylenediamine for novel carboxylated polyamides, *J. Polym. Sci., Part A: Polym. Chem.*, 44 (2006) 4259-4267. <https://doi.org/10.1002/pola.26170>
- [30] H. Drechsel, G. Jung, G. Winkelmann, Stereochemical characterization of rhizoferrin and identification of its dehydration products, *BioMetals*, 5 (1992) 141-148. <https://doi.org/10.1007/bf01061320>
- [31] S.H. Hsieh, Z.K. Huang, Z. Z. Huang, Z.S. Tseng, Antimicrobial and physical properties of woolen fabrics cured with citric acid and chitosan, *J. Appl. Polym. Sci.*, 94(2004) 1999-2007. <https://doi.org/10.1002/app.21104>
- [32] S. Mima, M. Miya, R. Iwamoto, S. Yoshikawa, Highly deacetylated chitosan and its properties, *J. Appl. Polymer Sci.*, 28(1983) 1909-1917. <https://doi.org/10.1002/app.1983.070280607>
- [33] J.A. Adorna, C.K. A. Aleman, I.L. E. Gonzaga, J.N. Pangasinan, K.M.D. Sisican, V.D. Dang, J.R.S. Ventura, Effect of lauric acid on the thermal and mechanical properties of polyhydroxy butyrate (PHB)/starch composite biofilms, *Int. J. Polym. Sci.*, 2020 (2020) 1-11. <https://doi.org/10.1155/2020/7947019>
- [34] D.I. Rudyardjo, S. Wijayanto, The synthesis and characterization of hydrogel chitosan alginate with the addition of plasticizer lauric acid for wound dressing application, *J. Phys. Conf. Series*, 853 (2017) 012042. <https://doi.org/10.1088/1742-6596/853/1/012042>
- [35] F. Gabriele, A. Donnadio, M. Casciola, R. Germani, N. Spreti, Ionic and covalent crosslinking in chitosan-succinic acid membranes: Effect on physicochemical properties, *Carbohydr. Polym.*, 251 (2021) 1-9. <https://doi.org/10.1016/j.carbpol.2020.117106>
- [36] N. Reddy, Y. Yang, Citric acid cross-linking of starch films, *Food Chem.*, 118 (2010) 702-711. <https://doi.org/10.1016/j.foodchem.2009.05.050>
- [37] N. Thessrimuang, J. Prachayawarakorn, Characterization and properties of high amylose Mung bean starch biodegradable films cross-linked with malic acid or succinic acid, *J. Polym. Environ.*, 27 (2018) 1-11. <https://doi.org/10.1007/s10924-018-1340-2>
- [38] J.R. Rodríguez-Núñez, T.J. Madera-Santana, D I. Sanchez-Machado, J. Lopez-Cervantes, H.S. Valdez, Chitosan/hydrophilic plasticizer-based films: Preparation, physicochemical and antimicrobial properties, *J. Polymer Environ.*, 22 (2014) 41-51. <https://doi.org/10.1007/s10924-013-0621-z>
- [39] H. Chen, C. Wu, X. Feng, M. He, X. Zhua, F. Teng, Effects of two fatty acids on soy protein isolate/sodium alginate edible films: Structures and properties, *LWT-Food Sci. Technol.*, 159 (2022) 1-10. <https://doi.org/10.1016/j.lwt.2022.113221>



# In-vitro evaluation of photoprotection, cytotoxicity and phototoxicity of aqueous extracts of *Cuscuta campestris* and *Rosa damascene* by MTT method and UV spectroscopy analysis

Payam Khazaeli <sup>a,b</sup>, Atefeh Ameri <sup>b</sup>, Mitra Mehrabani <sup>c</sup>, Morteza Barazvan <sup>a,d</sup>, Marzieh Sajadi Bami <sup>a</sup>, and Behzad Behnam <sup>c,a,e,\*</sup>

<sup>a</sup> *Pharmaceutics Research Center; Institute of Neuropharmacology, Kerman University of Medical Sciences, Kerman, Iran*

<sup>b</sup> *Pharmaceutical sciences and cosmetic products research center, Kerman University of Medical Sciences, Kerman, Iran*

<sup>c</sup> *Herbal and Traditional Medicines Research Center, Kerman University of Medical Sciences, Kerman, Iran*

<sup>d</sup> *Students Research Committee, Faculty of Pharmacy, Kerman University of Medical Sciences, Kerman, Iran*

<sup>e</sup> *Extremophile and Productive Microorganisms Research Center, Kerman University of Medical Sciences, Kerman, Iran*

## ARTICLE INFO:

Received 29 Jul 2022

Revised form 12 Oct 2022

Accepted 15 Nov 2022

Available online 30 Dec 2022

## Keywords:

*Cuscuta campestris*,  
UV-visible spectrophotometer,  
*Rosa damascene*,  
Sun protective factor,  
Phototoxicity

## ABSTRACT

Applying sunscreen is essential for protecting the skin from UV's acute and chronic effects. Some of these products on the market display side effects and are expensive. There is a great demand for effective, cheap, safe, and herbal sunscreens with a wide range of sun protection activities. This study aimed to evaluate the photoprotection, cytotoxicity, and phototoxicity of aqueous extracts of *Cuscuta campestris* (CC-AE) and *Rosa damascena* (RD-AE). The maceration method prepared the CC-AE and RD-AE from the aerial branch. In-vitro photoprotection was evaluated by determining the sun protective factor (SPF) of CC-AE and RD-AE by a UV-visible spectrophotometer. The cytotoxicity and phototoxicity studies were assessed using the MTT assay on 3T3 cells. In the final, the PIF (Photo Inhibitor Factor) was calculated. The SPF values of CC-AE and RD-AE were found at  $11.10 \pm 0.05$  and  $1.36 \pm 0.04$ , respectively, at the concentration of  $0.2 \text{ mg mL}^{-1}$ . The half maximal effective concentration ( $EC_{50}$ ) of CC-AE and RD-AE was obtained at  $35.05 \pm 0.91 \text{ } \mu\text{g mL}^{-1}$  and  $40.7 \pm 0.87 \text{ } \mu\text{g mL}^{-1}$ , respectively. The phototoxicity analysis showed that CC-AE and RD-AE had low PIF values and were considered as the probable phototoxic. Overall, regarding the considerable SPF and PIFs values plus the anti-inflammatory and antioxidant properties of these extracts, they can be evaluated for further pharmaceutical formulations.

## 1. Introduction

Solar ultraviolet (UV) radiation such as UVA (320–400 nm) and UVB (~295–320 nm) have acute and chronic influences on the skin; they might finally cause cancers of the skin [1]. UVB radiation can cause acute effects such as erythema and edema,

and chronic effects such as immunosuppression and carcinogenesis [2, 3]. However, UVA radiation can induce tanning by the oxidation of melanin, and photoaging by the destruction of dermal structures, as well as leading to damage of the macromolecules, and oxidative stress by the production of reactive oxygen species (ROS) [2, 3]. The main destructive factors of UV radiation on the skin are free radicals including superoxide anions, hydroxyl radicals, singlet oxygen,

\*Corresponding Author: Behzad Behnam

Email: [behnamb@kmu.ac.ir](mailto:behnamb@kmu.ac.ir)

<https://doi.org/10.24200/amecj.v5.i04.202>

hydrogen peroxide, ferric ion, nitric oxide, etc. [3]. Photoprotection which is caused with using of sunscreen, prevents the acute and chronic effects of UV radiation. UV protectors are classified as UV filters and UV absorbers based on types of cosmetic materials [2, 4]. UV filters are divided into two classes according to their chemical structure and mechanism of action: inorganic, such as titanium dioxide and zinc oxide, are of low irritation potential and exhibit photostability and wide-ranging absorption spectra and organic such as UVA, UVB, and broadband absorbers that absorb the radiations based on their chemical structure. The filter's ability of organic filters is classified as a photostable, photo-unstable, and photoreactive filters [2, 4, 5]. The sunscreens' formulations that protect the skin from harmful UV rays could be introduced as physical and chemical sunscreens by blocking, reflecting, scattering and absorbing the UV rays [2, 5]. The efficacy rate of sunscreens is usually measured by the sun protection factor (SPF) estimation, which represents an accepted global characteristic of protection from erythema after exposure to simulated solar radiation [6]. Generally, the components of sunscreens have shown side effects such as disruption in the endocrine system and changes in the hypothalamic-pituitary-thyroid (HPT) axis. In addition, they could be caused reproductive homeostasis during long-term use [4, 7]. However, some sunscreens may have environmental toxicity effects and can have detrimental effects on the ecosystem [2, 4]. Best sunscreens should have several characteristics, including safe, non-toxic, and photo-stable, and be able to protect the skin from UVA and UVB rays [4]. The natural photoprotectants can be included the obtained extracts of plants such as aloe vera, pomegranate, rambutan, grape, tomato, the green tea, and the oils obtained from soybean, olive, coconut, almond, and jojoba as well as the mycosporine-like amino acids (MAA), etc. [5, 8-10]. Several studies have described the use of plant extracts with photoprotection properties. For example, Rangel et al [2] assessed the photoprotective capability of extracts from red macroalgae. Permana et al [11] showed a potential absorption of UVA and UVB radiation by the hydrogel-containing propolis

extract-loaded phytosome and indicated their high SPF value of them [11]. Natural combinations have shown the desirable SPF and anti-inflammatory and antioxidant properties [9, 12]. *Rosa damascena* mill, commonly known as Gole Mohammadi in Iran [13], showed several medicinal properties including antiviral, antimicrobial, antioxidant, antitussive, hypnotic, anti-diabetic, and sedative effects on the respiratory system [14]. This plant contains different chemical compounds such as tannins, polyphenols, carotenoids, quercetin, eugenol, citronellol, geraniol, liquiritin, etc. [14, 15]. Generally, the extracts of rose petals have shown high antioxidant activity that correlated to the total phenolic, and flavonoid contents of rose [16, 17]. The analgesic and anti-inflammatory effects of rose have also been reported [18-20]. The hydroalcoholic extract of *R. damascena* can significantly reduce edema, which may be mediated by the inhibition of acute inflammation [13]. *Cuscuta campestris* Yuncker with the common name dodder has analgesic, antipyretic, anti-inflammatory, and anti-cancer properties [21, 22]. This holoparasitic plant has been applied to treat a liver injury, cancer prevention, sciatica, scurvy, and scrofula derma [22-24]. Based on reported works, polyphenolic compounds such as quercetin, sinapic acid, kaempferol, isorhamnetin hesperidin, and eugenol were identified in extracts from *C. campestris* [25, 26]. The ethyl acetate extract of the plant has the strongest antioxidant effect due to the highest content of flavonoid compounds kaempferol and quercetin [22]. A review of the literature did not expose any previous studies on the photoprotective, cytotoxicity, and phototoxicity activities of the aqueous extract of *Cuscuta campestris* (CC-AE) and *Rosa damascena* (RD-AE) plants by MTT method and UV spectroscopy analysis. Generally, the UV/visible spectrophotometric method were applied to analyze the UV radiation protection capability for probable sunscreen applications [2, 6]. One of the most important issue in pharmaceutical circles is to optimizing the wright method for analyzing the active ingredients in bulk drug materials, their impurities and decompositions substances, and also pharmaceutical formulations and biological

products. Spectrophotometry is the quantitative measurement of the reflection or transmission properties of a material as a function of wavelength. The use of UV-Vis spectrophotometry, especially in the analysis of pharmaceutical forms, has increased rapidly in recent years [2, 3, 26]. In vitro methods for evaluating the sunscreen potentials of materials are generally of two types. Methods that involve measuring the absorption or transmission of UV radiation through sunscreen product films on quartz plates or bio-membranes, and methods in which the absorption characteristics of sunscreen agents are determined based on spectrophotometric analysis of dilute solutions [2, 3, 26].

In the present study, the UV absorption of each sample was obtained and the Mansur equation was applied to find the final SPF. Afterwards the effects of extracts were evaluated in vitro in 3T3 cells to obtain their probable photo-toxic or photo-protective behaviors.

## 2. Materials and Methods

### 2.1. Chemicals

Trypsin, phosphate-buffered saline (PBS), and 3-(4, 5-dimethylthiazol-2-yl)-2, 5-diphenyl-2H-tetrazolium bromide (MTT) were supplied by Sigma company (St. Louis, MO, USA). Fetal bovine serum (FBS), Dulbecco's modified Eagle's medium (DMEM), and Penicillin-Streptomycin solution (100X) were obtained from Borna Pouyesh Gene Company (BPGene Co., Kerman, Iran).

### 2.2. Extracts preparation

The plants (*C. Campestris* and *R. Damascena*) were collected from Mahan, Kerman, Iran (30.0630° N, 57.2875° E). The plants were then identified by Dr. Mitra Mehrabani and kept in the Faculty of Pharmacy herbarium (Kerman University of Medical Sciences, Kerman, Iran). The aerial branches of plants were washed three times with deionized water and dried at room temperature. The dried aerial branches were ground with a mill to obtain a fine powder. The extracts of plants were prepared using the maceration method. For this purpose, 10 g of the fine powder was combined with the deionized water

(100 mL) in a laboratory flask with a volume of 500 mL. The mixture was heated at 80 °C for 30 min and filtrated through Buchner funnel linked with Watman filter paper (No.1). Finally, the filtrate was freeze-dried (freeze dryer FD-550 purchased from Tokyo Rikakikai Co., Ltd, Japan) [27]. The dried aqueous extract of *C. campestris* and *R. damascena* were labeled as CC-AE and RD-AE, respectively, and the SPF of compounds was determined by UV-visible spectrophotometer.

### 2.3. Determination of UV absorption spectra by UV-vis spectrophotometer

The characterizations of UV absorption spectra were carried out by analyzing an aqueous extract of *C. campestris* and *R. damascena* at concentrations 20000, 10000, 5000, 2500, and 1250 µg mL<sup>-1</sup>. The UV spectra were recorded using a Synergy TM 2 multi-mode microplate reader (BioTek Instruments, Inc., Winooski, VT, USA) from 200 to 900 nm.

### 2.4. Determination of photoprotection activity of plants extracts

The procedure of Khazaeli and Mehrabani [28], with some modifications, was used to measure the photoprotection activity of plant extracts. For this purpose, the obtained aqueous extracts of *C. campestris* and *R. damascena* were individually scanned in the range from 337.5 nm to 292.5 nm with interval five nm using a double beam UV/Vis spectrophotometer (Optizen 3220 UV). Then, in vitro SPF was measured by the following equation I [29].

$$\text{SPF} = \frac{\sum_{292.5}^{337.5} E(\lambda) \cdot \epsilon(\lambda)}{\sum_{292.5}^{337.5} E(\lambda) \cdot \epsilon(\lambda) \cdot T(\lambda)} \quad (\text{Eq.I})$$

Where  $T(\lambda)$ ,  $E(\lambda)$ , and  $\epsilon(\lambda)$  represents the transmittance of the sample at  $\lambda$ , the spectral irradiance of terrestrial sunlight at  $\lambda$ , and the erythemal action spectrum at  $\lambda$ , respectively. The  $E(\lambda) \times \epsilon(\lambda)$  values are showed in Table 1, the  $T(\lambda)$  was three times measured and the obtained means were applied to estimate the SPF value for each extract. Afterward, the graph relationship of SPF versus LnC was used to calculate SPF in 2.0 mg mL<sup>-1</sup> solution for each extraction.

Table 1. Normalized product function used in the calculation of SPF.

Wavelength (nm)	$E(\lambda) \times \epsilon(\lambda)$
292.5	1.139
297.5	6.510
302.5	10.00
307.5	3.577
312.5	0.973
317.5	0.567
322.5	0.455
327.5	0.289
332.5	0.129
337.5	0.046

$E(\lambda)$ : the spectral irradiance of terrestrial sunlight at each wavelength.  
 $\epsilon(\lambda)$ : the erythemal action spectrum at each wavelength.

### 2.5. Cell culture

The mouse embryonic fibroblast cells (3T3) (ATCC Number: IBRCC10100) were provided by the Iranian Biological Resource Center (IBRC) in Tehran, Iran. The cell line was cultured in DMEM medium supplemented with 10% (v/v) FBS, 100 U mL<sup>-1</sup> penicillin, and 100 µg mL<sup>-1</sup> streptomycin and incubated at 37 °C in a 5% CO<sub>2</sub> incubator [30].

### 2.6. Cytotoxicity assay

Based on methods reported in the literature [31-34], in the exponential growth stage, the cells were harvested and seeded into 96-well tissue culture plates (approximately 10<sup>4</sup> cells per well). After 24 h, the samples of serial concentrations of CC-AE and RD-AE (at the final concentration range of 3.9–125 µg mL<sup>-1</sup>) were separately poured into the desired wells. After 24 h, the medium in each well was switched with 20 µL of MTT solution (5 mg mL<sup>-1</sup>) and plates were incubated at 37 °C for a further 3 h. For dissolving the formazan crystals, the culture media were removed from the wells and 100 µL of fresh DMSO was added to each well of the plate. The optical density of final solutions was then read at 570 nm using a Synergy™ 2 multi-mode microplate

reader (BioTek Instruments, Inc., Winooski, VT, USA). Doxorubicin (12 µg mL<sup>-1</sup>) was applied as a positive control. All experiments were repeated in triplicate on different days and EC<sub>50</sub> values were determined and analyzed by non-linear regression analysis (SPSS software, SPSS inc., Chicago) and the data were reported as mean (m±SD).

### 2.7. Evaluation of phototoxicity and determination of PIF factor

For the purpose of evaluation of phototoxicity in the presence and absence of UVA radiation [35], cells were prepared as described in the cytotoxicity assay into two plates (A and B). Plate A was exposed to UVA light (1.8 mW cm<sup>-2</sup>) for 60 min. After 60 min, the medium was discarded and the fresh medium was added. Plate B was used as a non-irradiated control. Both plates were incubated for 24 h at 37 °C in a 5% CO<sub>2</sub> incubator. Afterward, the medium in each well was discarded and MTT solution (20 µL, 5 mg mL<sup>-1</sup>) was added. Plates were incubated at 37 °C for 3 h and following the culture, media were removed from the wells and 100 µL of fresh DMSO was added to each well to dissolve the formazan crystals. The absorption was then measured at 570

nm, and the  $EC_{50}$  values were estimated. The PIF (Photo Inhibitor Factor) was determined based on below equation II:

$$PIF = \frac{EC_{50(-UV)}}{EC_{50(+UV)}} \quad (\text{Eq.II})$$

In compliance with the OECD TG 432 [36], the below Table was considered for analyzing the PIF values (Table 2).

**Table 2.** The categorization of phototoxicity stages based on PIF values.

PIF value	Type of hazard
PIF < 2	Non phototoxic
PIF > 2 and < 5	Probable phototoxic
PIF > 5	Potential phototoxic

### 2.8. Investigation of protective effects of plant extracts against of phototoxic effects of chlorpromazine

In assessing of the ability of plant extracts to prevent of the phototoxic effects of chlorpromazine (CPZ), two culture plates (A and B) were seeded with about  $10^4$  cells per well. Then, the CC-AE and RD-AE were prepared at a concentration of  $31.25 \mu\text{g mL}^{-1}$ . The concentrations of chlorpromazine were also trained at the range of 0.1, 0.5, and  $1 \mu\text{g mL}^{-1}$ . After 24 h, the culture media on the cells were evacuated and  $100 \mu\text{L}$  of the prepared

concentration of extracts and  $100 \mu\text{L}$  of the concentrations of chlorpromazine were separately added into the desired wells of the culture plates. Subsequently, the plate A was exposed to UVA light ( $1.8 \text{ mW cm}^{-2}$ ) for 60 min. Over time, the cultural media were removed and the fresh media were added. The plate B was maintained in darkness (as a non-irradiated control). The culture plates (A and B) were incubated at  $37 \text{ }^\circ\text{C}$  for 24 h in a  $5\% \text{ CO}_2$  incubator. The subsequent steps were performed as in Section 2.8. All experiments were repeated three times in different days. Then, the cell viabilities (%) were determined, and data were stated as mean results ( $m \pm \text{SD}$ ).

### 2.9. Statistical analysis

Experimental data are presented as the mean ( $m \pm \text{SD}$ ) with at least three determinations for independent experiments. All data were analyzed by non-linear regression analysis (SPSS software, SPSS inc., Chicago) and the p-value ( $p < 0.05$ ) was considered to be statistically significant.

## 3. Results and Discussion

### 3.1. UV absorption spectra and critical wavelength

The UV absorption spectra of CC-AE and RD-AE are shown in Figure 1. The max absorbance of CC-AE (at  $2500 \mu\text{g mL}^{-1}$ ) and RD-AE (at  $2500 \mu\text{g mL}^{-1}$ )

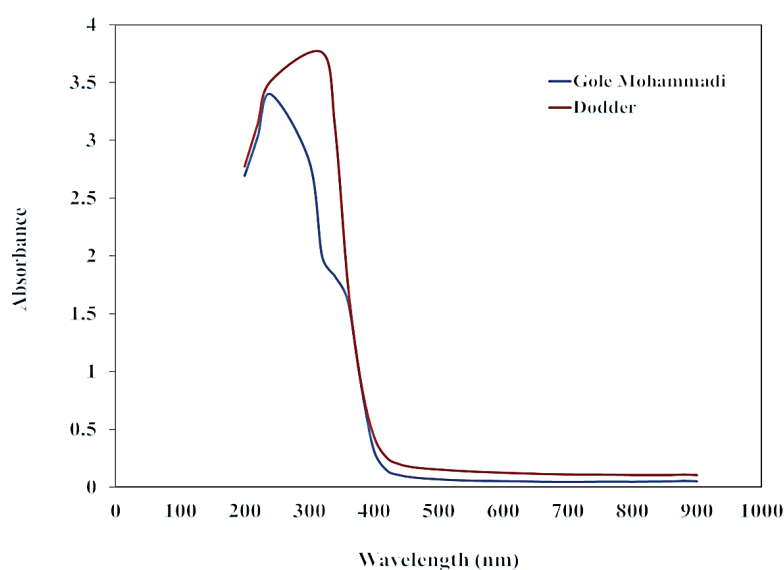


**Fig. 1.** The UV absorption spectra of aqueous extracts of *Rosa damascena* and *Cuscuta campestris* at concentration  $2500 \mu\text{g mL}^{-1}$

were at 240 nm and 320 nm, respectively (Fig. 1).

### 3.2. In vitro SPF assessment by UV

#### Spectrophotometry analysis

The SPF is a quantitative capacity of the efficiency of a sunscreen product. To prevent sunburn and other skin damage, a sunscreen product should have a broad absorption of between 290 and 400 nm. Antioxidants from natural resources, especially plants, might be offered as novel potentials for the treatment and prevention of diseases caused by UV rays. There are reports on the correlation between antioxidant activity and SPF values [2, 37]. Based on previous reports of the excellent antioxidant activity of CC-AE and RD-AE plants [16, 17, 25], the current study investigated the SPF values of aqueous extracts of plants by UV spectrophotometry applying Mansur mathematical equation [6]. In Table 3, the SPF values measured using the UV transmission spectra of CC-AE and RD-AE are listed. As shown in Table 3, the SPF values obtained at 2 mg mL<sup>-1</sup> were 11.10±0.05 and 1.36±0.04 for CC-AE and RD-AE, respectively. Ebrahimzadeh et al [38] assessed the SPF values of extracts from Sambucus ebulus, Zea maize, Feijoa sellowiana, and Crataegus pentagyna and reached the highest value (SPF = 24.47) using ultrasonic extract of Crataegus pentagyna. They also reported that there is a good correlation between SPF and phenolic contents. Hashemi et al [37] reported the highest SPF values (0.841 and 0.717) for Cucumis melo leaf ultrasonic extract and Artemisia absinthium shoots methanolic

extract, respectively. Da Silva Fernandes et al [36] obtained a low SPF (2.5±0.3) for an aqueous fraction (AF) from Antarctic moss Sanionia uncinata; however, the SPF values increased more than three times in association with UV-filters with AF. The highest value (25.8±0.3) was reported in AF plus 3-(4-methylbenzylidene)-camphor [36]. In another study, the sunscreen formulations prepared by using the combination of organic UV filters (w/w %), and Olea europaea leaf extract (OLE, w/w %) and measured in vitro photoprotective efficacy using a UV transmittance analyzer for the determination of SPF values [7]. The SPF values 56±3, 42±5, and 21±2 were obtained by formulations that contained 5%, 3%, and 1% OLE, respectively [7]. Therefore, the association of UV filters with different plant extracts can be increased the efficiency of sunscreen formulations [7, 36].

### 3.3. Phototoxicity Analysis

The toxicity effects of the CC-AE and RD-AE on the 3T3 cell line were analyzed using the MTT-based colorimetric test after 24 h; however, phototoxicity was evaluated by comparing the difference in toxicity between the sample plate that was not exposed to UVA light and the sample plate exposed to UV light. The half-maximal effective concentration (EC<sub>50</sub>), without UVA light, for 3T3 cell line treated with CC-AE, RD-AE, and was measured to be 35.05±0.91 µg mL<sup>-1</sup>, 40.7±0.87 µg mL<sup>-1</sup>, and 16.79±0.35 µg mL<sup>-1</sup>, respectively (Table 4). According to analyses of

**Table 3.** Calculation of SPF of the aqueous extracts of plants in different concentrations by UV–visible spectrophotometry

Plant	Concentration of aqueous extract (µg mL <sup>-1</sup> )	SPF <sup>a</sup>
<i>Cuscuta campestris</i>	10	0.070±0.04
	50	2.000±0.05
	500	7.450±0.04
	2000	11.10±0.05
<i>Rosa damascena</i>	10	0.027±0.04
	50	0.110±0.05
	500	1.072±0.05
	2000	1.360±0.04

<sup>a</sup> Data represent means±SE (n=3).

the PIF, CC-AE (PIF=3.55) and RD-AE (PIF=2.35) were exhibited as probable phototoxic in the tested doses (Table 2). Chlorpromazine (PIF=35.59) was a potential phototoxic hazard and results were obtained for the cell viability with a difference approximately 35-fold in  $EC_{50}$  values, with and without UV light (Table 4). Amaral et al [39] presented that the  $IC_{50}$  values for Caryocar brasiliense supercritical  $CO_2$  extract (CBSE) in the phototoxicity assay considered 6.50% w/v in dark conditions and 35.53% w/v in irradiated conditions. According to the PIF value, the CBSE not exhibited phototoxic potential (PIF=0.18). Da Silva Fernandes et al [36] reported that the AF presented non-phototoxic (PIF=1.089) and the AF in mixtures with UV filters did not offer any phototoxic potential (PIF < 2). Svobodová et al [40] assessed the phototoxic potential of silymarin, an identical extract of the seeds of *Silybum marianum*, and its bioactive components. The obtained results showed that silymarin and its major component had no phototoxicity. Nathalie et al [35] assessed the phototoxic of some essential oils and showed that the PIF values of lemongrass oil, orange oil, and CPZ were 2.34, 2.21, and 31.24, respectively, as probably phototoxic hazard by 3T3/MTT procedure [35]. Consequently, in the present study, *C. campestris* and *R. damascena* aqueous extracts can be identified as probable phototoxic ingredients; however, additional investigations are needed to evaluate the health risks associated with them in vivo.

### 3.4. Analysis and Evaluation of protective effects of plant extracts on prevention of phototoxic effects of chlorpromazine

The effect of combinations of *C. campestris* aqueous extract, and/or *R. damascena* aqueous extract and chlorpromazine as strong phototoxic substance were assessed using the MTT-assay on the 3T3 cell line. These experiments were evaluated using the combination of a concentration of CC-AE or RD-AE ( $31.25 \mu\text{g mL}^{-1}$ ) with three concentrations of CPZ (0.1, 0.5 and,  $1 \mu\text{g mL}^{-1}$ ) in the presence and absence of UVA light. The obtained results of cell viability (%) are shown in Table 5. After 24 h, the measured cell viabilities (%) for the 3T3 cell line treated with a combination of the CC-AE and the different ranges of CPZ were  $53.70 \pm 1.51\%$ ,  $49.15 \pm 1.01\%$ , and  $43.67 \pm 1.2\%$ , respectively, in the absence of UVA light; however, the measured cell viabilities (%) were  $49.59 \pm 2.00\%$ ,  $45.44 \pm 1.51\%$ , and  $37.47 \pm 0.93\%$ , for similar concentrations, in the presence of UVA light (Table 5). The measured cell viabilities (%) for the studied concentration of RD-AE on the different concentrations of CPZ were  $51.29 \pm 1.13\%$ ,  $46.43 \pm 1.64\%$ , and  $41.82 \pm 0.86$ , respectively, in the absence of UVA light. Measured cell viabilities were  $43.36 \pm 1.02\%$ ,  $35.53 \pm 1.33\%$ , and  $47.78 \pm 2.1\%$ , respectively, in the presence of UVA light (Table 5). Generally, in the fact of UVA light, the measured cell viabilities of CPZ alone were lower than the combination of CC-AE and CPZ. The measured cell viabilities of CPZ alone at concentrations  $0.5 \mu\text{g mL}^{-1}$  and  $1 \mu\text{g mL}^{-1}$  were higher than the combination of RD-AE and CPZ (Table 5).

**Table 4.** Evaluation of the cytotoxicity and phototoxicity of the aqueous extracts of plants and chlorpromazine in murine fibroblasts cell (3T3)

Sample	UV radiation <sup>a</sup>	$EC_{50}$ <sup>b</sup>	PIF
<i>Cuscuta campestris</i> aqueous extract (CC-AE)	-	$35.05 \pm 0.91$	3.55
	+	$9.86 \pm 0.61$	
<i>Rosa damascena</i> aqueous extract (RD-AE)	-	$40.7 \pm 0.87$	2.35
	+	$17.31 \pm 0.22$	
Chlorpromazine (CPZ)	-	$16.79 \pm 0.35$	35.59
	+	$0.467 \pm 0.06$	

<sup>a</sup> - or + represents the tests performed with and without UV light.

<sup>b</sup> Data represent the mean $\pm$ SD of three experiments in different days

**Table 5.** Evaluation of protective effects of plant extracts on prevention of phototoxic effects of chlorpromazine in murine fibroblasts (3T3).

Plant	CAE* ( $\mu\text{g mL}^{-1}$ )	Chlorpromazine ( $\mu\text{g mL}^{-1}$ )	UV radiation <sup>a</sup>	Cell viability <sup>b</sup> (%)
<i>Cuscuta campestris</i>	31.25	1	-	53.70±1.51
	31.25	0.5	-	49.15±1.01
	31.25	0.1	-	43.67±1.20
	31.25	1	+	49.59±2.00
	31.25	0.5	+	45.44±1.51
	31.25	0.1	+	37.47±0.93
<i>Rosa damascena</i>	31.25	1	-	51.29±1.13
	31.25	0.5	-	46.43±1.64
	31.25	0.1	-	41.82±0.86
	31.25	1	+	43.36±1.02
	31.25	0.5	+	35.53±1.33
	31.25	0.1	+	47.78±2.10
Chlorpromazine	-	1	-	55.22±1.09
	-	0.5	-	53.60±2.11
	-	0.1	-	53.60±1.21
	-	1	+	47.66±1.21
	-	0.5	+	38.04±0.98
	-	0.1	+	32.86±0.88

\* CAE: Concentration of aqueous extract

<sup>a</sup> - or + represents the tests performed with and without UVA light

#### 4. Conclusion

Ultraviolet rays cause numerous injuries to the skin, so there is a vital need to protect it against its harmful effects. Natural materials usually have the ability to protect against the toxic effects of ultraviolet rays. Based on favorable antioxidant and anti-inflammatory properties of *Cuscuta campestris* (CC-AE) and *Rosa damascena* (RD-AE) plants, the current study investigated the photoprotection, cytotoxicity and phototoxicity activities of aqueous extracts of CC-AE and RD-AE in mouse fibroblast cells (3T3 cells) by MTT method and UV spectroscopy analysis. In this research, the SPF values of CC-AE and RD-AE were evaluated by UV-visible spectrophotometry applying the Mansur equation. At the concentration of 0.2 mg mL<sup>-1</sup>, the SPF values of CC-AE and RD-AE were 11.10±0.05 and 1.36±0.04, respectively. The EC<sub>50</sub> of CC-AE and RD-AE was 35.05±0.91  $\mu\text{g mL}^{-1}$  and

40.7±0.87  $\mu\text{g mL}^{-1}$ , respectively. The PIF values for CC-AE and RD-AE are in the range of probable phototoxic materials (PIF > 2 and < 5), but as these numbers are deficient and near the range of non-phototoxic, they could be hypothesized for future anti-solar formulations. Moreover, in the presence of UVA light, the measured cell viabilities of CPZ alone were lower than the combination of CC-AE and CPZ. Overall, the presented data in this report showed that RD-AE, with SPF and PIF of 11 and 2.35 and various prominent biological effects, could be regarded as an efficient natural product to be considered in sunscreen formulations.

#### 5. Acknowledgements

We thank the Pharmaceutics Research Center, Institute of Neuropharmacology, Kerman University of Medical Sciences (Kerman, Iran) for their support (Grant number: 95000346).

## 6. References

- [1] S.R. Varma, T.O. Sivaprakasam, I. Arumugam, N. Dilip, M. Raghuraman, K. Pavan, M. Rafiq, R. Paramesh, In vitro anti-inflammatory and skin protective properties of Virgin coconut oil, *J. Tradit. Complement. Med.*, 9 (2019) 5-14. <https://doi.org/10.1016/j.jtcme.2017.06.012>.
- [2] K.C. Rangel, L.Z. Villela, K.d.C. Pereira, P. Colepicolo, H.M. Debonsi, L.R. Gaspar, Assessment of the photoprotective potential and toxicity of Antarctic red macroalgae extracts from *Curdiea racovitzae* and *Iridaea cordata* for cosmetic use, *Algal Res.*, 50 (2020) 101984. <https://doi.org/10.1016/j.algal.2020.101984>.
- [3] G. Bhandari, S. Baurai, Assessment of in vitro sun protection factor of plant extracts by ultraviolet spectroscopy method, *Univ. J. Phytochem. Ayurvedic Heights*, 2 (2020) 20-25. [https://doi.org/10.51129/ujpah-2020-29-2\(3\)](https://doi.org/10.51129/ujpah-2020-29-2(3)).
- [4] M. Majeed, S. Majeed, R. Jain, L. Mundkur, H.R. Rajalakshmi, P. Lad, P. Neupane, A randomized study to determine the sun protection factor of natural pterostilbene from *pterocarpus marsupium*, *Cosmetics*, 7 (2020) 16. <https://doi.org/10.3390/cosmetics7010016>.
- [5] D. Bhattacharjee, S. Preethi, A.B. Patil, V. Jain, A comparison of natural and synthetic sunscreen agents: a review, *Int. J. Pharm. Sci. Res.*, 13 (2021) 3494-3505. <https://doi.org/10.31838/ijpr/2021.13.01.524>.
- [6] T. Sharma, V. Tyagi, M. Bansal, Determination of sun protection factor of vegetable and fruit extracts using UV-Visible spectroscopy: A green approach, *Sustain. Chem. Pharm.*, 18 (2020) 100347. <https://doi.org/10.1016/j.scp.2020.100347>.
- [7] A.C. Da Silva, J.P. Paiva, R.R. Diniz, V.M. Dos Anjos, A.B.S. Silva, A.V. Pinto, E.P. Dos Santos, A.C. Leitão, L.M. Cabral, C.R. Rodrigues, Photoprotection assessment of olive (*Olea europaea* L.) leaves extract standardized to oleuropein: In vitro and in silico approach for improved sunscreens, *J. Photochem. Photobiol. B*, 193 (2019) 162-171. <https://doi.org/10.1016/j.jphotobiol.2019.03.003>.
- [8] M. Radice, S. Manfredini, P. Ziosi, V. Dissette, P. Buso, A. Fallacara, S. Vertuani, Herbal extracts, lichens and biomolecules as natural photo-protection alternatives to synthetic UV filters. A systematic review, *Fitoterapia*, 114 (2016) 144-162. <https://doi.org/10.1016/j.fitote.2016.09.003>.
- [9] B. Prasanth, A. Soman, J. Jobin, P.S. Narayanan, A.P. John, Plants and phytoconstituents having sunscreen activity, *World J. Curr. Med. Pharm. Res.*, 2 (2020) 14-20. <https://doi.org/10.37022/WJCMR.2020.02019>.
- [10] F. Merlin, W. Ratnasooriya, R. Pathirana, In vitro investigation of sunscreen activity and evaluation of phytochemical profile of methanolic leaf extract of *Rauvolfia tetraphylla*, *J. Pharmacogn. Phytochem.*, 9 (2020) 2063-2067. <https://www.phytojournal.com/>
- [11] A.D. Permana, R.N. Utami, A.J. Courtenay, M.A. Manggau, R.F. Donnelly, L. Rahman, Phytosomal nanocarriers as platforms for improved delivery of natural antioxidant and photoprotective compounds in propolis: An approach for enhanced both dissolution behaviour in biorelevant media and skin retention profiles, *J. Photochem. Photobiol.*, 205 (2020) 111846. <https://doi.org/10.1016/j.jphotobiol.2020.111846>.
- [12] M. Hupel, N. Poupard, E.A. Gall, Development of a new in vitro method to evaluate the photoprotective sunscreen activity of plant extracts against high UV-B radiation, *Talanta*, 86 (2011) 362-371. <https://doi.org/10.1016/j.talanta.2011.09.029>.
- [13] M.H. Boskabady, M.N. Shafei, Z. Saberi, S. Amini, Pharmacological effects of *Rosa damascena*, Iran. *J. Basic Med. Sci.*, 14 (2011) 295. <https://ijbms.mums.ac.ir/>
- [14] M. Mahboubi, *Rosa damascena* as holy ancient herb with novel applications, *J. Tradit.*

- Complement. Med., 6 (2016) 10-16. <https://doi.org/10.1016/j.jtcme.2015.09.005>.
- [15] N.Kumar, B. Singh, V.K. Kaul, Flavonoids from *Rosa damascena* Mill, Nat. Prod. Commun., 1 (2006) 1934578X0600100805. <https://doi.org/10.1177/1934578X0600100805>.
- [16] N.G. Baydar, H. Baydar, Phenolic compounds, antiradical activity and antioxidant capacity of oil-bearing rose (*Rosa damascena* Mill.) extracts, Ind. Crops Prod., 41 (2013) 375-380. <https://doi.org/10.1016/j.indcrop.2012.04.045>.
- [17] N. Yassa, F. Masoomi, R. Rohani, Chemical composition and antioxidant activity of the extract and essential oil of *Rosa damascena* from Iran, Population of Guilan, DARU J. Pharm. Sci., 17 (2009) 175-180. <http://daru.tums.ac.ir/index.php/daru/article/view/541>
- [18] V. Hajhashemi, A. Ghannadi, M. Hajiloo, Analgesic and anti-inflammatory effects of *Rosa damascena* hydroalcoholic extract and its essential oil in animal models, Iran. J. Pharm. Res., 9 (2010) 163. <https://pubmed.ncbi.nlm.nih.gov/24363723/>
- [19] G. Latifi, A. Ghannadi, M. Minaiyan, Anti-inflammatory effect of volatile oil and hydroalcoholic extract of *Rosa damascena* Mill. on acetic acid-induced colitis in rats, Res. Pharm. Sci., 10 (2015) 514. <https://www.rpsjournal.net/>
- [20] F. Fatemi, A. Golbodagh, R. Hojihosseini, A. Dadkhah, K. Akbarzadeh, S. Dini, M.R.M. Malayeri, Anti-inflammatory effects of deuterium-depleted water plus *Rosa damascena* mill. Essential oil via cyclooxygenase-2 pathway in rats, Turk. J. Pharm. Sci., 17 (2020) 99. <https://doi.org/10.4274/tjps.galenos.2018.24381>.
- [21] M. Behbahani, Evaluation of in vitro anticancer activity of *Ocimum basilicum*, *Alhagi maurorum*, *Calendula officinalis* and their parasite *Cuscuta campestris*, PloS One, 9 (2014) e116049. <https://doi.org/10.1371/journal.pone.0116049>.
- [22] E.K. Selvi, H. Turumtay, A. Demir, E.A. Turumtay, Phytochemical profiling and evaluation of the hepatoprotective effect of *Cuscuta campestris* by high-performance liquid chromatography with diode array detection, Anal. Lett., 51 (2018) 1464-1478. <https://doi.org/10.1080/00032719.2017.1382502>.
- [23] M. Moradzadeh, A. Hosseini, H. Rakhshandeh, A. Aghaei, H.R. Sadeghnia, *Cuscuta campestris* induces apoptosis by increasing reactive oxygen species generation in human leukemic cells, Avicenna J. Phytomed., 8 (2018) 237. <https://ajp.mums.ac.ir/>
- [24] W.H. Peng, Y.W. Chen, M.S. Lee, W.T. Chang, J.C. Tsai, Y.C. Lin, M.K. Lin, Hepatoprotective effect of *Cuscuta campestris* Yunck. whole plant on carbon tetrachloride induced chronic liver injury in mice, Int. J. Mol. Sci., 17 (2016) 2056. <https://doi.org/10.3390/ijms17122056>.
- [25] E. Jafari, A. Bahmanzadegan, G. Ghanbarian, V. Rowshan, Antioxidant activity and total phenolic content from aerial parts of three *Cuscuta* species, Anal. Chem. Lett., 5 (2015) 377-384. <http://dx.doi.org/10.1080/22297928.2016.1143394>.
- [26] M.M. Akiner, E.K. Selvi, M. Öztürk, I. Güney, U. Asu, Toxic efficacy of *Cuscuta campestris* Yunck. (Solanales: Convolvulaceae) and *Lupinus albus* L. (Fabales: Fabaceae) plant crude extracts against nymphs and adults of *Orosanga japonica* (Melichar, 1898) (Hemiptera: Ricaniidae) under laboratory conditions, Turk. Entomol. Derg., 45 (2021) 65-75. <https://doi.org/10.16970/entoted.743439>.
- [27] P. Khazaeli, M. Mehrabani, M.R. Heidari, G. Asadikaram, M.L. Najafi, Prevalence of aflatoxin contamination in herbs and spices in different regions of Iran, Iran. J. Public Health, 46 (2017) 1540. <https://ijph.tums.ac.ir/index.php/ijph>
- [28] P. Khazaeli, M. Mehrabani, Screening of sun protective activity of the ethyl acetate extracts of some medicinal plants, Iran. J. Pharm. Res., 1 (2010) 5-9. <https://doi.org/10.22037/IJPR.2010.738>.

- [29] J.D.S. Mansur, M.N.R. Breder, M.C.D.A. Mansur, R.D. Azulay, Determinação do fator de proteção solar por espectrofotometria, *An. Bras. Dermatol.*, 61 (1986) 121-124. [https://www.medscape.com/viewpublication/2466\\_33](https://www.medscape.com/viewpublication/2466_33)
- [30] M. Mostafavi, I. Sharifi, S. Farajzadeh, P. Khazaeli, H. Sharifi, E. Pourseyedi, S. Kakooei, M. Bamorovat, A. Keyhani, M.H. Parizi, Niosomal formulation of amphotericin B alone and in combination with glucantime: In vitro and in vivo leishmanicidal effects, *Biomed. Pharmacother.*, 116 (2019) 108942. <https://doi.org/10.1016/j.biopha.2019.108942>.
- [31] B. Behnam, M. Rezazadehkermani, S. Ahmadzadeh, A. Mokhtarzadeh, S.N. Nematollahi-Mahani, A. Pardakhty, Microniosomes for concurrent doxorubicin and iron oxide nanoparticles loading; preparation, characterization and cytotoxicity studies, *Artif. Cells Nanomed. Biotechnol.*, 46 (2018) 118-125. <https://doi.org/10.1080/21691401.2017.1296850>.
- [32] E. Mohammadi, M. Zeinali, M. Mohammadi-Sardoo, M. Iranpour, B. Behnam, A. Mandegary, The effects of functionalization of carbon nanotubes on toxicological parameters in mice, *Hum. Exp. Toxicol.*, 39 (2020) 1147-1167. <https://doi.org/10.1177/0960327119899988>.
- [33] R. Mohammadinejad, A. Dehshahri, H. Sassan, B. Behnam, M. Ashrafzadeh, A. Samareh Gholami, A. Pardakhty, A. Mandegary, Preparation of carbon dot as a potential CRISPR/Cas9 plasmid delivery system for lung cancer cells, *Minerva Biotechnol.*, 32 (2020) 106-113. <https://doi.org/10.23736/S1120-4826.20.02618-X>.
- [34] M. Moballeggh-Nasery, A. Mandegary, T. Eslaminejad, M. Zeinali, A. Pardakhti, B. Behnam, M. Mohammadi, Cytotoxicity evaluation of curcumin-loaded affibody-decorated liposomes against breast cancerous cell lines, *J. Liposome Res.*, 31 (2021) 189-194. <https://doi.org/10.1080/08982104.2020.1755981>.
- [35] D. Nathalie, G. Yannick, B. Caroline, D. Sandrine, F. Claude, C. Corinne, F. Pierre-Jacques, Assessment of the phototoxic hazard of some essential oils using modified 3T3 neutral red uptake assay, *Toxicol. In Vitro*, 20 (2006) 480-489. <https://doi.org/10.1016/j.tiv.2005.08.018>.
- [36] A. Da Silva Fernandes, L.B. Brito, G.A.R. Oliveira, E.R.A. Ferraz, H. Evangelista, J.L. Mazzei, I. Felzenszwalb, Evaluation of the acute toxicity, phototoxicity and embryotoxicity of a residual aqueous fraction from extract of the Antarctic moss *Sanionia uncinata*, *BMC Pharmacol. Toxicol.*, 20 (2019) 1-10. <https://doi.org/10.1186/s40360-019-0353-3>.
- [37] Z. Hashemi, M.A. Ebrahimzadeh, M. Khalili, Sun protection factor, total phenol, flavonoid contents and antioxidant activity of medicinal plants from Iran, *Trop. J. Pharm. Res.*, 18 (2019) 1443-1448. <https://doi.org/10.4314/tjpr.v18i7.11>.
- [38] M.A. Ebrahimzadeh, R. Enayatifard, M. Khalili, M. Ghaffarloo, M. Saeedi, J.Y. Charati, Correlation between sun protection factor and antioxidant activity, phenol and flavonoid contents of some medicinal plants, *Iran. J. Pharm. Res.*, 13 (2014) 1041. <https://brieflands.com/journals/iranian-journal-of-pharmaceutical-research/>
- [39] L.F. Amaral, P. Moriel, M.A. Foglio, P.G. Mazzola, Evaluation of the cytotoxicity and phototoxicity of *Caryocar brasiliense* supercritical carbon dioxide extract, *BMC Complement. Altern. Med.*, 14 (2014) 1-6. <https://doi.org/10.1186/1472-6882-14-450>.
- [40] A.R. Svobodová, B. Zálešák, D. Biedermann, J. Ulrichová, J. Vostálová, Phototoxic potential of silymarin and its bioactive components, *J. Photochem. Photobiol. B*, 156 (2016) 61-68. <https://doi.org/10.1016/j.jphotobiol.2016.01.011>.



# Evaluating the effect of ethanol foliar feeding on the essential oil, phenolic content, and antioxidant activities of *Ducrosia anethifolia*

Aliyeh Sarabandi<sup>a</sup>, Amirhossein Sahebkar<sup>b,c,d,e</sup>, Javad Asilif, Moharam Valizadeh<sup>g</sup>, Khalilollah Taheri<sup>h</sup>, Jafar Valizadeh<sup>h,\*</sup>, and Maryam Akaberi<sup>f,\*</sup>

<sup>a</sup> Department of Phytochemistry, Faculty of Science, University of Sistan and Baluchistan, Zahedan, Iran.

<sup>b</sup> Applied Biomedical Research Center, Mashhad University of Medical Sciences, Mashhad, Iran.

<sup>c</sup> Biotechnology Research Center, Pharmaceutical Technology Institute, Mashhad University of Medical Sciences, Mashhad, Iran.

<sup>d</sup> School of Medicine, The University of Western Australia, Perth, Western Australia, Australia.

<sup>e</sup> Department of Biotechnology, School of Pharmacy, Mashhad University of Medical Sciences, Mashhad, Iran.

<sup>f</sup> Department of Pharmacognosy, School of Pharmacy, Mashhad University of Medical Sciences, Mashhad, Iran.

<sup>g</sup> Faculty of Environmental Sciences and Sustainable Agriculture, Sistan and Baluchistan University, Zahedan, Iran.

<sup>h</sup> Department of Biology, Faculty of Science, University of Sistan and Baluchistan, Zahedan, Iran

## ARTICLE INFO:

Received 27 Jul 2022

Revised form 11 Oct 2022

Accepted 23 Nov 2022

Available online 28 Dec 2022

## Keywords:

*Ducrosia anethifolia*,  
 GC-MS,  
 Spectrophotometry,  
 Foliar feeding,  
 Essential oil,  
 Antioxidant

## ABSTRACT

*Ducrosia anethifolia* (Asteraceae) is a medicinal aromatic plant distributed in Iran and Afghanistan. This research aims to investigate the composition of the plant essential oil, determine the total flavonoid and phenolic contents, and evaluate its antioxidant activities after ethanol foliar feeding. For this purpose, 0, 10, 20, 40, and 80% v/v of aqueous ethanol solutions were sprayed on different batches of the plants. Then, the essential oils were obtained using water distillation. Compounds were analyzed by Gas chromatography-mass spectrometry technique (GC-MS) using a validated method. The method was validated as per the ICH guidelines for linearity, precision, accuracy, robustness, LOD, and LOQ. The total contents of phenols and flavonoids were measured using spectrophotometric methods. The antioxidant activity was evaluated using DPPH and FRAP assays. The results showed that n-decanal, cis-verbenyl acetate and dodecanal were the major compounds in all treatments. However, alcohol could cause significant differences in the essential oils qualitatively and quantitatively. The results showed that 40% ethanol could increase the number of phenolics and flavonoids and consequently the antioxidant activity. Thus, ethanol foliar feeding can be used as an appropriate approach to increase the essential oil of *D. anethifolia* as well as its phenolic and flavonoid contents.

## 1. Introduction

*Ducrosia anethifolia* (DC.) Boiss. (Asteraceae) is an aromatic herbaceous and biennial plant with a height of 10–30 cm. The stems are glabrous and branched mostly from the base. The leaves are ovate-oblong, 2–6 cm long, and branched,

with a petiole length of 5–18 cm. The edges of the petals are jagged and slightly shaggy and the compound umbel inflorescence has white flowers. In Iran, the plant is known as Moshgak, Mushk Boo, Darvishan Ginger, Reshgak, Khorkhundai, Gavarshkh, and mount Coriander [1]. The genus

*Ducrosia* has three species in Iran including *D. anethifolia*, *D. assadii* Alava, and *D. flabellifolia* Boiss. *Ducrosia anethifolia* grows wildly in mountainous and plain areas on sandy soils in

\*Corresponding Author: Maryam Akaberi and Jafar Valizade

Email: [akaberim@mums.ac.ir](mailto:akaberim@mums.ac.ir) and [djafar.walisade@gmail.com](mailto:djafar.walisade@gmail.com)  
<https://doi.org/10.24200/amecj.v5.i04.213>

different regions of Iran such as Kerman, Khorasan, Zanjan, Shushtar, Behbahan, Shiraz, Kazerun, Borazjan, Noorabad, Farashband, Firoozabad, Jahrom, Darab, and Sistan Baluchestan [2]. It also grows natively in countries from the Mediterranean range to W. Pakistan such as Afghanistan, Pakistan, Iraq, Syria, Lebanon, and some Arab countries [3]. *Ducrosia assadii* is endemic to Iran and *D. flabellifolia* is native to Syria, W. Iran, and Arabian Peninsula [4]. Essential oils are one of the most pharmacologically important constituents in plants belonging to *Ducrosia*. Terpene compounds are reported to be responsible for many medicinal activities of the oil of this medicinal plant. The volatile compounds of this aromatic plant are used as a flavoring additive in various beverages and desserts. Besides, Moshgak is also used as an edible vegetable [5, 6]. Several studies have investigated the essential oil composition of *D. anethifolia* revealing that the long chain oxygenated hydrocarbons such as decanal, dodecanal, and decanol constitute the major compounds in the essential oil. In addition, monoterpenes including  $\alpha$ -pinene,  $\alpha$ -thujene, linalool, cis-citronellyl acetate, and oxygenated sesquiterpenes such as chrysanthenyl acetate have been reported as the main constituents of the essential oil [7]. In Iranian traditional medicine, the aerial parts of *D. anethifolia* have been used to relieve various pains such as headaches, back pain, and colic pain. It has been also used for the treatment of seizures, insomnia, heartburn, cataract, inflammation of the inner wall of the nose, and colds. Pharmacological studies show that the plants belonging to this genus have muscle relaxant, CNS depressant, and anti-depressant properties. In addition, the essential oils obtained from *D. anethifolia* have antimicrobial properties against gram-positive bacteria, yeasts, and some dermatophytes. The essential oil of *D. anethifolia* is reported to have antifungal properties by preventing the growth of parasitic fungi such as *Candida albicans* on the skin [8-10]. It could also improve kidney function and lower the lipid levels of the blood. Alpha-pinene as one of the major compounds in essential oil is probably responsible

for the anti-anxiety effect of the plant. Myrcene, as another main component of the plant, has several pharmacological activities including anti-radical, inhibitory effects, anti-cancer, and anti-tumor properties [11-13]. The use of methanol and ethanol foliar feeding is one of the most important approaches for increasing plant growth and harvest yield. Research has shown that ethanol becomes acetaldehyde after penetration into the plant tissue. Acetaldehyde is transformed into acetate (acetic acid) by the acetaldehyde dehydrogenase enzyme. Acetic acid also converts to acetyl coenzyme A, which eventually turns into carbon dioxide and dioxido. Methanol, ethanol, and other alcohols are non-toxic to plants and can simply penetrate the membrane of plant cells. The absorption rate directly depends on the density of alcohol. Therefore, the application of methanol and ethanol foliar feeding on the aerial parts of C3 plants (the plants that only use the standard method of carbon dioxide fixation by the enzyme Rubisco) [14], in which their light breathing is large can compensate for part of the stabilized carbon losses and in this way, increase pure photosynthesis and dry matter production per unit area. As a result, some studies conducted in the field of agronomic C3 plants have shown that methanol could affect the performance of these plants positively [15]. Thus, the aim of this study was to evaluate the effect of ethanol foliar feeding on the essential oil composition and yields of *D. anethifolia*. In addition, the antioxidant activities of the plant extract were investigated and the total phenol and flavonoid contents of the plant were measured.

## 2. Material and Methods

### 2.1. Planting and harvesting

This study was performed at the research farm of the research center for medicinal and ornamental plants of Sistan and Baluchestan University with a latitude of 29°27'N and a longitude of 60°51'E at an altitude of 1410 m from sea level. In this experiment, seeds of the plant samples were planted in 7 rows of binary, each row was about 80 centimeters and the distance between every two rows was 20

centimeters. The plants were divided into five treatment groups including control (distilled water) and four concentrations of ethanol solution (10, 20, 40, and 80%). The ethanol spraying was performed before the flowering stage of the plants every three days 6 times. The spraying process began in early May and the plants were harvested in early June (spring 2016). After harvesting, the aerial parts of the plants were dried in the shade and stored until use. After collecting, the plants were transferred to the laboratory and dried in the shade. Then, the plants were milled, powdered, and prepared for essential oil.

### 2.2. Extraction Procedure

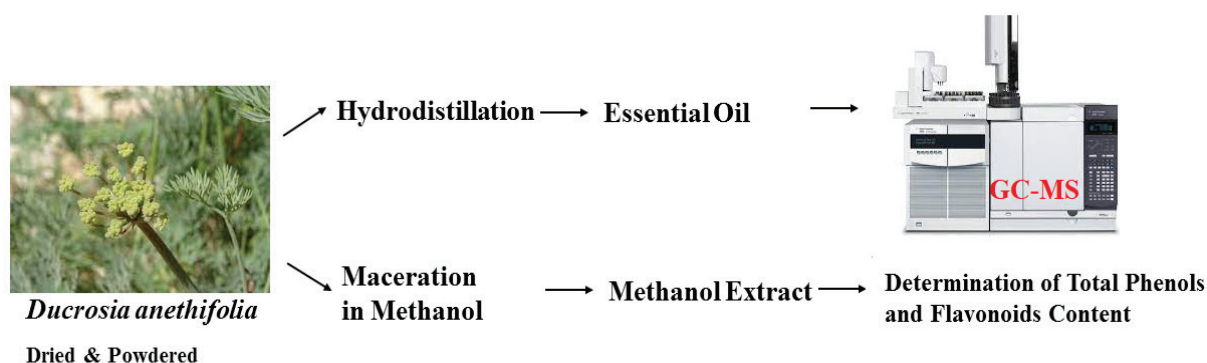
The dried aerial parts of the plants for each treatment were powdered separately with an electric mill. Then, the powdered samples were subjected to extraction. The essential oil of the samples was obtained by water distillation. For this purpose, 50 g of each dried plant sample was subjected to hydrodistillation for 3 h using a Clevenger-type apparatus (1000 ml water). The essential oils were collected in separate glass vials and were dehydrated with aid of sodium sulfate and magnesium sulfate salts. In order to obtain the extracts of the samples, the maceration method was used. About 5.0 g of the powdered samples were weighed accurately and added to separate Erlenmeyer flasks containing 50 ml methanol (covered with aluminum sheets) and placed on a magnetic stirrer for 24 hours. Then, the extracts were filtered with Watman filter paper and the solvent was removed by a rotary evaporator to obtain dry extracts (Schema 1).

### 2.3. GC-MS Analysis

In the next step, the essential oils were subjected to the GC-MS analysis to separate the chemical constituents and identify them according to their mass characteristics and retention times. The analysis of the essential oils was carried out using an Agilent system equipped with an HP-5S column (30 m × 250 μm, film thickness 0.25 μm) interfaced with a quadrupole mass detector (MS 5977A). Oven temperature 50-250°C (3°C per minute), injector temperature 250°C, injection volume: 0.1 μL, split injection with a split ratio of 1:50 helium as the carrier gas with flow rate 1 mL min<sup>-1</sup>, ion source: 70 eV, ionization current: 150 μA, and scan range: 35-465. The method was validated as per the ICH guidelines for linearity, precision, accuracy, robustness, LOD, and LOQ according to our previous study [16]. Identification of the chemical constituents of the essential oil was carried out using AMDIS software (www.amdis.net) and identified by its retention indices with reference to the n-alkanes series (C6-C20), comparison of their retention time, mass spectra, and computer matching with the Wiley 7 nL and NIST library database.

### 2.4. Determination of total phenolic content

Total phenol content was determined by the Folin-Ciocalteu reagent. A dilute solution of the extracts (0.05:1 g mL<sup>-1</sup>) or gallic acid (standard phenolic compound) was mixed with the Folin-Ciocalteu reagent (2.5 ml, 1:10 diluted with distilled water) and aqueous Na<sub>2</sub>CO<sub>3</sub> (2 ml, 5%). The mixture was allowed to stand for 30 min and the phenolic contents were determined by colorimetry at 765 nm. The total phenolic content was determined as mg of gallic



**Schema 1.** Procedure for determination of flavonoid, phenolic contents in *Ducrosia anethifolia*

acid equivalent using an equation obtained from the standard gallic acid calibration curve [17].

### 2.5. Determination of total flavonoid content

The flavonoid contents of the extracts were measured by aluminum chloride coloration using quercetin as standard [18]. To extract flavonoids, 0.1 g of each extract was solved in 10 mL ethanol 80%. Then, 100  $\mu$ L of the solution was added to a test tube, and 100  $\mu$ L of 10%  $\text{AlCl}_3$ , 100  $\mu$ L of 1 M sodium acetate, 1.5 mL of ethanol 96%, and 3.2 mL of distilled water were added and vortexed for 1 minute. The control treatment included 3.4 mL of distilled water, 100  $\mu$ L of 1 M sodium acetate, and 1.5 mL ethanol 96%. After 30 minutes, adsorption was read at 415 nm.

### 2.6. DPPH free radical scavenging activity

This spectrophotometric method was used to evaluate the antioxidant activity of the extracts. DPPH is a reagent that measures free radical scavenging activity [19]. Zero, 0.01, 0.02, 0.03, 0.04, 0.05 mL of concentration 2000  $\text{mg L}^{-1}$  of the extracts and positive control (ascorbic acid) were added to 1.0 mL of 0.1 mM solution of DPPH (Sigma, St Louis) in methanol. The reaction mixture was shaken and then incubated for 30 min at room temperature. The remaining amount of DPPH was determined at 517 nm against a blank using a spectrophotometer (Milton Roy Company Spectronic 20D). All tests were carried out five times.

### 2.7. Ferric-reducing antioxidant power (FRAP) assay

The antioxidant capacity of the plant extracts was done by Iron reduction (FRAP assay) according to Sadeghi et al [17]. For this purpose, 300 mM acetate buffer (pH 3.610) mM TPTZ solution in 40 mM HCl, and 20 mM  $\text{FeCl}_3 \cdot 6\text{H}_2\text{O}$  solution were mixed for the preparation of stock. FRAP reagent was prepared right away before analysis by mixing 25 mL acetate buffer, 2.5 mL TPTZ solution, and 2.5 mL  $\text{FeCl}_3 \cdot 6\text{H}_2\text{O}$  solution. Plant extracts ( $1000 \mu\text{g mL}^{-1}$ ) were prepared. 200  $\mu\text{g mL}^{-1}$  of the extracts was mixed with 1.8 mL of the FRAP reagent and was incubated at 37  $^\circ\text{C}$  for 30 min in the dark condition before being

used. Then, readings of the colored products (ferrous tripyridyltriazine complex) were determined at 595 nm against a distilled water blank.  $\text{FeSO}_4 \cdot 7\text{H}_2\text{O}$  (100-1000  $\mu\text{M}$ ) was used for calibration. Ascorbic acid was used as a positive control. Results are expressed as mM  $\text{Fe}^{2+}$  per mg sample [17].

## 3. Results

### 3.1. Chemical composition of the essential oils

Table 1 shows the major components of the essential oil in the different treatments and control along with the percentage of each compound. The results revealed that ethanol spraying had a significant effect on the amount and yield of the essential oils. The yield of the essential oil was enhanced by increasing the amount of alcohol from 10% to 40% treatment with a decline in 80% alcohol-treated samples. The chemical composition of the essential oil of the control and that of the 10% treatment were to some extent similar. Interestingly, while in the two treatments 20% and 40%, the chemical composition is rather the same, their chemical composition is different from the blank and 10% treatment. Although the chemical composition of the 80% treatment was similar to 20% and 40%, there were some differences. For instance, compound 2-isopropyl-5-methyl-3-cyclohexene-1-one was only identified in the 80% treatment. Decanal, cis-verbenyl acetate, and dodecanal were major components in all samples with variations in different treatments.

Table 2 shows that monoterpenes and other compounds including alkanes are dominated in the essential oil samples. The number of oxygenated monoterpenes is increased in 20%, 40%, and 80% treatments while hydrocarbon monoterpenes are decreased in these samples compared to the control. Hydrocarbon monoterpenes are absent in the 20% sample.

The number of oxygenated sesquiterpenes is almost the same in all treatments with a small increase of 20% and 40%. The highest number of hydrocarbon sesquiterpenes were observed for 20% sample.

### 3.2. Determination of total flavonoid content

The highest and the lowest amount of total phenol per 1g of the plant powder were observed for 40%

**Table 1.** The major compounds identified in the essential oil of the different treatments.

<sup>a</sup> Rt	<sup>b</sup> RI	Compound	Control	10%	20%	40%	80%
4.936	939	$\alpha$ -Pinene	5.272	4.678	-	-	0.564
5.52	975	Sabinene	0.936	0.876	-	-	-
5.589	979	$\beta$ -Pinene	0.251	0.223	-	-	-
5.737	990	$\beta$ -Myrcene	1.428	1.341	-	-	-
6.287	1024	$\rho$ -Cymene	4.217	3.593	-	-	0.330
6.355	1029	d-Limonene	5.178	4.575	-	-	0.348
7.271	1088	Terpinolene	0.343	0.329	-	0.523	-
7.46	1100	Nonanal	0.849	1.018	0.425	-	1.057
8.135	1137	cis-Verbenol	0.809	0.682	0.779	-	0.927
8.204	1140	Citronellal	0.801	0.902	-	-	-
8.364	1150	trans-Verbenol	0.247	0.210	0.962	0.607	0.253
8.432	1169	1-Nonanol	0.732	0.783	-	-	0.710
8.713	1179	$\rho$ -Cymen-8-ol	0.458	0.419	-	-	0.620
8.776	1185	Cryptone	0.606	0.696	-	-	-
8.965	1200	Decanal	20.044	20.681	9.098	10.596	13.571
9.274	1250	3,7-Dimethyl-2-octen-1-ol	1.709	1.479	-	-	0.353
9.754	1274	<sup>c</sup> IMC Hexane	-	-	-	-	10.191
9.817	1282	cis-Verbenyl acetate	20.598	18.151	36.274	42.415	21.766
9.88	1286	5-Undecanol	1.816	1.560	1.038	0.778	1.311
10.155	1290	Lavandulyl acetate	0.915	0.828	1.562	1.315	0.623
10.367	1298	trans-Pinocarvyl acetate	-	-	0.420	1.093	-
10.395	1306	Undecanal	1.008	1.183	-	-	1.131
10.498	1352	Citronellyl acetate	0.659	0.634	2.058	2.255	1.019
11.408	1381	Geranyl acetate	1.387	1.467	0.958	1.243	0.331
11.677	1408	Z-Caryophyllene	0.451	0.575	0.490	-	0.243
11.757	1410	Dodecanal	10.768	11.953	6.777	6.431	11.053
12.072	1420	$\beta$ -Caryophyllene	1.666	1.731	1.359	1.308	0.351
12.501	1436	$\gamma$ -Elemene	3.458	3.246	22.994	1.055	2.038
13.25	1510	<sup>d</sup> CPCP	-	-	-	18.913	16.705
14.029	1578	Spathulenol	1.898	2.096	2.287	1.577	1.417
14.12	1583	Caryophyllene oxide	1.568	1.709	1.304	0.796	1.161
14.252	1612	Tetradecanal	0.342	0.452	0.467	0.425	0.814
14.515	1620	Unknown	2.536	2.689	1.287	1.165	0.604
14.652	1632	$\gamma$ -Eudesmol	0.264	0.266	2.008	3.832	1.287
14.738	1677	Z-Nerolidyl acetate	0.778	0.833	0.724	0.462	0.225
14.887	1680	$\beta$ -Eudesmol	0.506	0.576	1.168	-	1.723
14.939	1685	n-Tetradecanol	1.092	1.334	0.990	0.665	1.582
<b>Total</b>			73.176	90.761	95.429	97.454	94.287

<sup>a</sup>Retention time; <sup>b</sup>Kovats Index<sup>c</sup>MC Hexane: 2-Isopropyl-5-methyl-3-cyclohexen-1-one<sup>d</sup>CPCP: 2-Cyclopentylidene cyclopentanone

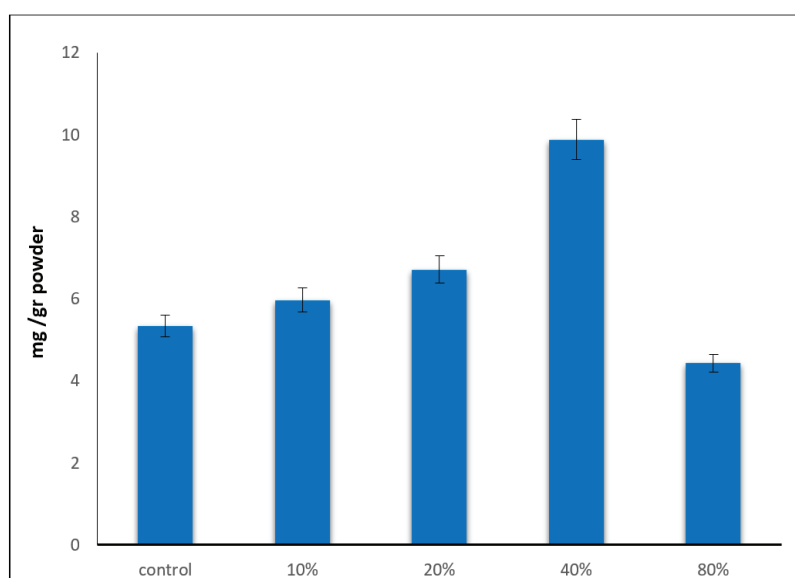
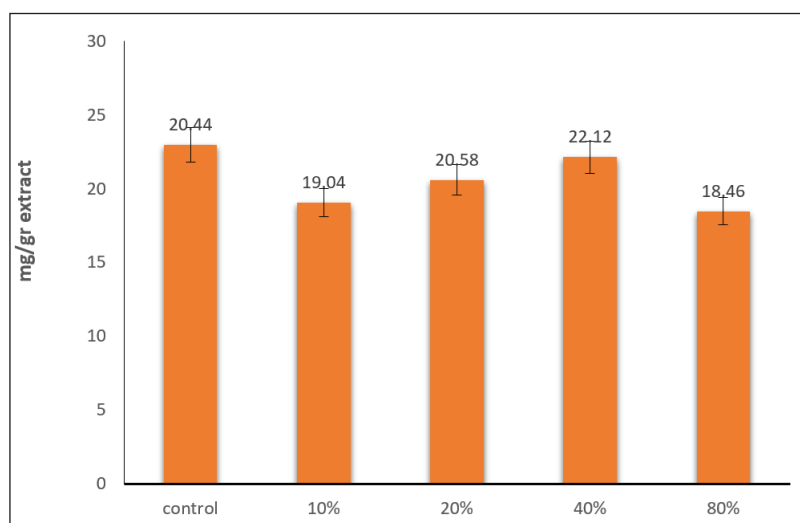
**Table 2.** The amount of different volatile compounds in different treatments.

Compounds	Control	10%	20%	40%	80%
Oxygenated Monoterpenes	28.189	25.468	43.013	59.524	36.083
Hydrocarbon Monoterpenes	17.625	16.453	-	0.523	1.272
Oxygenated Sesquiterpenes	5.014	5.480	7.491	6.667	5.813
Hydrocarbon Sesquiterpenes	5.575	5.552	24.843	2.363	4.670
Other Compounds	25.883	38.964	18.795	37.808	47.934

and 80% ethanol samples, respectively (Fig. 1). The highest and the lowest amount of total phenol per 1.0 g of the plant extract were observed for 40% and 10% ethanol samples, respectively (Fig. 2).

### 3.3. Determination of total flavonoid content

As shown in Figure 3, the 40% ethanol treatment showed the highest amount of flavonoid compared to the rest of the treatments.

**Fig. 1.** The total phenol content in the plant powder of different treatments.**Fig. 2.** The total phenol content of the extracts from different treatments.

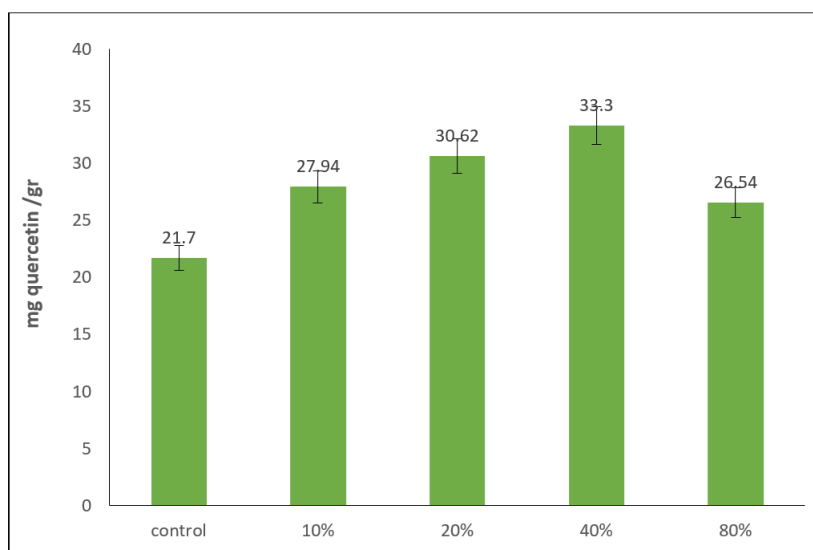


**Fig. 3.** The total flavonoid content of the extracts from different treatments.

### 3.4. DPPH free radical scavenging activity

The results of DPPH radical-scavenging activity assay are shown in Figure 4. Considering the large variation of  $IC_{50}$ , the lowest antioxidant activity was observed for 80% treatment compared to the control. Treatments with 10%, 20%, and 40% showed almost the same antioxidant activity, all higher than that of the control.

### 3.5. FRAP assay

All analyzed extracts demonstrated significant antioxidant capacities with FRAP test. The 40% treatment showed 53.00  $mMFe^{2+}/mg$  sample

with the highest antioxidant activity compared to reducing power of ascorbic acid (69.00  $mMFe^{2+}/mg$  sample) (Fig. 5).

Totally, the results from the determination of phenolic and flavonoid contents of the samples as well as DPPH and FRAP assays revealed that the amount of these compounds and the antioxidant capacity of the plant samples were influenced by the use of ethanol spraying which was shown in Table 3. By increasing the concentration of alcohol from 10% to 40%, the phenol and flavonoid contents and consequently the antioxidant activity reached their maximum rate.

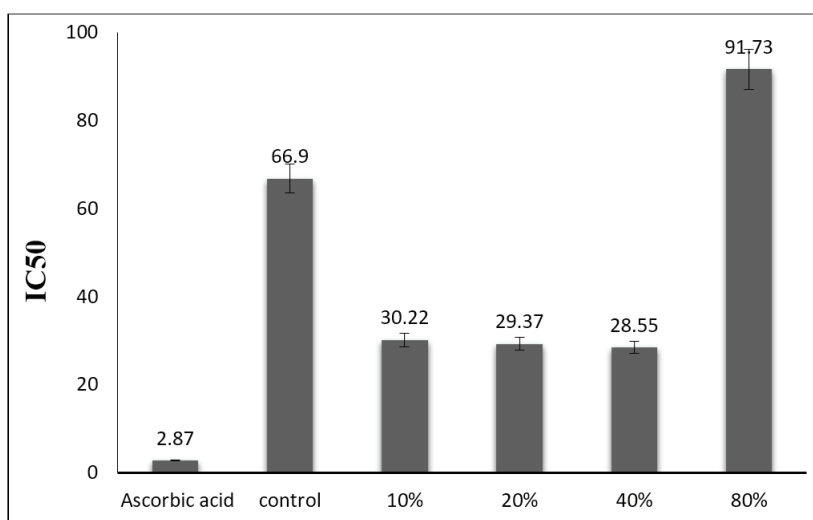


**Fig. 4.** DPPH free radical scavenging activities observed for different treatments compared to ascorbic acid as positive control

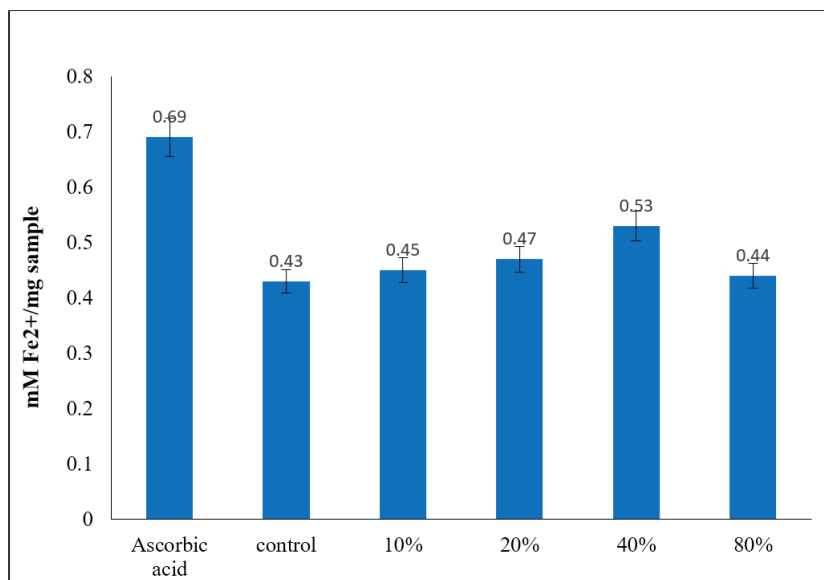


**Fig. 5.** The antioxidant capacity of different treatments compared to ascorbic acid as a positive control

**Table 3.** Comparing the phenolic and flavonoid contents as well as antioxidant activities of the samples.

Plant samples	IC <sub>50</sub>	Fe <sup>2+</sup> mM/ mg sample	mg total phenol/ 1 gr powder	mg total phenol/ 1 gr extract	mg quercetin/ 1 gr extract
Control	2.87	0.69	5.33	20.44	21.7
10%	66.9	0.43	5.97	19.04	27.94
20%	30.22	0.45	6.71	20.58	30.62
40%	28.55	0.47	9.88	22.12	33.3
80%	91.73	0.44	4.43	18.46	26.54

#### 4. Discussion

Foliar feeding is a technique of feeding plants by applying liquid fertilizer directly to the leaves. Due to the increased rate of absorption through the aerial parts of plants, it is an excellent method to deliver food and elements required for plants much faster [19]. Studies show that using alcohols with different concentrations would exert different effects on different plant species. The most important role for methanol operating in C<sub>3</sub> plants is to prevent light respiration, probably due to increased CO<sub>2</sub> concentration in leaves. If the concentration of CO<sub>2</sub> increases in leaves, ribulose 1,5-bisphosphate will react with CO<sub>2</sub> instead of O<sub>2</sub>, and the carboxylation function will occur. Therefore, the alcohol-induced biomass increase of the C<sub>3</sub> plants might cause the plant to use methanol as a direct source of carbon for serine biosynthesis and reduce carbon waste

through light respiration [15]. There are several reports investigating the effect of alcohol on the function of different plants. For instance, Zbiec and Podsiad (2003) investigated the effect of alcohol spraying and reported the increasing quantitative and qualitative yield of this technique on plants such as geranium, wheat, turnip, and sugar beet [21]. Iqbal Makhdum et al. studied the effect of methanol spraying on cotton plants and observed that 30% methanol treatment has been able to increase plant function compared with the control treatment [22]. In another research, performed by Safarzadeh Vishkaei who studied the effect of methanol on peanuts, 30% methanol treatment could increase the height of plant and grain function. Methanol and ethanol (30%) spraying could increase plant growth and the essential oil amount of peppermint [23]. The application of alcohol foliar feeding

would induce increasing the production of cytokinin and plant growth [24]. In addition, foliar feeding of alcohols in plants might induce increasing the plant metabolites including essential oils. Studies show that plants exposed to environmental stresses might increase the production of their specialized metabolites to confront the stimulant leading to more metabolite synthesis.

The current study showed that alcohol foliar feeding had effects on the amount of essential oil of the medicinal plant *D. anethifolia* and its composition. Our results showed that monoterpenes and alkanes such as n-decanal were the major components in the essential oil of *D. anethifolia*. In most of the studies investigating the essential oil composition of this medicinal plant, n-decanal was reported as the main constituent [25,26]. For example, Salari et al. have reported n-decanal (22.29%) as the most abundant constituent of *D. anethifolia* essential oil (Kerman), followed by alkanes decanol (22.18%) and dodecanol (11/79%) [27]. There are also some studies in which decanal has not been reported as the major compound [3,28,29]. The results of Arbabi et al. showed that cis-chrysanthenyl acetate with an average amount of 44.77% was the main compound of the essential oil of *D. anethifolia* from Sistan & Baluchistan [2].

Besides, our results revealed that this technique had beneficial effects on the amount of phenolic and flavonoid contents and consequently on the antioxidant activity of the plant. In total, the best efficiency was observed for 40% ethanol treatment. This can be due to the nutritional role of ethanol as a carbon source, stimulus, and active substance in metabolic reactions. In addition, ethanol plays an essential role in the biosynthetic pathway for the production of terpenoids. The opposite effect observed in the higher percentages of alcohol might be due to the plant poisoning leading to the decreased level of specialized metabolites and antioxidant capacity. The results of this experiment showed that the use of the hydroalcohol spraying could increase essential oil production, so it is suggested to use of hydroalcoholic foliar feeding to increase *D. anethifolia* metabolites in future research.

## 5. Conclusion

Taken together, the results of this experiment showed that ethanol spraying could increase the production of essential oil as well as phenolic and flavonoid compounds in *D. anethifolia*. Since the plant is an important medicinal plant, this might increase its efficacy. Thus, hydroalcoholic foliar feeding can be a valuable strategy to increase the specialized metabolites of *D. anethifolia* in future research.

## 6. Acknowledgements

The authors would like to thank the University of Sistan and Baluchestan for their help and support (Grant No. 2376081).

## 7. References

- [1] J. Mottaghipisheh, A. Boveiri Dehsheikh, M. Mahmoodi Sourestani, T. Kiss, J. Hohmann, D. Csupor, *Ducrosia* spp., rare plants with promising phytochemical and pharmacological characteristics: An updated review, *Pharmaceuticals* (Basel), 13 (2020) 175. <https://doi.org/10.3390/ph13080175>
- [2] M. Arbabi, H. Naghdi Badi, M. Labbafi, A. Mehrafarin, E. Saboki, Investigating the essential oil composition of *Ducrosia anethifolia* (DC.) Boiss. in different altitudes of Sistan and Baluchestan province, Iran, *J. Med. Plants*, 19 (2020) 343-355. <https://doi.org/10.29252/jmp.19.74.343>
- [3] J. Mottaghipisheh, M.T. Maghsoudlou, J. Valizadeh, R. Arjomandi, Antioxidant activity and chemical composition of the essential oil of *Ducrosia anethifolia* (DC.) Boiss. from Neyriz, *J. Med. Plant. By-prod.*, 2 (2014) 215-218. <https://doi.org/10.22092/JMPB.2014.108737>.
- [4] E.R. Elsharkawy, E.M. Abdallah, M.H. Shiboob, S.M. Alghanem, Phytochemical, antioxidant and antibacterial potential of *Ducrosia anethifolia* in northern border region of Saudi Arabia, *J. Pharm. Res. Int.*, 31 (2019) 1-8. <https://doi.org/10.9734/jpri/2019/v31i630361>

- [5] N.M. Shalaby, H.I. Abd-Alla, H.F. Aly, M.A. Albalawy, K.H. Shaker, J. Bouajila, Preliminary in vitro and in vivo evaluation of antidiabetic activity of *Ducrosia anethifolia* Boiss. and its linear furanocoumarins, *Biomed. Res. Int.*, 2014 (2014) 480545. <https://doi.org/10.1155/2014/480545>
- [6] M. Zamyad, M. Abbasnejad, S. Esmaeili-Mahani, A. Mostafavi, Alpha-Pinene as the main component of *Ducrosia anethifolia* (Boiss) essential oil is responsible for its effect on locomotor activity in rats, *Avicenna J. Neuro. Psycho. Physiol.*, 3 (2016) 29-34. <https://doi.org/10.17795/ajnpp-38787>.
- [7] M. Akaberi, Z. Tayarani-Najaran, I. Mehregan, J. Asili, A. Sahebkar, M. Hassanzadeh-Khayyat, S.A. Emami, Review of the essential oil composition of Iranian endemic and native taxa of Apiaceae (Umbelliferae), *Curr. Org. Chem.*, 24 (2020) 909-1009. <https://doi.org/10.2174/1385272824999200513103632>.
- [8] M. Abbasnejad, A. Mostafavi, R. Kooshki, P. Hamzenejad, S. Esmaeili-Mahani, Effect of *Ducrosia anethifolia* (Dc.) Bioss essential oil on spatial learning and memory in rats, *J. Gorgan Univ. Med. Sci.*, 18 (2017) 9-15. [http://goums.ac.ir/journal/browse.php?a\\_id=2949&sid=1&slc\\_lang=en](http://goums.ac.ir/journal/browse.php?a_id=2949&sid=1&slc_lang=en)
- [9] L. Obeidi, A.A. Mehrabi, M. Omid, A. Oladzad, Meiotic behavior and pollen viability of *Ducrosia anethifolia* (DC), Iran. *J. Rangelands For. Plant Breed. Genet. Res.*, 20 (2012) 124-133. <https://doi.org/10.22092/IJRFPBGR.2012.6631>
- [10] M. Zamyad, M. Abbasnejad, S. Esmaeili-Mahani, A. Mostafavi, V. Sheibani, The anticonvulsant effects of *Ducrosia anethifolia* (Boiss) essential oil are produced by its main component alpha-pinene in rats, *Arq. Neuropsiquiatr.*, 77 (2019) 106-114. <https://doi.org/10.1590/0004-282X20180147>.
- [11] M. Karami, F. Ghassemi, Effects of aqueous-alcoholic extract of *Ducrosia anethifolia* (DC.) Boiss. leaves on fetal heart tissue in diabetic rats, *Iran. J. Med. Aromatic Plants Res.*, 37 (2021) 52-64. <https://doi.org/10.22092/IJMAPR.2021.342950.2791>
- [12] N. Rahimi, E. Samani Jahromi, S. Zolghadri Jahromi, The effect of the hydro-alcoholic extract of (*Ducrosia anethifolia*) on testosterone hormone and the histological changes of the testicle in male adult rats, *Armaghane-danesh, Yasuj Univ. Med. Sci. J.*, 21 (2016) 682-693. <https://armaghanj.yums.ac.ir/article-1-1389-en.pdf>
- [13] L. Shooshtari, M. Omid, E. Majidi, M. R. Naghavi, M. Ghorbanpour, A. Etminan, Assessment of somaclonal variation of regenerated *Ducrosia anethifolia* plants using AFLP markers, *J. Hortic. For. Biotechnol.*, 17 (2013) 99-106. [https://journal-hfb.usab-tm.ro/romana/2013/Lista%20Lucrari%20PDF/Lucrari%20Vol%2017\(4\)%20PDF/22Lia%20Shooshtari.pdf](https://journal-hfb.usab-tm.ro/romana/2013/Lista%20Lucrari%20PDF/Lucrari%20Vol%2017(4)%20PDF/22Lia%20Shooshtari.pdf)
- [14] C. Wang, L. Guo, Y. Li, Z. Wang, Systematic comparison of C3 and C4 plants based on metabolic network analysis, *BMC Syst. Biol.*, 6 (2012) S9. <https://doi.org/10.1186/1752-0509-6-S2-S9>
- [15] S. Sajedi Moghadam, A. Mehrafarin, H. Naghdi Badi, A.R. Pazoki, N. Qavami, Evaluation of phytochemical yield of thyme (*Thymus vulgaris* L.) under foliar application of hydroalcohols, *J. Med. Plants*, 4 (2012) 130-140. <https://doi.org/10.1001.1.2717204.2012.11.44.12.4>
- [16] J. Asili, Z. Tayarani-Najaran, S.A. Emami, M. Iranshahi, A. Sahebkar, S. Eghbali, Chemical composition, cytotoxic and antibacterial activity of essential oil from aerial parts of *Salvia tebesana* Bunge, *J. Essen. Oil-Bear. Plants*, 24 (2021) 31-39. <https://doi.org/10.1080/0972060X.2021.1886996>
- [17] Z. Sadeghi, J. Valizadeh, O. Azyzian Shermeh, M. Akaberi, Antioxidant activity and total phenolic content of *Boerhavia elegans* (choisy) grown in Baluchestan, Iran, *Avicenna J. Phytomed.*, 5 (2015) 1-9. <https://www.ncbi.nlm.nih.gov/pmc/articles/>

- PMC4352527/
- [18] E.V. Beketov, V. P. Pakhomov, O.V. Nesterova, Improved method of flavonoid extraction from bird cherry fruits, *Pharm. Chem. J.*, 39 (2005) 316-318. <https://doi.org/10.1007/s11094-005-0143-7>
- [19] M. Jahani, M. Akaberi, M. Hasanzadeh Khayyat, S.A. Emami, Chemical composition and antioxidant activity of essential oils from *Cupressus sempervirens*. var. *sempervirens*, *C. sempervirens* cv. *Cereiformis* and *C. sempervirens* var. *horizontalis*, *J. Essent. Oil-Bear. Plants*, 22 (2019) 917-931. <https://doi.org/10.1080/0972060X.2019.1646672>
- [20] H. Nourafcan, Z. Kalantari, The effect of methanol and ethanol foliar application on peppermint morpho-physiological characteristics, *Agroecol. J.*, 12 (2017) 1-9. <http://www.Agroecology Journal.com>
- [21] I. Zbiec, C.O. Podsiad, Response of some cultivated plants to methanol as compared to supplemental irrigation, *Electron. J. Pol. Agric. Univ.*, 6 (2003) 1-7. <http://www.ejpau.media.pl>
- [22] M.I. Makhdum, M.N.A. Malik, S. Din, F. Ahmad, F.I. Chaudhry, Physiological response of cotton to methanol foliar application, *J. Res. Sci.*, 13 (2002) 37-43. <https://www.bzu.edu.pk/jrscience/vol13no1/5.pdf>
- [23] M.N. Safarazade Vishgahi, G. Nourmohamadi, H. Magidi, H. Effect of methanol on peanut function and yield components, *Iran. J. Agric. Sci.* 103 (2007) 88. <https://jijas.ut.ac.ir>
- [24] H. Hadadi, P. Moradi, F. Matlabi, The Effect of methanol and manganese salt spraying on the amount and components of essential oil of melissa (*Melissa officinalis* L.), *J. Med. Plants*, 2 (2016) 80-88. <https://doi.org/10.1001.1.2717204.2016.15.58.13.1>
- [25] V. Hajhashemi, M. Rabbani, A. Ghanadi, E. Davari, Evaluation of antianxiety and sedative effects of essential oil of *Ducrosia anethifolia* in mice, *Clinics*, 21 (1985) 5103-5121. <https://doi.org/10.1590/S1807-59322010001000020>
- [26] F. Sefidkon, I. Javidtash, Essential oil composition of *Ducrosia anethifolia* (DC.) Boiss. from Iran, *J. Essential Oil Res.*, 14 (2002) 278-279. <https://doi.org/10.1001.1.2717204.2020.19.74.24.2>
- [27] S. Salari, M. Shamsaddini, The production of nanoliposomal system containing *Ducrosia anethifolia* (DC.) Boiss essential oil made by sonication and filtration methods, *J. Med. Plants*, 19 (2020) 229-238. <https://doi.org/10.1001.1.2717204.2020.19.74.13.1>
- [28] Z. Karimi, A. Ghani, S. Mohtashami, Comparative study of essential oil content and composition of *Ducrosia anethifolia* at two phenological stage, *Res. J. Pharm.*, 44 (2017) 29-30. <http://rjpharmacognosy.ir>
- [29] M. Keshavarzi, A. Sharifan, S.A. Yasini Ardakani, Effect of the essential oil of *Ducrosia anethifolia* (DC.) Boiss. and *Teucrium polium* L. on physicochemical, sensory, and microbial characteristics of probiotic yogurt during storage time, *Iran. J. Food Sci. Technol.*, 18 (2021) 265-276. <https://doi.org/10.52547/fsct.18.117.265>



# Determination of tetrafluoroborate in wastewaters by ion chromatography after ion pair liquid-liquid dispersive microextraction

Roman Grigorievich Sirotkin<sup>a,\*</sup>, Elena Valerievna Elipasheva<sup>a</sup>, Alexander Vladimirovich Knyazev<sup>a</sup>,  
 and Viktoriya Alekseevna Bobrova<sup>a</sup>

<sup>a</sup> Lobachevsky State University of Nizhny Novgorod - National Research University (UNN), Nizhny Novgorod, Russian Federation

## ARTICLE INFO:

Received 6 Aug 2022  
 Revised form 19 Oct 2022  
 Accepted 25 Nov 2022  
 Available online 29 Dec 2022

## Keywords:

Tetrafluoroborate,  
 Microextraction,  
 Ion chromatography,  
 Ion pair,  
 Wastewaters

## ABSTRACT

The ion chromatographic method was developed to determine tetrafluoroborate ion ( $\text{BF}_4^-$ ) in different types of water using ion pair liquid-liquid dispersive microextraction. Tetrafluoroborate was extracted into an organic phase (1,2-dichloroethane) as an ion pair with a tetrabutylammonium cation ( $\text{TBA}^+$ ). The most complete formation of  $[(\text{TBA}^+)(\text{BF}_4^-)]$  was observed at ion-pair reagent concentration of at least  $5 \text{ mmol L}^{-1}$  ( $C(\text{BF}_4^-) \leq 1 \text{ mg L}^{-1}$ ). Ultrasonic irradiation was used to disperse the extractant. The achieved concentration factor (K) was  $29 \pm 3$ , and the degree of extraction (R) was  $50 \pm 5\%$ . The limit of detection of tetrafluoroborate using the microextraction technique was  $7 \times 10^{-3} \text{ mg L}^{-1}$ . The method applies to the analysis of different water origins. The presence of the main contained anions does not interfere with the microextraction and chromatographic determination of tetrafluoroborate. The maximum molar ratio of  $\text{BF}_4^-$  to diverse ions is  $1:10^4$  for fluoride, chloride, bromide, nitrate ions, and  $1:10^2$  for sulfate and perchlorate ions.

## 1. Introduction

Today, the concept of “green chemistry” remains one of the main trends in analytical chemistry [1-4]. Decreased volumes of toxic reagents, automation, and miniaturization of analytical methods are the critical points of this concept [3]. One of the leading trends in green chemistry is using ionic liquids containing tetrafluoroborate ions [5, 6]. The control of its concentration in various objects is necessary at the stages of the synthesis and use of ionic liquids. Industrial wastewater can also contain various amounts of tetrafluoroborate. It's known that  $\text{BF}_4^-$  use in the composition of non-aqueous electrolytes for chemical reactions and electrochemical

processes [7], as well as in electroplating to improve the quality of the electroplated layer [8]. Another alternative application area for  $\text{BF}_4^-$  is agriculture. It is used there as a “green fungicide” [9] and an herbicide [10]. The wide use of  $\text{BF}_4^-$  means a substantial difference in the composition of the analyzed samples. This necessitates the development of a universal method for analyte determination.

Spectrophotometry [11, 12, 13] and ion chromatography [14, 15] are the most common methods for determining tetrafluoroborate in aqueous solutions. The works [11, 12] are based on the conversion of all boron forms in the sample to the  $\text{BF}_4^-$ , reaction with an organic dye, and photometric determination of the product. However, the reaction stability depends on the temperature, the sample

\*Corresponding Author: [Roman G. Sirotkin](mailto:roman_g_sirotkin@mail.ru)

Email: [roman\\_sirotkin94@mail.ru](mailto:roman_sirotkin94@mail.ru)

<https://doi.org/10.24200/amecj.v5.i04.214>

pH, and the dye concentration. Also, the high consumption of toxic reagents is the disadvantage of this work. In addition, these methods make it possible to determine the concentration of total boron in the sample. The ion pair preconcentration of  $\text{BF}_4^-$  and spectrophotometric determination are described in [13]. But large amounts of sample (20 ml) and toxic extractant (10 ml) were used in this work.

The determination of  $\text{BF}_4^-$  in water samples by ion chromatography is often not sensitive enough ( $0.2 \text{ mg L}^{-1}$  -  $1.4 \text{ mg L}^{-1}$ ) [14,15]. In this work, a procedure for ion pair liquid-liquid microextraction of  $\text{BF}_4^-$  is proposed to increase the determination's selectivity and lower the detection limit. This method involves forming a neutral ion pair between the anion of the analyte and the cation of the ion-pair reagent due to electrostatic interaction [16]. It is known that cations of quaternary ammonium bases (QABs) can form ion pairs with inorganic anions from aqueous solutions [17]. The solubility of such compounds in organic solvents is higher than in water [18]. In addition to the lower detection limits, microextraction also makes it possible to reduce the load on the chromatographic system at high concentrations of diverse ions. It is important for the analysis of various samples, including industrial wastewater.

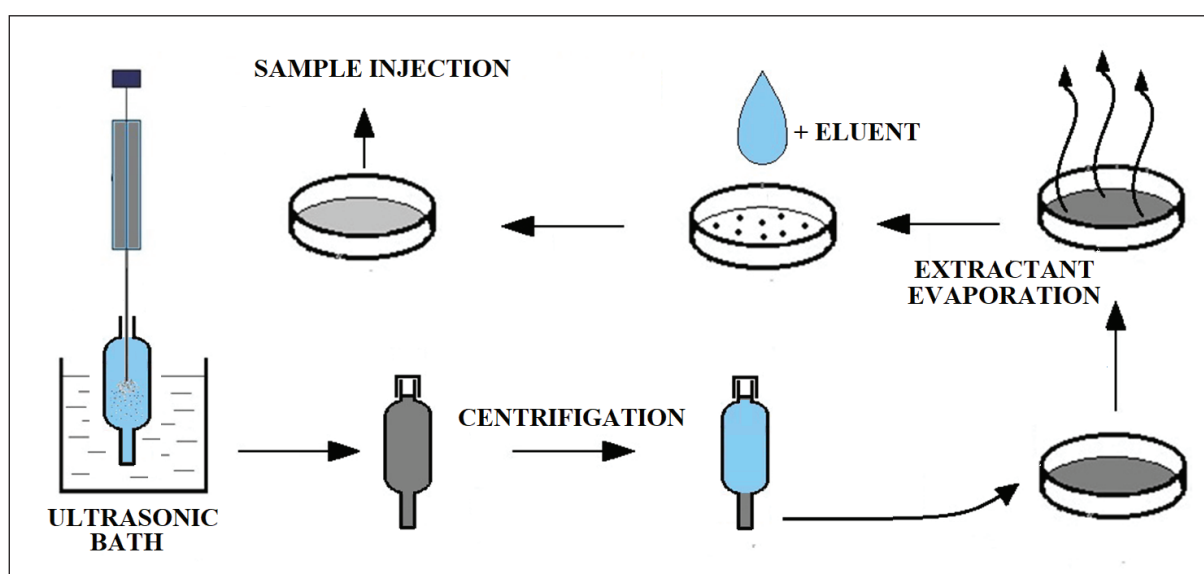
## 2. Materials and methods

### 2.1. Microextraction technique

A specially designed centrifuge tube (4.5 mL volume) was used for microextraction. 3.0 ml of analyzed water was placed in a tube, and a solution of the ion-pair reagent was added. Then the tube was placed in an ultrasonic bath, and 500  $\mu\text{L}$  of the extractant was added. The resulting emulsion was separated by centrifugation. Further, the replacement of the organic matrix with an aqueous one was held. To do this, the extract (400  $\mu\text{L}$ ) was transferred in a Teflon vial, and the extractant was evaporated by using an infrared lamp. Then 50  $\mu\text{L}$  of eluent was added to the dry residue. This solution was injected into the chromatograph for the determination of tetrafluoroborate ion ( $\text{BF}_4^-$ ) in water samples (Schema 1).

### 2.2. Chromatographic conditions

All experiments were carried out on an LC-20A ion chromatograph (Shimadzu, Japan), which consisted of a Model LP-20ADsp liquid delivery pump and a conductivity detector Model CDD-10Avp. The separating column was OKA (50x4 mm i.d., Vagos, Tallinn, Estonia), and the suppressor column was KU-2x8 (100x4 mm i.d., Ekos-1, Moscow, Russia). Both columns and the conductivity detection cell



**Schema 1.** Microextraction technique for determination of tetrafluoroborate ions ( $\text{BF}_4^-$ ) in water and wastewater samples based on ion chromatography

were placed inside the CTO-20AC column oven for temperature control (32 °C). The eluent was obtained by a mixture of 1.0 mmol L<sup>-1</sup> Na<sub>2</sub>CO<sub>3</sub> with 4.0 mmol L<sup>-1</sup> NaHCO<sub>3</sub>, and the flow rate was set at 3 ml min<sup>-1</sup>. This eluent has the optimum eluting power for the selective and fast determination of tetrafluoroborate. The volume of the injection loop was 50 µL.

### 2.3. Reagents

Ammonium tetrafluoroborate was used to prepare a standard solution supplied by JSC Vekton, Russia. The solution was kept in a polyethylene container for no more than a month. Sodium carbonate and sodium bicarbonate were used to prepare an eluent solution (JSC Vekton, Russia). All solutions were prepared using deionized water. 1,2-dichloroethane, chloroform, dichloromethane, and carbon tetrachloride were used as extractants (JSC Vekton, Russia). All reagents were analytical grade or better. Ion-pair reagents were tetrabutylammonium hydroxide TBAOH (40% aqueous solution, Sigma-Aldrich, Switzerland, CAS Number: 2052-49-5) and tetraethylammonium hydroxide TEAOH (25% aqueous solution, Acros Organics, India).

### 2.4. Other Equipment

The extractant was dispersed using a PSB-Gals 1335-05 ultrasonic bath with a radiation generator power of 50 W and a frequency of 35 kHz. SM-6M centrifuge with a rotor speed of 1200 rpm was used for separating the organic and aqueous phases. During replacing the matrix, the extractant was evaporated using a 300 W mirror infrared lamp. The Anion 4100 conductometer was used to control of purity of deionized water. Laboratory scales AUX 320 Shimadzu, micro doses HTL 20-200 µL, and Dragon LAB TopPette Pipette 2-20 µL were also used in work.

## 3. Results and discussions

### 3.1. Stability of tetrafluoroborate ion (BF<sub>4</sub><sup>-</sup>)

Hydrolysis of BF<sub>4</sub><sup>-</sup> ions occurs in aqueous solutions at pH>1. Also, the rate of this process depends on the temperature [19]. About 0.7% of BF<sub>4</sub><sup>-</sup> decomposes in alkaline solutions within a day at 20°C [20]. So, we have studied the stability of a standard solution containing 1 mg L<sup>-1</sup> of BF<sub>4</sub><sup>-</sup>. The results (Fig. 1) showed that the standard solution is stable for a month at a temperature of 3 ± 1°C in a polyethylene container.

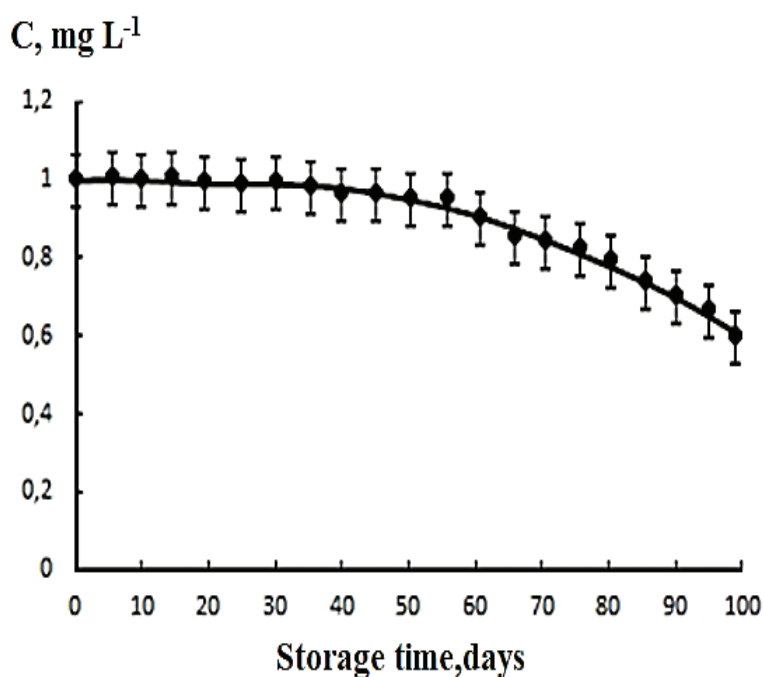
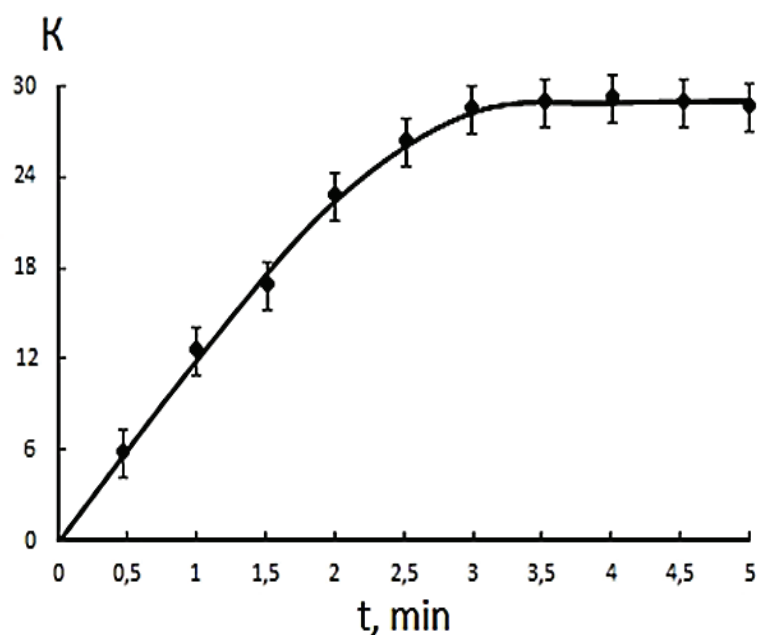


Fig. 1. The stability of BF<sub>4</sub><sup>-</sup> standard solution concentration.

Conditions: T = 3±1°C, polyethylene container



**Fig. 2.** Effect of ultrasonic irradiation time. Extractant: 1,2-dichloroethane; ion-pair reagent: TBAOH, concentration 5 mM (n=3, P=0.95)

### 3.2. Effect of ultrasonic irradiation time

The maximum concentration factor of  $\text{BF}_4^-$  is reached at 3 min of ultrasonic irradiation and does not change further (Fig. 2). This dependence is valid for all chosen extractants and ion-pair reagents.

### 3.3. Effect of different extractants and ion pair reagents

Using tetrabutylammonium hydroxide as an ion-pair reagent made it possible to achieve better microextraction parameters (Table 1). Obviously, this is explained by the longer alkyl chain of tetrabutylammonium compared to tetraethylammonium cation. So, the extraction of ion pairs from the aqueous phase increases [21].

Parameters of microextraction depend on the polarity of the extractant solvent. Both the

permittivity of solvent  $\epsilon_r$  and its dipole moment  $\mu$  are important complementary characteristics, so the polarity of the extractant was estimated using the electrostatic coefficient EF [22], defined as the product of  $\epsilon_r$  and  $\mu$ . Thus, the simultaneous influence of both parameters is taken into account. The dependence of the concentrating factor of tetrafluoroborate on the electrostatic coefficient of the used extractant is shown in Figure 3. The higher the EF value of the solvent, the higher the efficiency of  $[(\text{TBA}^+)(\text{BF}_4^-)]$  extraction.

### 3.4. Effect of ion pair reagent concentration

The minimum concentration of QAB was 5 mmol  $\text{L}^{-1}$  for analyte concentrations range of 0.01–1

**Table 1.** The concentrating factor (K) and the degree of  $\text{BF}_4^-$  extraction (R) (n=3, P=0.95).

QAB	(%), K (R)			
	chloroform	1,2-dichloroethane	carbon tetrachloride	dichloromethane
Tetraethyl-ammonium hydroxide	$0.1 \pm 1.3$ ( $0.2 \pm 2.2$ )	$0.3 \pm 3.1$ ( $0.5 \pm 5.3$ )	$0.1 \pm 0.8$ ( $0.1 \pm 1.4$ )	$0.2 \pm 2.4$ ( $0.3 \pm 4.1$ )
Tetrabutyl-ammonium hydroxide	$2 \pm 19$ ( $3 \pm 27$ )	$3 \pm 29$ ( $5 \pm 50$ )	$0.2 \pm 1.8$ ( $0.3 \pm 3.0$ )	$3 \pm 26$ ( $4 \pm 44$ )

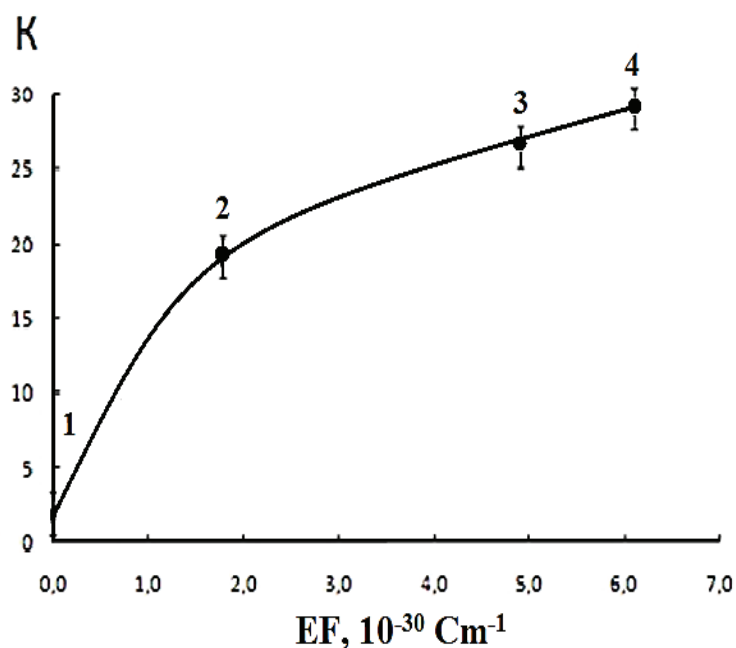


**Fig. 3.** Effect of extractant EF. Ion-pair reagent TBAOH, concentration 5 mM. 1 – carbon tetrachloride, 2 – chloroform, 3 – dichloromethane, 4 – 1,2-dichloroethane. ( $n=3$ ,  $P=0.95$ )  $\text{EF}, 10^{-30} \text{ Cm}^{-1}$

$\text{mg L}^{-1}$  (Fig. 4). Abundance of ion pair reagents in the sample does not make the concentration results worse. It is necessary to shift the chemical equilibria to the formation of ion pairs.

Excess reagent was contained in the extract [23]. So, tetrabutylammonium hydroxide and

tetraethylammonium hydroxide were chosen as ion-pair reagents. The fact was that hydroxide ions were neutralized by hydrogen ions in a suppression column and entered the detector as water molecules. It helped to decrease the background signal.

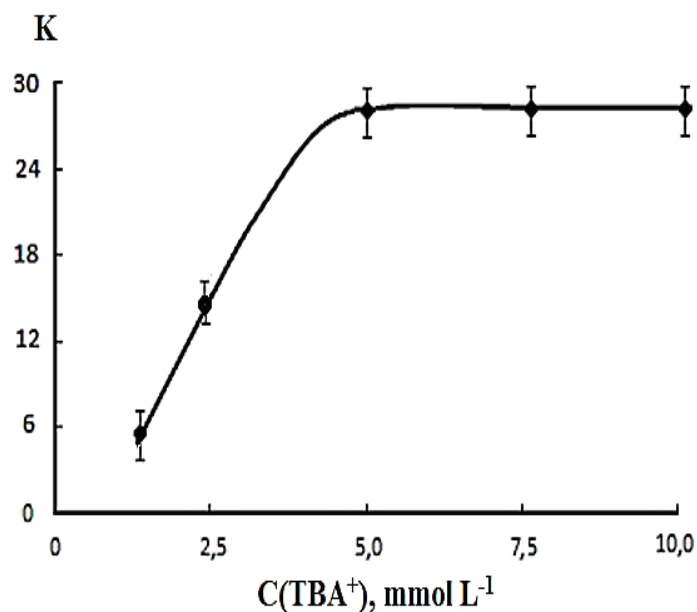


**Fig. 4.** Effect of ion pair reagent concentration. Extractant: 1,2-dichloroethane. Ion-pair reagent: TBAOH, concentration 5 mM.  $C(\text{BF}_4^-) = 1 \text{ mg L}^{-1}$  ( $n=3$ ,  $P=0.95$ )  $C(\text{TBA}^+), \text{ mmol L}^{-1}$

**Table 2.** Summary of method parameters (Extractant : 1,2-dichloroethane. Ion-pair reagent:TBAOH, concentration 5 mM; n=3, P=0.95)

Parameter name	Value
Linear Regression Equation	$S = 4011C \pm 180$ , where S – value of $\text{BF}_4^-$ peak area, $\text{mV} \times \text{min}$ , C – $\text{BF}_4^-$ concentration, $\text{mg L}^{-1}$
Linearity Range of the calibration curve, $\text{mg L}^{-1}$	100 - 0.5
% R	$50 \pm 5$
K	$29 \pm 3$
$C_{\text{min}}$ , $\text{mg L}^{-1}$	$10^{-1} \times 2$
$C_{\text{min, ex}}$ , $\text{mg L}^{-1}$	$10^{-3} \times 7$

### 3.5. Detection limits

The limit of chromatographic detection  $C_{\text{min}}$  was defined as  $3.3\sigma$  ( $\sigma$ : the standard deviation of measurements of blank samples) [24]. The detection limit using microextraction  $C_{\text{min, ex}}$  was calculated by dividing  $C_{\text{min}}/K$  (Table 2).

### 3.6. Synthetic wastewaters analysis and effect of diverse anions

The microextraction efficiency and chromatographic determination are also affected by the sample composition. Many anions can compete with tetrafluoroborate in forming ion pairs with QABs.

Synthetic wastewater samples were prepared and analyzed to assess the interfering effect of diverse anions. The results are shown in Table 3.

Sulfate and perchlorate ions can have the greatest interfering effect. These anions also form stable ion pairs with tetrabutylammonium cation. When its concentration is over than shown in Table 3, the co-eluting occurs with  $\text{BF}_4^-$ . The peak geometry is violated, and the calculation of its area is difficult. However, under the chosen conditions, the separation of all components is not difficult. It is illustrated by the synthetic wastewater chromatograms (Fig. 5a, 5b).

**Table 3.** Effect of diverse anions

(Extractant – 1,2-dichloroethane. Ion-pair reagent – TBAOH, concentration 5 mM; n=3, P=0.95)

$\text{BF}_4^-$ concentration in synthetic samples, $\text{mgL}^{-1}$	Interfering ions (maximum molar ratio)	Results of $\text{BF}_4^-$ determination, $\text{mgL}^{-1}$
1.0	$\text{F}^-$ , $\text{Cl}^-$ , $\text{Br}^-$ , $\text{NO}_3^-$ (1:10 <sup>4</sup> )	$1.00 \pm 0.17$
0.2	$\text{SO}_4^{2-}$ , $\text{ClO}_4^-$ (1:10 <sup>2</sup> )	$0.20 \pm 0.04$
0.05		$0.05 \pm 0.01$

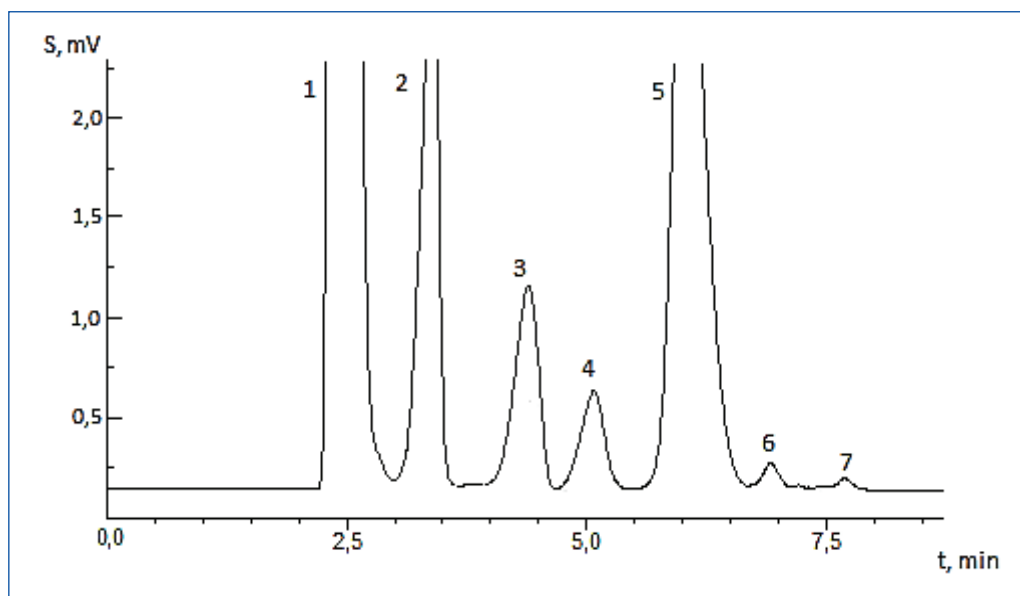


**Fig. 5a.** Chromatograms of synthetic wastewater samples with direct analysis of samples,  
1 – F<sup>-</sup>, 2 – Cl<sup>-</sup>, 3 – Br<sup>-</sup>, 4 – NO<sub>3</sub><sup>-</sup>, 5 – SO<sub>4</sub><sup>2-</sup>, 6 – BF<sub>4</sub><sup>-</sup>, 7 – ClO<sub>4</sub><sup>-</sup>

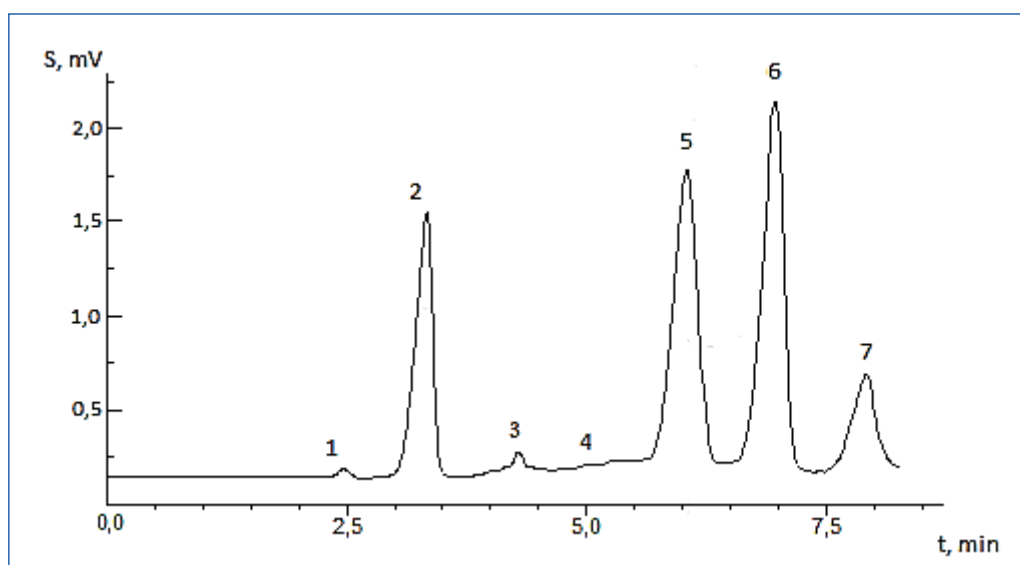


**Fig. 5b.** Chromatograms of synthetic wastewater samples after microextraction.  
1 – F<sup>-</sup>, 2 – Cl<sup>-</sup>, 3 – Br<sup>-</sup>, 4 – NO<sub>3</sub><sup>-</sup>, 5 – SO<sub>4</sub><sup>2-</sup>, 6 – BF<sub>4</sub><sup>-</sup>, 7 – ClO<sub>4</sub><sup>-</sup>

### 3.7. Example of waste waters analysis and recoveries of BF<sub>4</sub><sup>-</sup>

Using the proposed method, 3 samples of wastewater were analyzed to determine BF<sub>4</sub><sup>-</sup>. Samples 1 and 2 were taken from the drain of the university electrochemical laboratory, and sample 3 was wastewater from the electroplating industry. All samples were filtered twice: firstly, with an ash-

free paper filter with a pore size of 5-8 μm (Melior XXI LLC, Russia), then with a syringe filter with a pore size of 0.22 μm (Hawach Scientific Co., Ltd, China). BF<sub>4</sub><sup>-</sup> concentration was calculated using the calibration curve method. The results (Table 4) show that the proposed method is suitable for analyzing various origins samples. Recoveries of BF<sub>4</sub><sup>-</sup> are shown in Table 5.

**Table 4.** The concentration of some components of different wastewater (n=3, P=0.95)

Component	Concentration, mg L <sup>-1</sup>		
	Sample № 1	Sample № 2	Sample № 3
*Fe	10 <sup>-1</sup> ·(2.0±0.4)	10 <sup>-1</sup> ×(1.5±0.3)	0.4±1.9
*Ni	10 <sup>-2</sup> ×1>	10 <sup>-2</sup> ×1>	10 <sup>-2</sup> ×(2.0±0.4)
*Cu	10 <sup>-2</sup> ×1>	10 <sup>-2</sup> ×1>	10 <sup>-2</sup> ×(8.0±1.5)
*Cr	10 <sup>-2</sup> ×1>	10 <sup>-2</sup> ×1>	10 <sup>-2</sup> ×(3.0±0.8)
·F	1.1±0.1	10 <sup>-1</sup> ×(9.3±0.9)	11±2
·Cl	25±3	32±4	68±7
SO <sub>4</sub> <sup>2-</sup>	5.0±0.6	8.1±0.9	36±5
BF <sub>4</sub> <sup>-</sup>	10 <sup>-2</sup> ×(7.2±1.4)	10 <sup>-2</sup> ×(2.2±0.4)	10 <sup>-1</sup> ×(4.0±0.4)

\* determined by atomic absorption analysis

**Table 5.** Recoveries of BF<sub>4</sub><sup>-</sup> (n=3, P=0.95)

Original, mg L <sup>-1</sup>	Added, mg L <sup>-1</sup>	Found, mg L <sup>-1</sup>	Recovery, %
10 <sup>-1</sup> ×(4.0±0.4)	10 <sup>-1</sup> ×1.0	10 <sup>-1</sup> ×(5.1±0.6)	102.5
	10 <sup>-1</sup> ×2.5	10 <sup>-1</sup> ×(6.4±0.7)	97.5
	10 <sup>-1</sup> ×5.0	10 <sup>-1</sup> ×(9.0±0.9)	100.0
10 <sup>-2</sup> ×(2.2±0.2)	10 <sup>-2</sup> ×1.0	10 <sup>-2</sup> ×(3.3±0.9)	104.5
	10 <sup>-2</sup> ×2.5	10 <sup>-2</sup> ×(4.9±1.1)	109.1
	10 <sup>-2</sup> ×5.0	10 <sup>-2</sup> ×(7.1±1.3)	95.5
10 <sup>-2</sup> ×(7.2±1.4)	10 <sup>-2</sup> ×1.0	10 <sup>-2</sup> ×(8.0±1.6)	97.2
	10 <sup>-2</sup> ×2.5	10 <sup>-2</sup> ×(9.6±2.0)	98.6
	10 <sup>-2</sup> ×5.0	10 <sup>-1</sup> ×(1.3±0.2)	111.1

#### 4. Conclusion

A simple ion chromatographic method was developed to determine BF<sub>4</sub><sup>-</sup> using ion-pair liquid-liquid dispersive microextraction. The parameters of microextraction (concentration factor and degree of extraction) were calculated using ion-pair reagents with different hydrophobicity and extractants of various polarities. The higher the ion-pair reagent hydrophobicity and the electrostatic coefficient of the extractant, the higher the extraction efficiency. The best combination is using 1,2-dichloroethane and tetrabutylammonium hydroxide. The maximum molar ratios of analyte to diverse anions were established using synthetic wastewater. Analysis of real samples of industrial wastewater showed that other contained components don't interfere with the determination of BF<sub>4</sub><sup>-</sup>. The proposed method can generally be applied to analyze water samples of various origins.

#### 5. Acknowledgment

The authors are sincerely grateful to the laboratory attendants of the chemistry department of the Lobachevsky State University of Nizhny Novgorod for their efforts.

#### 6. References

- [1] P.T. Anastas, Green chemistry and the role of analytical methodology development, *Crit. Rev. Anal. Chem.*, 29 (1999) 167–175. <https://doi.org/10.1080/10408349891199356>
- [2] M. Koel, M. Kaljurand, Application of the principles of green chemistry in analytical chemistry, *Pure Appl. Chem.*, 78 (2006) 1993–2002. <https://doi.org/10.1351/pac200678111993>
- [3] S. Armenta, S. Garrigues, M. de la Guardia, Green Analytical Chemistry, *TrAC-Trends Anal. Chem.*, 27 (2008) 497–511. <https://doi.org/10.1016/j.trac.2008.05.001>

- org/10.1016/j.trac.2008.05.003
- [4] B.A. de Marco, B.S. Rechelo, E.G. Tócoli, A.C. Kogawa, H.R.N. Salgado, Evolution of green chemistry and its multidimensional impacts: A review, *Saudi Pharm. J.*, 27 (2019) 1–8. <https://doi.org/10.1016/j.jsps.2018.07.011>
- [5] R. Goutham, P. Rohit, S.S. Vigneshwar, A. Swetha, J. Arun, K.P. Gopinath, A. Pugazhendhi, Ionic liquids in wastewater treatment: A review on pollutant removal and degradation, recovery of ionic liquids, economics and future perspectives, *J. Mol. Liq.*, 349 (2021) 118150. <https://doi.org/10.1016/j.molliq.2021.118150>
- [6] M. Khraisheh, F. AlMamani, M. Inamdar, M.K. Hassan, M.A. Al-Chouti, Ionic liquids application for wastewater treatment and biofuel production: A mini review, *J. Mol. Liq.*, 337 (2021) 116421. <https://doi.org/10.1016/j.molliq.2021.116421>
- [7] H. Kim, S. Baek, T. Lim, J.J. Kim, Electrochemical reduction of nitrous oxide in 1-butyl-3-methylimidazolium tetrafluoroborate ionic liquid electrolyte, *Electrochem. Commun.*, 113 (2020) 106688. <https://doi.org/10.1016/j.elecom.2020.106688>
- [8] A.N. Araújo, M.B. Etxebarria, J.L.F.C. Lima, M.C.B.S.M. Montenegro, R. Pérez Olmos, Tubular detectors for flow-injection potentiometric determination of tetrafluoroborate in electroplating baths, *Anal. Chim. Acta*, 293 (1994) 35–41. [https://doi.org/10.1016/0003-2670\(94\)00073-5](https://doi.org/10.1016/0003-2670(94)00073-5)
- [9] Y. Dong, X. Liang, H. Yuan, S. Qi, F. Chen, D. Wang, Potential green fungicide: 16-oxo-1-oxa-4-azoniacyclohexadecan-4-ium tetrafluoroborate, *Green Chem.*, 10 (2008) 990–994. <https://doi.org/10.1039/b805797d>
- [10] R. Biczak, Quaternary ammonium salts with tetrafluoroborate anion: Phytotoxicity and oxidative stress in terrestrial plants, *J. Hazard. Mater.*, 304 (2016) 173–185. <https://doi.org/10.1016/j.jhazmat.2015.10.055>
- [11] L. Rusnakova, V. Andruch, I.S. Balogh, J. Škrliková, A dispersive liquid-liquid microextraction procedure for determination of boron in water after ultrasound-assisted conversion to tetrafluoroborate, *Talanta*, 85 (2011) 541–545. <https://doi.org/10.1016/j.talanta.2011.04.030>
- [12] A. Bayati-Comitaki, M.M. Zahedi, Ultrasound-assisted formation of tetrafluoroborate: methylene blue for microextraction and flow based spectrophotometric determination of the boron, *Int. J. Environ. Sci. Technol.*, 19 (2022) 10869–10876. <https://doi.org/10.1007/s13762-022-04278-6>
- [13] I. Kasahara, S. Hosokawa, N. Hata, S. Taguchi, K. Goto, Selective and sensitive spectrophotometric determination of tetrafluoroborate in wastewater after ion-pair extraction using bis[2-(5-chloro-2-pyridylazo)-5-diethylaminophenolato] cobalt(II) as a counter ion, *Analyst*, 118 (1993) 1205–1208. <https://doi.org/10.1039/AN9931801205>
- [14] S. Zhou, H. Yu, L. Yang, H. Ai, Fast determination of tetrafluoroborate by high-performance liquid chromatography using a monolithic column, *J. Chromatogr. A.*, 1206 (2008) 200–203. <https://doi.org/10.1016/j.chroma.2008.08.048>
- [15] J. Katagiri, T. Yoshioka, T. Mizoguchi, Basic study on determination of total boron by conversion to tetrafluoroborate ion ( $\text{BF}_4^-$ ) followed by ion chromatography, *Anal. Chim. Acta*, 570 (2006) 65–72. <https://doi.org/10.1016/j.aca.2006.03.084>
- [16] N. Phadungcharoen, N. Pengwanput, A. Nakapan, U. Sutitaphan, P. Thanomkloma, N. Jongudomsombuta, A. Chinsriwongkulb, T. Rojanarata, Ion pair extraction coupled with digital image colorimetry as a rapid and green platform for pharmaceutical analysis: an example of chlorpromazine hydrochloride tablet assay, *Talanta*, 219 (2020) 121271. <https://doi.org/10.1016/j.talanta.2020.121271>

- [17] M.L. Magnuson, E.T. Urbansky, C.A. Kelty, Determination of perchlorate at trace levels in drinking water by ion-pair extraction with electrospray ionization mass spectrometry, *Anal. Chem.* 72 (2000) 25-29. <https://doi.org/10.1021/ac9909204>
- [18] M. M. Baiser, H. Lund, *Organic Electrochemistry: An Introduction and a Guide*, M. Dekker, New York, *J. Polym. Sci.: Polymer Letters Edition*, 22 (1983) 459. <https://doi.org/10.1002/pol.1984.130220809>
- [19] A. Nemodruk, Z. Karalova, *Boron analytical chemistry*, Nauka, Moscow, 1964. <https://agris.fao.org/agris-search/search.do?recordID=US201300591908>
- [20] Me. G. Ryss, *The chemistry of fluorine and its inorganic compounds*, Goshimizdat, Moscow, 1956. <https://www.osti.gov/etdeweb/biblio/1512919>
- [21] V.S. Shmidt, S.D. Nikitin, Regularities in interfacial tension and emulsion unmixing for solvent-extraction systems, *At. Energ.*, 60 (1986) 467–475. <https://doi.org/10.1007/BF01124091>
- [22] K. Rajhardt, *Solvents and solvent effects in organic chemistry*, Mir Publ., Moscow, 1991. <https://www.bestbookcentre.com/books/russian-books-mir-publishers-moscow>
- [23] E.A. Mezhov, *Extraction with amines and quaternary ammonium bases*, Energoatomizdat Publ., Moscow, 1999. <https://openlibrary.org/publishers/Energoatomizdat>
- [24] L.P. Eksperiandova, K.N. Belikov, S.V. Khimchenko, T.A. Blank, Once again about the limits of detection and determination, *J. Anal. Chem.*, 65 (2010) 229–234. <https://doi.org/10.1134/S1061934810030020>



# Photocatalytic degradation of methyl orange using cerium doped zinc oxide nanoparticles supported bentonite clay

Safoora Javan<sup>a</sup>, Mohammad Reza Rezaei Kahkha<sup>b\*</sup>, Fahimeh Moghaddam<sup>a</sup>,

Mohsen Faghihi-Zarandi<sup>c</sup>, and Anahita Hejazi<sup>d</sup>

<sup>a</sup> Department of Environmental Health Engineering, Neyshabour University of Medical Sciences, Neyshabur, Iran

<sup>b</sup> Department of Environmental Health Engineering, Zabol University of Medical Sciences, Zabol, Iran

<sup>c</sup> Foreign Language Department, Shahid Bahonar University of Kerman, Kerman, Iran

<sup>d</sup> Engineering Department of Occupational Health & Safety at Work, Kerman University of Medical Sciences, Kerman, Iran

## ARTICLE INFO:

Received 3 Aug 2022

Revised form 20 Oct 2022

Accepted 17 Nov 2022

Available online 30 Dec 2022

## Keywords:

Photocatalyst,  
Degradation,  
Clay,  
Bentonite,  
Methyl Orange,  
Dye

## ABSTRACT

Methyl orange (MO) is a common anionic azo dye that is a serious harmful pollutant to the environmental aquatic systems, so it must be treated before it can be discharged. Photocatalysts are usually semiconducting solid oxides that create an electron-hole pair by absorbing photons. These electron holes can react with molecules on the surface of the particles. Photocatalysts are used in water purification, self-cleaning glasses, the decomposition of organic molecules, etc. Photocatalysts are environmental cleaning materials that remove pollution from surfaces and can destroy organic compounds when exposed to sunlight or fluorescence. The photocatalytic process follows the following principles. Bentonite mineral is a natural adsorbent material that has good adsorption capacity. In this work, zinc oxide nanoparticles doped with cerium were prepared by the sol-gel method (SGM) and deposited on bentonite clay to degrade methyl orange (MO) dye. Important parameters that affected degradation efficiency such as contact time, amount of nanocatalyst, and initial dye concentration were investigated and optimized. Results showed that 100% degradation efficiency was obtained at 60 mg of nanocatalyst and 50 mg L<sup>-1</sup> of methyl orange in 120 minutes. The Kinetics of the degradation process was consistent with pseudo-second-order and the adsorption isotherm of MO dye on nanocatalyst was fitted with the Langmuir isotherm model. The reusability of the synthesized nanocatalyst showed that the nanocatalyst was applied successfully seven times without a significant change in degradation efficiency.

## 1. Introduction

Photocatalysts are one of the essential elements for advanced oxidation processes (AOPs) [1, 2]. Zinc oxide (ZnO) is often the first choice due to its cheapness, non-toxicity, chemical stability, and high photocatalytic activity. Photocatalysts

absorb light radiation (ultraviolet or visible) by the catalyst, and electrons are transferred from the semiconductor's valence band to the conduction band. This transition creates a hole in the valence band, and an electron is produced in the conduction band (Schema 1).

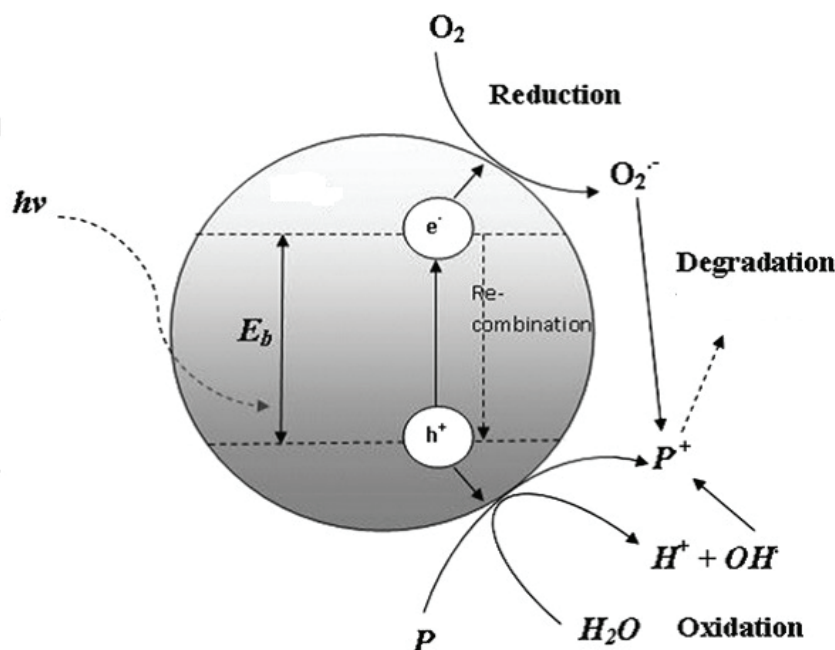
The hole in the reaction with water molecules produces active hydroxyl radicals [3, 4].

Moreover, the produced electron is transferred to the dissolved oxygen and forms a superoxide

\*Corresponding Author: Mohammad Reza Rezaei Kahkha

Email: [m.r.rezaei.k@gmail.com](mailto:m.r.rezaei.k@gmail.com)

<https://doi.org/10.24200/amecj.v5.i04.216>



**Schema 1.** Photocatalytic process

radical. These radicals can remove pollutants in aqueous media. Since the produced electron and holes are unstable and can recombine and return to their original state, doping elements were used with ZnO to prevent these phenomena [5]. Cerium is one of the elements of the lanthanide family whose redox couple Ce (III)/Ce (IV) causes the production of  $CeO_2$  and  $Ce_2O_3$  oxides. Ce (IV) traps the electron created in the conduction band, which has lost its stable electron configuration, tends to donate its electron and become stable, which is possible by electron migration to oxygen absorbed on the surface and the formation of superoxide radicals. Therefore, the electron of the conduction band enters a new cycle, which reduces the possibility of its access to the hole [6, 7]. Despite the advantages of nanocatalysts, their use in water purification processes is limited due to the small size of the particles. Problems such as the separation of suspended particles, non-recycling and secondary pollution are among the limitations of this method. One proposed method to solve this problem is fixing nanocatalysts on suitable substrates [8]. Many researchers developed different types of substrates such as silica gel [9], activated carbon [10], stainless steel

[11], glass fibers [12] and wood foam [13], has been used. Recently, ZnO nanoparticles were immobilized on cellulose paper [14], which was used to treat textile wastewater in a photoreactor. Natural clays such as bentonite, montmorillonite, and perlite are used as catalyst substrates due to their high porosity, chemical inertness, non-degradability, and high mechanical and thermal resistance compared to the other mentioned substrates [15]. In this work, ZnO-Ce nanoparticles were first synthesized by the sol-gel method. Then, nanoparticles were fixed on bentonite. The performance of the synthesized nanocatalyst as a catalyst was investigated in the removal of methyl orange in a batch photoreactor.

## 2. Material and methods

### 2.1. Reagents and instrumental

All reagents and chemicals are analytical grade and used as received. Zinc acetate dihydrate  $Zn(CH_3COO)_2 \cdot 2H_2O$ ; CAS Number: 5970-45-6), cerium (CAS Number: 7440-45-1), nitrate (SRM from NIST:  $NaNO_3$  in  $H_2O$  1000  $mgL^{-1}$   $NO_3$ , Sigma), hydrochloric acid (CAS Number: 7647-01-0), sodium hydroxide (CAS Number: 1310-73-2), absolute ethanol (CAS Number: 64-17-5) and MO

dye (Content 85 %; CAS Number: 547-58-0; EC Number: 208-925-3; Sigma) were obtained from Sigma and Merck (Germany). Bentonite (CAS Number: 1302-78-9) was purchased from Sigma (Sigma, USA). The pH of the solutions was adjusted using a Metrohm (Metrohm, Switzerland) pH meter. The color concentration was measured using a double beam-Unico 4802 spectrophotometer at its maximum wavelength (584 nm). FTIR spectrum was recorded by Bruker Tensor 27 device.

### 2.2. Synthesis of ZnO-Ce nanoparticles

The sol-gel method was used to prepare ZnO-Ce nanoparticles. First, 8.5 mL of zinc acetate was added to 40 mL of absolute ethanol and the solution was placed in an ultrasonic bath for 30 minutes (Solution A). Then 0.12 g of cerium nitrate was dissolved in 20 mL of absolute ethanol and 3 mL of deionized water and 2 mL of hydrochloric acid were added to it. Then, the solution was placed in an ultrasonic bath for 10 minutes (solution B). Solution B was added drop by drop to solution A while stirring to form a gel. To evaporate the ethanol, the gel was placed in an oven with a temperature of 80°C for 12 hours and then calcined for 3 hours in an oven at a temperature of 550°C.

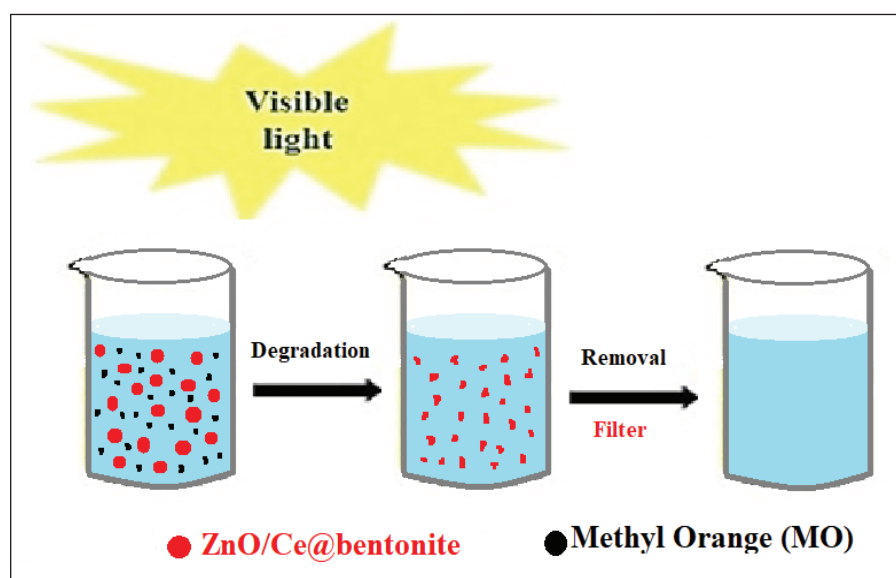
### 2.3. Synthesize bentonite nanocatalyst

The immersion method was used to synthesize

bentonite nanocatalysts coated with ZnO-Ce nanoparticles. For this purpose, 0.1 g of ZnO-Ce nanoparticles was added to one liter of ethanol and water with a ratio of 3:1. For homogenization, the slurry solution was placed in an ultrasonic bath (35 kHz, 40 W) for 30 minutes. Next, bentonite was immersed in the solution for one minute. Then the bentonite was first dried at room temperature and then dried in an oven at 80°C for 2 hours. To increase the adhesion of nanoparticles to the surface of bentonite, the granular bentonite was heated in an oven at a temperature of 550°C for 2 hours.

### 2.4. Removal procedure

Photocatalytic removal of MO by ZnO-Ce nanoparticles was studied using a batch reactor, equipped with a UVC lamp at room temperature (25 °C). To enhance removal efficiency, the reactor was covered with aluminum sheets. The appropriate dose of ZnO nanoparticle was mixed with different amounts of MO dye. The solution was stirred at 300 rpm for 30 minutes while the UV lamp at 3800 W irradiated the solution. After the experiment, 30 ml of the sample was taken and in order to separate the zinc oxide nanoparticles, the sample was centrifuged at 5000 rpm and filtered. Residual concentration was measured by spectrophotometer at 530 nm (Schematic 2) shows the diagram of degradation of MO).



Schema 2. Schematic diagram of degradation of MO

The removal percentage of MO dye (%removal) was calculated as Equation 1.

$$\%Removal = \frac{C_{eq}-C_0}{C_0} * 100$$

(Eq.1)

Parameters affecting the removal of MO dye, including the amount of the nanocomposite (10-100 mg), initial concentration of MO dye (25–150 mg L<sup>-1</sup>), and contact time (30-210 min), were investigated.

### 3. Results and discussion

#### 3.1. Characterization of nanocatalyst

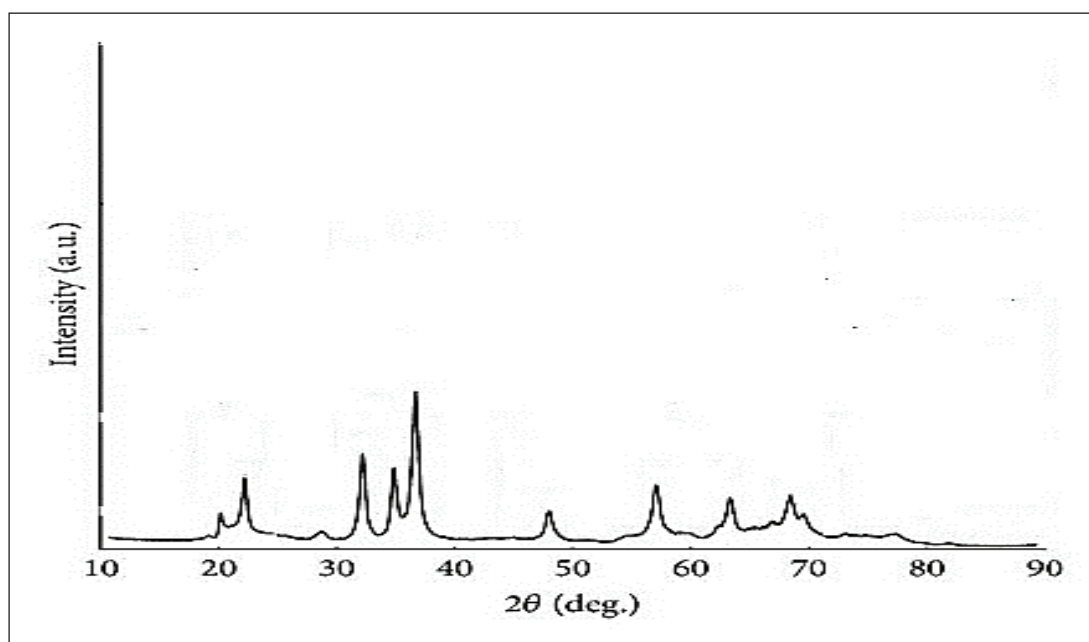
##### 3.1.1. XRD pattern of ZnO/Ce/ bentonite

Schematic 3 showed an XRD pattern of the

synthesized nanocomposite. It can be seen in schematic 3 that by doping cerium as an impurity, the peaks related to the rutile phase are removed and only the anatase phase is observed. In other words, the presence of cerium as an impurity greatly improves the growth of anatase phase crystals and prevents the transfer of the anatase phase to rutile.

##### 3.1.2. SEM image of synthesized ZnO/Ce/ bentonite

Schematic 4 showed an SEM image of a synthesized nanocatalyst. It can be concluded that the presence of cerium in the ZnO structure reduces the size of nanoparticles. Considering the strong dependence of the properties of nanoparticles on their size, we can expect significant changes in the properties of ZnO/Ce/ bentonite nanoparticles.



Schematic 3. XRD pattern of ZnO/Ce adsorbent

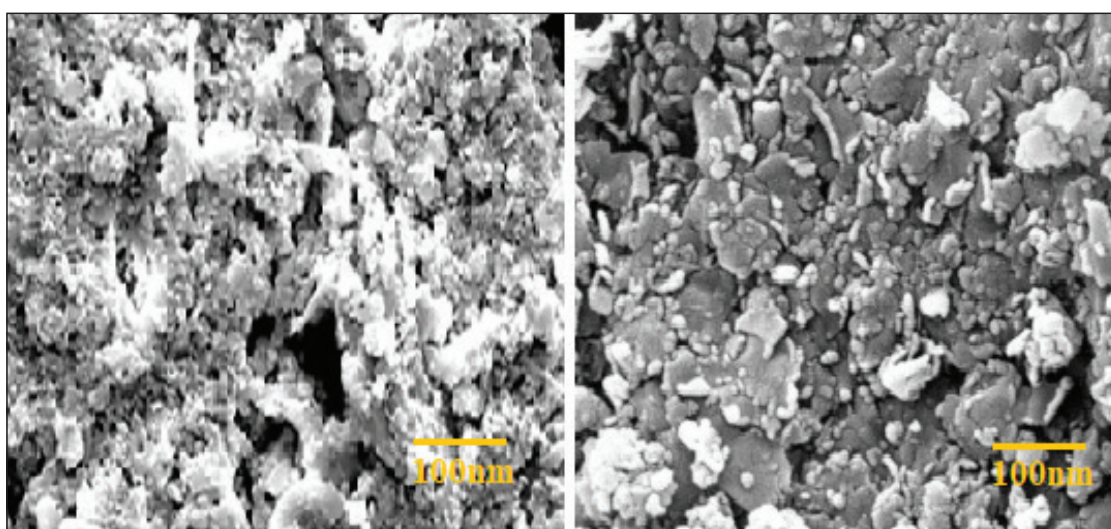
### 3.2. The optimized parameters for photocatalytic removal of MO

#### 3.2.1. Effect of amount of nanocatalyst

The amount of ZnO /Ce / bentonite nanocatalyst impacts the adsorption of the MO dye. The removal efficiency and the adsorption capacity were investigated. For this purpose, experiments were conducted using an adsorbent dosage in the range of 10 to 120 mg. As depicted in Figure 1, the uptake of the MO dye was significantly increased, up to 60 mg. Furthermore, by increasing the amount of nanocatalyst, the removal efficiency was increased.

#### 3.2.2. Effect of initial concentration of MO dye on removal efficiency

The effect of the initial concentration of dye on removal percentage by ZnO/Ce/Bentonite nanocatalyst was investigated in the range of 20 to 150 mg L<sup>-1</sup>. The result is shown in Figure 2. In the early stages of adsorption, the results showed a significant increase. The maximum percent removal was achieved at 50 mg L<sup>-1</sup> of MO dye. After this point, the saturation of active sites on the nanocatalyst has occurred, resulting decrease in the adsorbent's ability to the sorbent.



Schema 4. SEM image of synthesized adsorbent

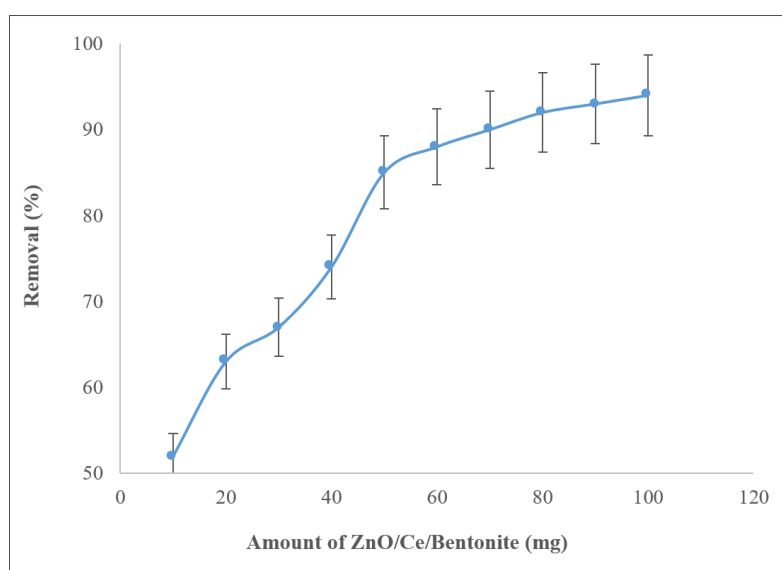
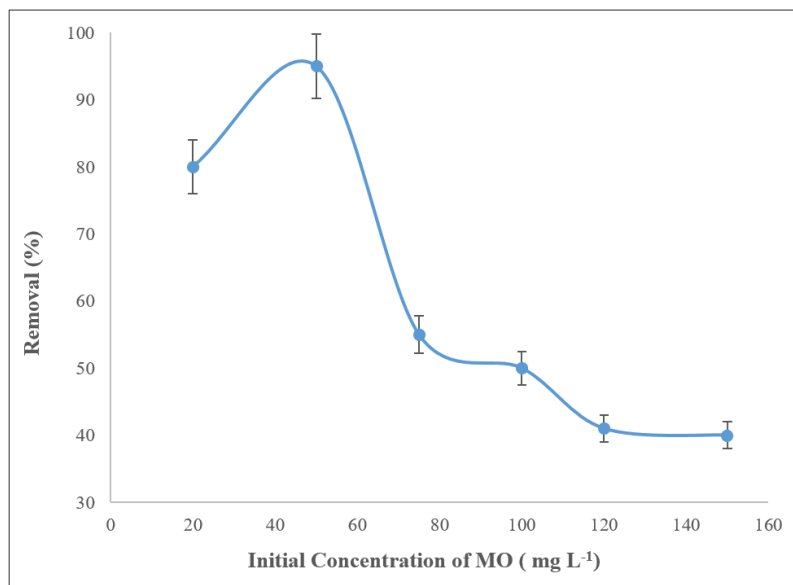


Fig. 1. Effect of ZnO/Ce/Bentonite amount on degradation efficiency



**Fig. 2.** Effect of dye concentration on degradation efficiency

### 3.2.3. Effect of time on degradation efficiency

The effect of contact time on the degradation efficiency of MO dye by ZnO/ Ce/ Bentonite nanocatalyst was investigated. The results are depicted in Figure 3. The removal percentages of MO dye increased significantly in the early stages. After a while, the percentage degradation will rise slightly until an equilibrium is reached. The results showed that the best dye removal percentage was obtained at 120 minutes. Hence, this time was selected for subsequent experiments.

### 3.2.4. Kinetic study

Adsorption kinetic studies of MO dye onto ZnO/ Ce/ Bentonite nanocatalyst were investigated using pseudo-first-order and pseudo-second-order kinetics. The results are shown in Figure 4 and at summarized in Table 1. The kinetic model that best fits the adsorption of MO dye on the nanocatalyst was determined by  $R^2$  values. Considering the reported  $R^2$  values, the adsorption of MO dye on ZnO/ Ce/ Bentonite nanocatalyst was followed by a pseudo-second-order kinetics model.

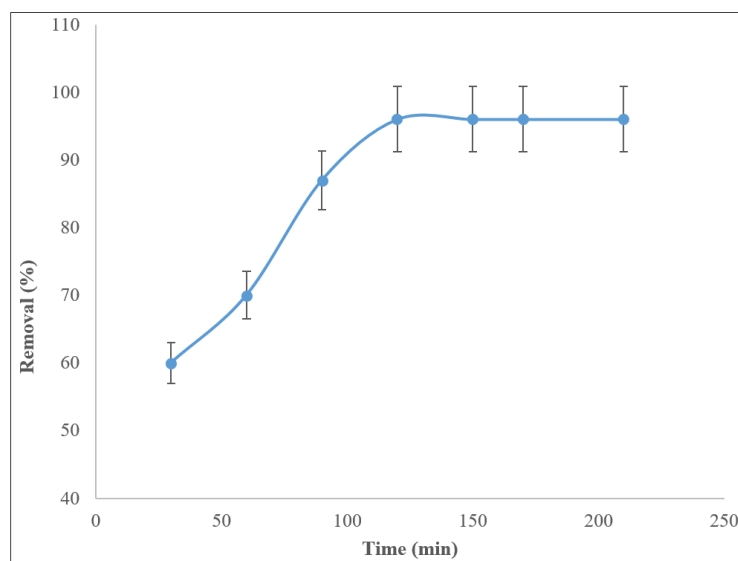


**Fig. 3.** Effect of time on degradation efficiency

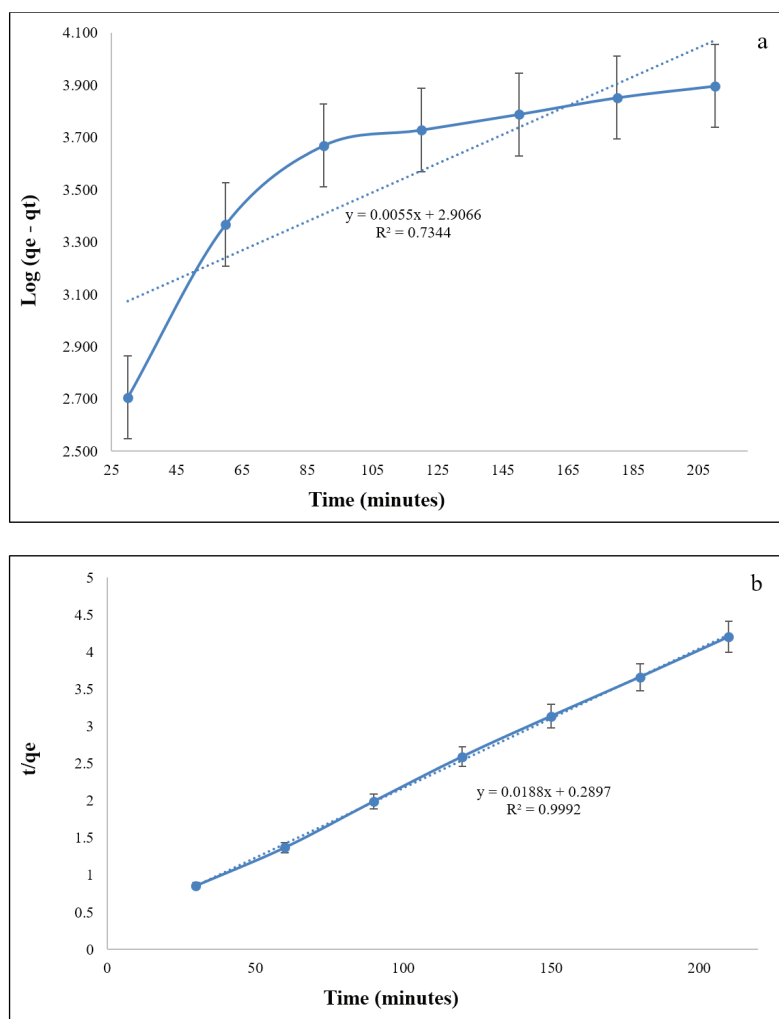


Fig. 4. Kinetic studies of the adsorption of MO dye on nanocatalyst.

a) Pseudo First order      b) Pseudo second order

Table 1. Kinetics parameters for MO dye

MO dye	First order kinetics		Second order kinetics	
	$R^2$	$K_1$ ( $\text{min}^{-1}$ )	$R^2$	$K_1$ ( $\text{g} \cdot \text{mg}^{-1} \cdot \text{min}^{-1}$ )
	0.8344	$-6.51 \times 10^{-3}$	0.9992	$1.88 \times 10^{-2}$

### 3.2.5. Adsorption isotherms

For the evaluation of adsorption isotherms, Langmuir and Freundlich's isotherms were used to illustrate the mechanism. The Langmuir and Freundlich isotherms for MO dye on nanocatalyst were depicted in Figure 5 and Table 2. It was found that the adsorption of Mo dye on ZnO/Ce/Bentonite nanocatalyst followed from Langmuir isotherm.

### 3.2.6. Reusability of Nanocatalyst

Evaluating the reusability of ZnO/Ce/Bentonite nanocatalyst on the degradation of MO dye photocatalytic experiments in optimal conditions was repeated several times. Afterward, the nanocatalyst was washed, dried, and reused for the next run. Results showed that degradation efficiency was decreased from 100 to 98.1 after 7 repeated experiments that confirmed the reusability of the nanocatalyst. Also, for the evaluation of the

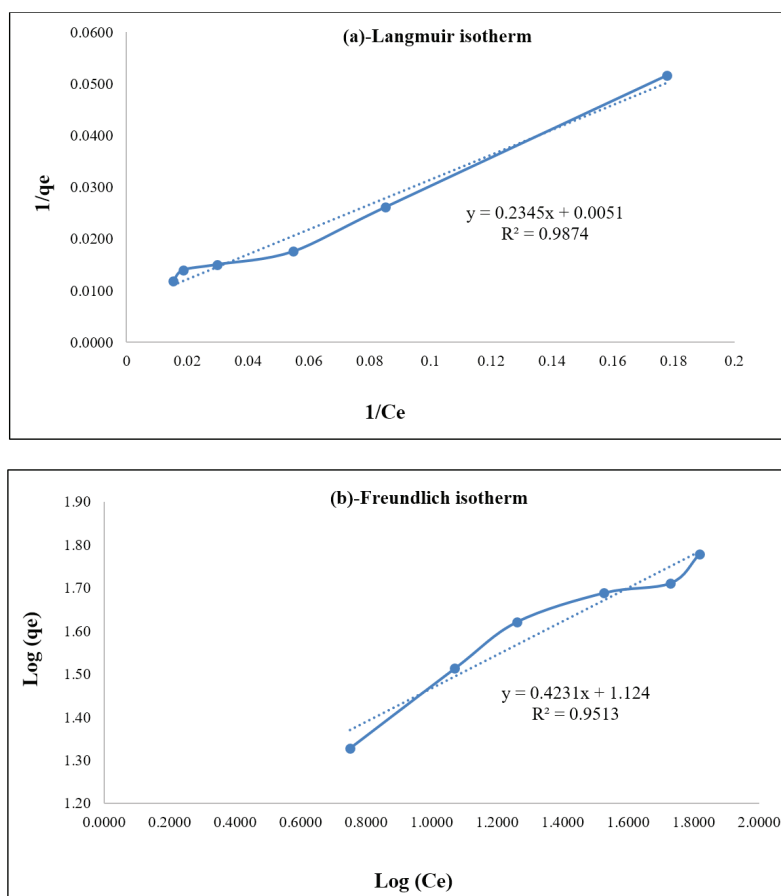


Fig. 5. a) Langmuir isotherm of MO dye onto nanocatalyst, b) Freundlich isotherm of MO dye onto nanocatalyst

Table 2. Isotherms parameter of MO dye

MO dye	Langmuir		Freundlich		
	$R_L$	$K_L$	$K_F$	N	
Results	0.9874	0.3989	0.9513	11.9674	2.5713

sorption capacity of the nanocatalyst, a standard solution containing  $100 \text{ mgL}^{-1}$  of MO was applied. The initial and final amounts of MO dye were determined by spectrophotometer after adsorption on ZnO/Ce/ Bentonite. The maximum adsorption capacity was defined as the total amount of adsorbed MO per gram of the nanocatalyst. The obtained capacity was found to be  $115 \text{ mg g}^{-1}$ .

#### 4. Conclusion

The degradation efficiency of methyl orange using ZnO/Ce/Bentonite nanocatalyst as photocatalyst and adsorbent was investigated. The optimal conditions

for the degradation efficiency of the dye were found at a nanocatalyst dosage of  $60 \text{ mg}$ , a contact time of  $120 \text{ min}$  yellow. At optimum conditions, 100% of methyl orange was removed by synthesized nanocomposite. Also, the nanocatalyst was reused after 7 repeated cycles, and adsorption capacity was obtained  $115 \text{ mg g}^{-1}$ . The isotherm data of MO dye were fitted with the Langmuir model, while the kinetic data were modeled by the pseudo-second-order, revealing that the nature of the kinetic adsorption is chemical. The present study showed that the ZnO/ Ce/ Bentonite nanocatalyst is an effective adsorbent for the degradation of MO dye from aqueous solutions.

## 5. Acknowledgements

Authors at this moment thank from health laboratory of Zabol University for their cooperation to perform experiments.

## 6. References

- [1] A. Rafiq, M. Ikram, S. Ali, F. Niaz, M. Khan, Q. Khan, M. Maqbool, Photocatalytic degradation of dyes using semiconductor photocatalysts to clean industrial water pollution, *J. Ind. Eng. Chem.*, 97 (2021) 111-128. <https://doi.org/10.1016/j.jiec.2021.02.017>
- [2] B. Viswanathan, Photocatalytic degradation of dyes: an overview, *Curr. Catal.*, 7 (2018) 99-121. <http://dx.doi.org/10.2174/2211544707666171219161846>
- [3] J. Singh, Biogenic synthesis of copper oxide nanoparticles using plant extract and its prodigious potential for photocatalytic degradation of dyes, *Environ. Res.*, 177(2019) 108569. <https://doi.org/10.1016/j.envres.2019.108569>
- [4] S. Alkaykh, A. Mbarek, E.E. Ali-Shattle, Photocatalytic degradation of methylene blue dye in aqueous solution by MnTiO<sub>3</sub> nanoparticles under sunlight irradiation, *Heliyon*, 6 (2020) e03663. <https://doi.org/10.1016/j.heliyon.2020.e03663>
- [5] L. Yang, Three-dimensional bacterial cellulose/polydopamine/TiO<sub>2</sub> nanocatalyst membrane with enhanced adsorption and photocatalytic degradation for dyes under ultraviolet-visible irradiation, *J. Colloid Interface Sci.*, 562 (2020) 21-28. <https://doi.org/10.1016/j.jcis.2019.12.013>
- [6] H. Chaker, A statistical modeling-optimization approach for efficiency photocatalytic degradation of textile azo dye using cerium-doped mesoporous ZnO: A central composite design in response surface methodology, *Chem. Eng. Res. Des.*, 171 (2021) 198-212. <https://doi.org/10.1016/j.cherd.2021.05.008>
- [7] R. Jasrotia, Photocatalytic degradation of environmental pollutant using nickel and cerium ions substituted Co<sup>0</sup>. 6ZnO. 4Fe<sub>2</sub>O<sub>4</sub> nanoferrites, *Earth Syst. Environ.*, 5 (2021) 399-417. <https://doi.org/10.1007/s41748-021-00214-9>
- [8] A. Mohammad, Adsorption promoted visible-light-induced photocatalytic degradation of antibiotic tetracycline by tin oxide/cerium oxide nanocatalyst, *Appl. Surface Sci.*, 565 (2021) 150337. <https://doi.org/10.1016/j.apsusc.2021.150337>
- [9] M.R. AbuKhadra, Enhanced photocatalytic degradation of acephate pesticide over MCM-41/Co<sub>3</sub>O<sub>4</sub> nanocatalyst synthesized from rice husk silica gel and Peach leaves, *J. Hazard. Mater.*, 389 (2020) 122129. <https://doi.org/10.1016/j.apsusc.2021.150337>
- [10] M.S. Nasrollahzadeh, Synthesis of ZnO nanostructure using activated carbon for photocatalytic degradation of methyl orange from aqueous solutions, *Appl. Water Sci.*, 8 (2018) 1-12. <https://doi.org/10.1007/s13201-018-0750-6>
- [11] J. Singh, A. Dhaliwal, Electrochemical and photocatalytic degradation of methylene blue by using rGO/AgNWs nanocatalyst synthesized by electroplating on stainless steel, *J. Phys. Chem. Solids*, 160 (2020) 110358. <https://doi.org/10.1016/j.jpcs.2021.110358>
- [12] S. Fukugaichi, Fixation of titanium dioxide nanoparticles on glass fiber cloths for photocatalytic degradation of organic dyes, *ACS omega*, 4 (2019) 15175-15180. <https://doi.org/10.1021/acsomega.9b02067>
- [13] Z. Wang, Efficient and sustainable photocatalytic degradation of dye in wastewater with porous and recyclable wood foam@ V<sub>2</sub>O<sub>5</sub> photocatalysts, *J. Clean. Prod.*, 332 (2022) 130054. <https://doi.org/10.1016/j.jclepro.2021.130054>
- [14] S. Li, Promoting effect of cellulose-based carbon dots at different concentrations on multifunctional photocatalytic degradation of dyes by ZnO, *Opt. Mater.*, 121(2021) 111591. <https://doi.org/10.1016/j.optmat.2021.111591>
- [15] A. Mishra, A. Mehta, S. Basu, Clay supported TiO<sub>2</sub> nanoparticles for photocatalytic degradation of environmental pollutants: A review, *J. Environ. Chem. Eng.*, 6 (2018) 6088-6107. <https://doi.org/10.1016/j.jece.2018.09.029>